Integrability of rank-two web models

Augustin Lafay, Azat M. Gainutdinov, Jesper Lykke Jacobsen

Nucl. Phys. B 1002 (2024) 116530

Contents lists available at ScienceDirect

Nuclear Physics, Section B

journal homepage: www.elsevier.com/locate/nuclphysb

Quantum Field Theory and Statistical Systems

Integrability of rank-two web models

Augustin Lafay [a,b,*], Azat M. Gainutdinov [c], Jesper Lykke Jacobsen [b,d,e]

[a] Department of Mathematics and Systems Analysis, Aalto University, Finland
[b] Laboratoire de Physique de l'École Normale Supérieure, ENS, Université PSL, CNRS, Sorbonne Université, Université de Paris, F-75005 Paris, France
[c] Institut Denis Poisson, CNRS, Université de Tours, Parc de Grandmont, F-37200 Tours, France
[d] Sorbonne Université, École Normale Supérieure, CNRS, Laboratoire de Physique (LPENS), F-75005 Paris, France
[e] Université Paris Saclay, CNRS, CEA, Institut de Physique Théorique, F-91191 Gif-sur-Yvette, France

ARTICLE INFO

Editor: Hubert Saleur

ABSTRACT

We continue our work on lattice models of webs, which generalise the well-known loop models to allow for various kinds of bifurcations [1,2]. Here we define new web models corresponding to each of the rank-two spiders considered by Kuperberg [3]. These models are based on the A_2, G_2 and B_2 Lie algebras, and their local vertex configurations are intertwiners of the corresponding q-deformed quantum algebras. In all three cases we define a corresponding model on the hexagonal lattice, and in the case of B_2 also on the square lattice. For specific root-of-unity choices of q, we show the equivalence to a number of three- and four-state spin models on the dual lattice.

The main result of this paper is to exhibit integrable manifolds in the parameter spaces of each web model. For q on the unit circle, these models are critical and we characterise the corresponding conformal field theories via numerical diagonalisation of the transfer matrix.

In the A_2 case we find two integrable regimes. The first one contains a dense and a dilute phase, for which we have analytic control via a Coulomb gas construction, while the second one is more elusive and likely conceals non-compact physics. Three particular points correspond to a three-state spin model with plaquette interactions, of which the one in the second regime appears to present a new universality class. In the G_2 case we identify four regimes numerically. The B_2 case is too unwieldy to be studied numerically in the general case, but it found analytically to contain a simpler sub-model based on generators of the dilute Birman-Murakami-Wenzl algebra.

Contents

* Corresponding author.
E-mail address: augustin.lafay@aalto.fi (A. Lafay).

https://doi.org/10.1016/j.nuclphysb.2024.116530
Received 22 December 2023; Received in revised form 3 March 2024; Accepted 31 March 2024

Available online 9 April 2024

1. Introduction

One of the most striking applications of conformal invariance in two dimension is the study of random geometrical objects. The specific case of random curves has been the object of much interest in the theoretical physics literature since the 1980s, where the so-called loop models have been investigated both in their lattice discretisation, notably using quantum integrability and lattice algebras of the Temperley-Lieb type, and in the continuum limit, via Conformal Field Theories (CFT); see [4–6] for reviews. Interestingly,

these CFT are in general not only non-unitary, but also logarithmic [7], and in certain cases of physical interest they may even possess a non-compact target space [8,9]. In parallel with these developments, random curves have been extensively studied in probability theory since the 2000s, where they have spearheaded the development of frameworks such as Schramm-Loewner Evolution (SLE) [10,11] and the Conformal Loop Ensemble (CLE) [12]. More recent work on loop models aims at the rigorous construction of the field theory [13–15] and the computation of correlation functions [16–20].

Notwithstanding all these interesting developments, it is known that many applications of random geometry need to go beyond the concept of curves, and focus instead on more general random graphs that allow for branchings and bifurcations. In two recent papers [1,2] we have initiated a study of so-called web models, which are generalisations of lattice models of loops, in which algebraic spiders play a prominent role. These spiders have their root in the study of invariants for quantum deformations of the classical Lie algebras, and our first objective has been to show that they lead naturally to lattice models for random geometries with the required properties. The spiders provide a convenient geometrical or graph-like description of quantum group invariants in tensor product representations, and they are known for a number of root systems, following the seminal work by Kuperberg [3] on the rank-two cases A_2, G_2 and B_2.

Our first paper introduced the A_n web models which gives rise to a lattice model on the hexagonal lattice much like the well-known Nienhuis loop model [21], but now allowing for bifurcations at nodes that are incident on three links. The web configurations are identical to domain walls in an n-state spin model, but they carry a non-local weight parameterised by q. At a specific parameter value, $q = e^{i\pi/(n+2)}$, the non-local weights become trivial so that the partition functions of the web and spin models agree. In general the web model provides a continuous, non-local deformation of the spin model, just like the well-known $O(N)$ loop model is a non-local deformation of the Ising model (the case $n = 1$).

Our second paper focused on the physics of the simplest member of this family, the A_2 model. In particular, we reformulated the geometrical model as a local vertex model with complex weights. This was used to interpret geometrically some of its critical exponents, as well as numerically determining its phase diagram. In this case, the resulting geometrical structures take the form of a collection of mutually avoiding bipartite cubic graphs embedded in the lattice. Each graph has a statistical weight that is a product of local Boltzmann weights for links and nodes, and a non-local weight for each graph component that generalises the usual Boltzmann weight of a loop. The non-local weight depends on the deformation parameter q in the quantum algebra $U_q(A_2)$, and it can be unambiguously evaluated by the "reduction" relations that define the A_2 spider.

Meanwhile, the Nienhuis loop model [21] is recovered in the rank-one A_1 case. The most striking feature of this simple and elegant model is without doubt that it is *quantum integrable* [22,23]. This is the reason why this model has been at the centre of an immense activity for more than forty years, leading to important methodological developments and practical applications spanning several fields of research in mathematics and physics. Sadly the web models studied in our previous papers [1,2] lack this very desirable feature.

The purpose of the present paper is to make up for this deficiency. We here define new web models for all rank-two spiders (with symmetries A_2, G_2 and B_2) and show that these are quantum integrable. All of these models contain a special point where they describe interfaces in spin models with plaquette interactions. These spin models were not studied before, and by construction they are also integrable.

Our starting point is to propose a slight modification of the A_2 web model from [2]. The modification may look innocuous from a physics point of view, because it does not change the universality class, but it is crucial from a mathematical point of view, because it makes the model quantum integrable. The modification consists in assigning an extra weight conjugate to the angle by which a piece of web bends in-between two successive bifurcations. Moreover we define, for the first time, statistical models for the other rank-two spiders, G_2 and B_2, and show their integrability. As a result we have ensured, as announced, the quantum integrability of web models based on all rank-two spiders.

The resulting models are defined on the hexagonal lattice for all three spiders, while for the B_2 case we also define a variant model on the square lattice.

Regarding the link to spin interfaces, recall that in our first paper [1] we showed how the A_2 web model possesses a special point, when $q = e^{i\pi/4}$, for which the partition function becomes proportional to that of a three-state chiral spin model on the dual (triangular) lattice. With the bending parameter included, this construction carries through, but the spin model now has an extra three-spin plaquette interaction. We show here that the two other web models also have special points, with q a root of unity, for which they are dual to three- or four-state spin models with various symmetries.

To study the continuum limit of web models, either analytically or via numerical diagonalisation of the transfer matrix, it turns out that we need an equivalent formulation as a vertex model with purely local weights. In our second paper [2] we provided this construction for the (unmodified) A_2 model, based on a representation-theoretical analysis of its underlying quantum group $U_q\,\mathfrak{sl}(3)$. We extend here this local reformulation to the modified-by-bending-weight A_2 model, as well as to the G_2 and B_2 models. In all cases the local Hilbert space of the vertex models consists of trivial and fundamental representations.

The main result of this piece of work is then that the corresponding vertex models are quantum integrable, for any value of q, provided that the various local weights are carefully adjusted. A general idea behind this discovery was to find a 'big' affine quantum group that contains the quantum symmetry of our models: it corresponds in each case to a certain (possibly twisted) affine Dynkin diagram that reduces, after erasing one of its nodes, to the (finite) Dynkin diagram of the web model. This affine quantum group—which is the analogue of $A_2^{(2)}$ for the A_1 loop model [23,24]—then generates solutions of the spectral-parameter dependent Yang-Baxter equation through analysis of intertwining conditions on the tensor product of its evaluation representations. We found these solutions in all three cases explicitly and decomposed them in terms of spider diagrams. After a fine tuning, we found a complete agreement with the local transfer matrices from the vertex-model formulation (see Section 7 for more details). Achieving

this connection with integrable models was in fact the principal motivation for the proposed modification of the A_2 model by the bending weight.

In the A_2 and G_2 cases, the solutions to Yang-Baxter equations already appeared in another context [25,26], but the solution in the B_2 case is new to the best of our knowledge. However, in all three cases, the geometrical interpretation was not discussed before. As usual we expect the continuum limit of these integrable models to be critical, and in fact conformally invariant, when q belongs to the unit circle. The question thus arises, what are the characteristics of the corresponding CFT?

In [2] we already provided some first numerical results on the central charge of the A_2 model, based on the scan of a two-dimensional parameter space of local weights for each choice of q. It was found that the model possesses both a dilute and a dense critical phase, just like the Nienhuis loop model (the A_1 model). Based on experience with the loop model [27], we can hope that each of these universality classes can be retrieved within the integrable sub-manifold of the (modified) model, hence making the numerical work much easier. This turns out to be the case indeed. Varying q along the unit circle for the integrable model, the diagonalisation of the transfer matrices for cylinders of circumference up to size $L = 9$ leads, in fact, to the identification of two distinct critical regimes (see Fig. 6), with distinct analytical behaviour of the central charge.

The first of these regimes encompasses the dilute and dense critical points, confirming our expectations that the A_2 models with and without modification belong to the same universality class. The numerically determined central charge in this regime is in excellent agreement with [2] and with an analytical Coulomb gas computation, that will be exposed in a separate publication [28]. The ground state of the second regime exists only when L is a multiple of 3, and its central charge takes larger values ($c \gtrapprox 3$) than expected for a rank-two model, with a conspicuously slow convergence. All of these observations hint at a larger symmetry, and possibly a non-compact continuum limit, like the one found for the Nienhuis loop model in regime III [8,9]. We did not find this regime in [2], presumably because we only focused on real, positive fugacities there.

Along the integrable line, three particular points correspond to a three-state spin model. Within the first regime, one finds two such points, with $c = \frac{4}{5}$ and $c = 0$, which are the expected results for a three-state Potts model in the dilute (critical for the spin model) and dense (infinite-temperature) phases, respectively. The third point is in the second regime, and has a value $c \approx 1.5$ that has not previously been reported for a three-state Potts model, to our best knowledge.

We present a similar numerical investigation of the G_2 model along its integrable sub-manifold (see Fig. 7), this time up to size $L = 8$. We identify here four different regimes for which the numerical results are well-behaved, leaving one or two further regimes for subsequent analytical investigations. In addition we find two handfuls of special points for which mappings to other well-understood models can be made. These include dense and dilute $O(N = -1)$ loop models, three-state spin models, spanning trees and loop-erased random walks.

Finally, for the B_2 model, the dimension of the transfer matrix is too large in order for us to obtain exploitable results. However, by adjusting certain local Boltzmann weights, we obtain a reduction of the size of the Hilbert space, leading to a more amenable model. In fact, we demonstrate that in this case the local transfer matrices can be written in terms of the dilute Birman-Murakami-Wenzl (BMW) algebra. Mathematically, the appearance of this algebra is not surprising because the BMW algebra is known to be Schur-Weyl dual to $U_q(B_2)$ in the tensor product of its natural representations, and here we have the diluted version of this well-known B_2 type Schur-Weyl duality. The corresponding integrable solution is in agreement with the baxterisation of the dilute BMW algebra [29].

The paper is structured as follows. In section 2 we specify the lattices and boundary conditions needed to define the models of this paper. The next three sections (3, 4 and 5) deal with respectively the A_2, G_2 and B_2 models. In each of them we first discuss the corresponding spider, define the lattice model, and establish the equivalence with spin models on the dual lattice. Section 6 provides the analysis of the quantum groups necessary to define the local vertex models and the corresponding transfer matrices. The integrable models are then constructed in section 7, as sketched above. Finally we gather some discussion and concluding remarks in section 8. A few technical ingredients are dispatched in four appendices.

2. Lattices

We will consider lattice models defined on the hexagonal lattice $\mathbb{H}$, the square lattice $\mathbb{S}$ and their duals, $\mathbb{H}^* = \mathbb{T}$ and $\mathbb{S}^*$ respectively. To fix notations, we will say that these lattices are comprised of *nodes* and *links* connecting them. To be more precise, the primal lattices $\mathbb{H}$ and $\mathbb{S}$ will be finite subgraphs of the infinite hexagonal and square lattices respectively, embedded either in the plane or the infinite cylinder as defined in the following way.

In the plane, consider a self avoiding closed path C on the dual infinite lattice, either the triangular lattice, or a shifted square lattice. The path C separates the plane in two open sets, one of which is bounded and denoted by $\mathring{C}$. The primal lattice is then comprised of all nodes and links that are inside $\mathring{C}$, in particular its intersection with $\mathcal{E}_b$—the set of links crossed by C—is empty. By dual lattices $\mathbb{H}^*$ and $\mathbb{S}^*$, we mean the subgraphs of the dual infinite lattices that are inside $\mathring{C} \cup C$. The nodes of the dual lattices that are inside C are called *boundary* nodes. Informally, the dual lattices contain an external layer comprised of boundary nodes, surrounding the primal lattices. An example for the plane case is given in Fig. 1.

On the cylinder, we pick two self avoiding and mutually avoiding non contractible paths C and C' on the dual infinite lattices, C' being on top of C when we orient the cylinder vertically. There is a bounded open set $C\mathring{C}'$ between C and C'. The primal lattices are defined to be the subgraphs contained in $C\mathring{C}'$. Denote by $\mathcal{E}_b$ the set of links crossed by C or C'. The dual lattices are defined to be the subgraphs contained in $C\mathring{C}' \cup C \cup C'$. We will call boundary nodes, the nodes inside $C \cup C'$. Note that, in this case, the boundary nodes split in two connected components, C and C'.

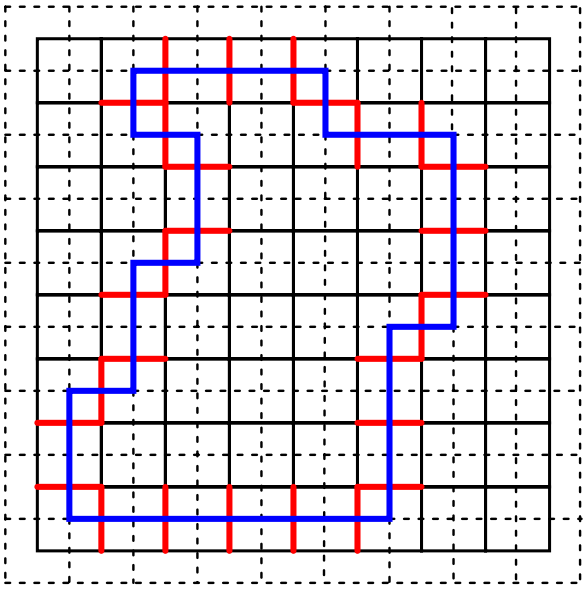

Fig. 1. The primal square lattice (undashed) and its dual (dashed). The path C is drawn in blue and the set $\mathcal{E}_b$ of edges crossed by C is drawn in red.

We will consider two types of lattice models. The first of them is the well-known setting of spin models where we assign on each node of the dual lattices a variable, the "spin", which takes a finite number of values, identified with elements of $\mathbb{Z}_n$ for some integer n. We will always consider monochromatic boundary conditions, i.e. the spins at the boundary nodes of a given connected component of the boundary are forced to take the same value. One may equivalently imagine the boundary nodes to be contracted into a single node, one for each connected component of the boundary.

The second type of lattice model is the web model outlined in the Introduction, for which we now recall a few definitions (see also [1]). Its configurations are called *webs*. A configuration can be represented abstractly as a graph with *vertices* and *edges*, or—for the purpose of defining the lattice model—as embedded in a lattice of *nodes* and *links*, in which case we shall call a link covered by the web a *bond*, while a link not covered is said to be *empty*. Given an embedded web, its abstract representation is obtained by deleting all the empty links, and contracting any path of consecutive bonds in between two vertices into a single edge. Obviously there will in general be many embedded webs that correspond to a given abstract one. The properties of the abstract web are described by the corresponding *spider*, an algebraic object which will be defined precisely in the next section. The first step in the definition of a web model is therefore to "lift" the spider to the lattice embedding. This must be done in a suitable way, so that the algebraic properties are preserved, while keeping the lattice model as simple and elegant as possible.

We here embed the webs in the primal lattice. The Boltzmann weights of a configuration G in the web models will be expressed as the product of two factors. The first of these is the product of local weights, such as the fugacity of a bond or of a specific arrangement around a given vertex. The other factor, called the Kuperberg weight $w_{\mathrm{K}}(G)$, is a priori non-local and depends only on G seen as an abstract web, regardless of its embedding.

3. The A_2 web models

We previously defined and studied the A_2 web models on the hexagonal lattice in [1]. Here, we give a more general definition that will prove exhibiting integrable points. We begin by recalling the definition of the A_2 spider as well as the mapping of webs to spin interfaces of the 3 states Potts models.

3.1. The A_2 spider

A_2 webs are planar oriented graphs embedded in a simply connected domain whose connected components are either closed loops or graphs with trivalent vertices inside the domain or univalent vertices connected to the boundary of the domain. Webs that do not have univalent vertices connected to the boundary of the domain will be called closed webs, otherwise, we will call them open webs. There are two types of trivalent vertices, called sinks and sources:

A number can be assigned unambiguously to any closed A_2 web from the following relations [3]:

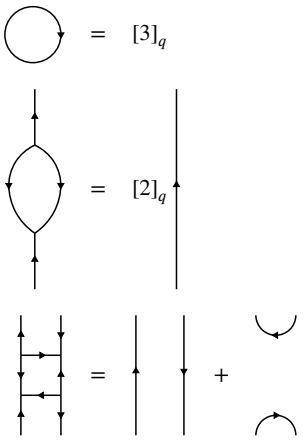

$$= [3]_q \tag{1a}$$

$$= [2]_q \tag{1b}$$

$$= + \tag{1c}$$

Indeed, it is a result of [3] that any closed web is proportional to the empty one. For an A_2 web G, we call the proportionality factor the *Kuperberg weight* of G and denote it by $w_{\mathrm{K}}(G)$.

The q-numbers $[k]_q$ appearing in (1) and *passim* are defined in Appendix C. They depend on a deformation parameter $q \in \mathbb{C}$. We can consider q as parameterising a family of web models having the symmetry of a given spider.

3.2. Definition of the models

Similarly as in [1], we define the A_2 web models on the hexagonal lattice $\mathbb{H}$. Configurations are given by closed A_2 webs embedded in $\mathbb{H}$. We will denote the configuration space by $\mathcal{K}$. Let G be one such configuration. We assign fugacities x to bonds and fugacities y and z to vertices that are sinks and sources respectively. In addition to the previous local fugacities that were present in the original definition of [1], we give a fugacity to each node of $\mathbb{H}$ that is adjacent to precisely two bonds. The two bonds inherit orientations from the web G, so that one of them is directed into the common node and the other goes out of the node. An observer that follows the bonds along that orientation, turns through an angle $\pi/3$ (anticlockwise) or $-\pi/3$ (clockwise) at the node: we call this the *bending* at the node. To this we assign a fugacity $e^{i\phi}$ for an anticlockwise bending, or $e^{-i\phi}$ for a clockwise bending. Here, ϕ is a new parameter at our disposal: the work [1] corresponds to $\phi = 0$.

The product of the local fugacities and the non local weight given by the Kuperberg weight defines the Boltzmann weight of a configuration. The partition function then reads:

$$Z_{A_2} = \sum_{c \in K} x^N (yz)^{N_V} e^{i\theta} w_{\mathrm{K}}(c), \tag{2}$$

where N is the number of bonds, and N_V is the number of sink/source pairs of vertices. We have defined $\theta = \sum_i \phi_i$, where the sum is over all nodes and $\phi_i = \pm\phi$ is the bending at node i, so that $e^{i\theta}$ is the total weight given by the bending of edges. An example of a configuration with its Boltzmann weight is given in Fig. 2.

Remark that the Boltzmann weights are invariant under discrete rotations of the lattice but not reflections when $e^{i\phi} \notin \mathbb{R}$. It is also clear that Z_{A_2} is invariant under the transformation $\phi \to -\phi$. Assuming, x, y, z and ϕ to be real, the Boltzmann weight of a configuration is sent to its complex conjugate under a spatial reflection, or the reversal of all orientations within a given web. Since the partition function Z_{A_2} comprises a sum over orientations, it follows that it is real. It is also clear that Z_{A_2} is invariant under

$$q \to q^{-1}, \tag{3}$$

since this transformation keeps the q-numbers unchanged. Furthermore, we show in Appendix A that the Boltzmann weights are of the form $x^N (yz)^{N_V} e^{iM\phi} w_{\mathrm{K}}(c)$ with

$$N + N_V + M = 0 \bmod 2$$

$$M = 0 \bmod 3.$$

This implies the invariance of Z_{A_2} under the following transformations

$$e^{i\phi} \to \tau e^{i\phi} \tag{4}$$

where τ is a third root of unity, or

$$x \to -x \tag{5a}$$

$$y \to iy \tag{5b}$$

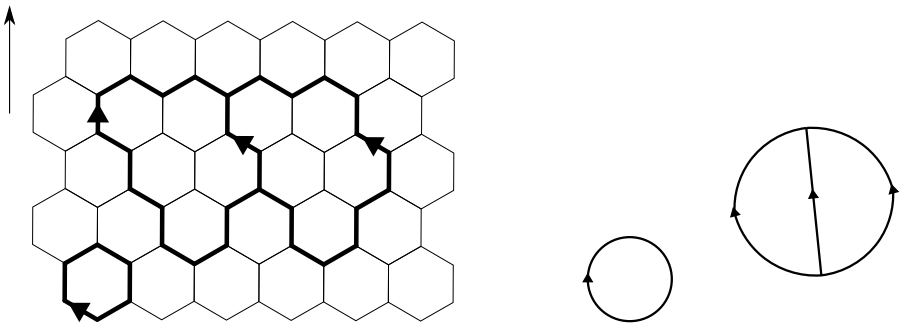

Fig. 2. Left panel: A configuration on $\mathbb{H}$ of weight $x^{35}yze^{6i\phi}[2]_q[3]_q^2$. The arrow is parallel to the axis of the cylinder. The left and right sides of the drawing are identified by periodic boundary conditions. Right panel: The same configuration drawn as a web.

$$z \to iz \tag{5c}$$

$$e^{i\phi} \to -e^{-i\phi} \tag{5d}$$

We finally note that the partition function is invariant under the following transformation

$$q \to -q \tag{6a}$$

$$y \to iy \tag{6b}$$

$$z \to iz \tag{6c}$$

because the factors of i can be absorbed in the Kuperberg rules (1). This will be explained in more detail in the next section. See also Fig. 2.

3.3. Relation with $\mathbb{Z}_3$ spin interfaces

In [1], we defined a mapping from the A_2 web model to the 3 states Potts model on the triangular lattice dual to $\mathbb{H}$ with nearest neighbour interactions. Here, we slightly generalise this mapping to account for three site plaquette interactions. Given two spins σ_i and σ_j in $\mathbb{Z}_3 \equiv \{0,1,2\}$ at sites i and j respectively, the nearest neighbour interaction is given by a local Boltzmann weight $x_{|\sigma_i-\sigma_j|}$. It follows that $x_1 = x_2 =: x$, and we set $x_0 = 1$. Given three sites i, j, k situated in a clockwise manner around a plaquette, the three site plaquette interaction is given by

$$\begin{aligned} p_{\sigma_i,\sigma_j,\sigma_k} =& \delta_{\sigma_i,\sigma_j}\delta_{\sigma_j,\sigma_k} + 2^{\frac{1}{4}} y \delta_{\sigma_i,\sigma_j+1}\delta_{\sigma_j,\sigma_k+1} + 2^{\frac{1}{4}} z \delta_{\sigma_i,\sigma_j-1}\delta_{\sigma_j,\sigma_k-1} \\ &+ e^{-i\phi}\left(\delta_{\sigma_i,\sigma_j+1}\delta_{\sigma_j,\sigma_k} + \delta_{\sigma_j,\sigma_k+1}\delta_{\sigma_k,\sigma_i} + \delta_{\sigma_k,\sigma_i+1}\delta_{\sigma_i,\sigma_j}\right) \\ &+ e^{i\phi}\left(\delta_{\sigma_i,\sigma_j-1}\delta_{\sigma_j,\sigma_k} + \delta_{\sigma_j,\sigma_k-1}\delta_{\sigma_k,\sigma_i} + \delta_{\sigma_k,\sigma_i-1}\delta_{\sigma_i,\sigma_j}\right). \end{aligned} \tag{7}$$

Notice that the plaquette interactions reduce the S_3 symmetry to $\mathbb{Z}_3$; in our previous work [1,2] we did not include plaquette interactions, so in that case the symmetry was actually S_3. In the present model, ϕ, y and z are adjustable parameters. Setting $\phi = 0$ and $y = z = 2^{-1/4}$ the plaquette interaction becomes the identity operator and we recover the previous model [1,2].

The partition function then reads

$$Z_{\mathbb{Z}_3} = \sum_{\sigma}\left(\prod_{\langle ij\rangle} x_{|\sigma_i-\sigma_j|}\right)\left(\prod_{\langle ijk\rangle} p_{\sigma_i,\sigma_j,\sigma_k}\right) \tag{8}$$

where $\langle ij\rangle$ denotes nearest neighbours pairs of sites and $\langle ijk\rangle$ denotes plaquettes of three sites. We have used the subscript $\mathbb{Z}_3$ to emphasise that the interaction (7) is invariant under cyclic permutations of the colours. The integrable solutions for the A_2 web models that will be described in Section 7.2 contain points that can be mapped to $\mathbb{Z}_3$ spin models only for a non-trivial plaquette interaction.

We now reformulate the partition function in terms of its domain walls. For two neighbouring spins σ_i and σ_j, if $|\sigma_i - \sigma_j| = 1$, we draw a bond on the link of $\mathbb{H}$ separating the two spins and we orient the bond such that the when going from the node i to the node j, the spin value increases (respectively decreases by) 1 when traversing a right-pointing (respectively left-pointing) bond. If $|\sigma_i - \sigma_j| = 0$ we let the link empty. We obtain this way a closed simple A_2 web G embedded in $\mathbb{H}$. The mapping is many to one and onto. The number of spin configurations having G as their domain wall is exactly 3 corresponding to the choice for the spin of an arbitrary face. We thus have that

$$Z_{\mathbb{Z}_3} = 3\sum_{G\in\mathcal{K}} x^N (\sqrt{2}yz)^{N_V} e^{i\theta} \tag{9}$$

Set $q = e^{i\frac{\pi}{4}}$. In order to relate $Z_{\mathbb{Z}_3}$ to Z_{A_2}, we follow the idea of [1]. Remark that the product of the vertex fugacities and the Kuperberg weight do not depend on the embedding of the web into $\mathbb{H}$. Given a closed simple web G, rewriting the product of vertex fugacities as

$$(yz)^{N_V} = (\sqrt{2}yz)^{N_V}\left(\frac{1}{\sqrt{2}}\right)^{N_V}$$

we call the product $\left(\frac{1}{\sqrt{2}}\right)^{N_V} w_{\mathrm{K}}(G)$, the *topological* weight of the web, $w_{\mathrm{top}}(G)$. Similarly as in [1] for the A_2 case, it can be computed thanks to modifications of the relations (1) in order to incorporate the vertex fugacity in the reduction process. This can be seen as a rescaling of the vertices of webs:

(10)

The rules computing the topological weight are then

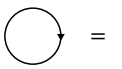

(11a)

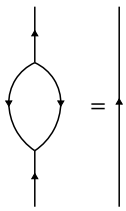

(11b)

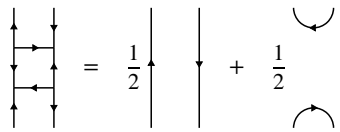

(11c)

The stochastic nature of these rules, i.e., the fact that the sum of prefactors appearing on each side of any of a given rule is the same implies that [1]

$$w_{\mathrm{top}}(G) = 1$$

We conclude that

$$Z_{\mathbb{Z}_3} = 3Z_{A_2} \tag{12}$$

where the spin interfaces are mapped to A_2 webs.

4. The G_2 web models

We now turn to web models based on the G_2 spider. In contrast to the A_2 case there are no orientations involved, and hence no bending. This will also lead to some other physical consequences, as we shall soon see.

4.1. The G_2 spider

G_2 webs are planar graphs embedded in a simply connected domain whose connected components are either closed loops or graphs with trivalent vertices inside the domain or univalent vertices connected to the boundary of the domain. Webs that do not have univalent vertices connected to the boundary of the domain will be called closed webs, otherwise, we will call them open webs. Edges come in two types and are called simple and double edges, depicted respectively as

There are two types of trivalent vertices:

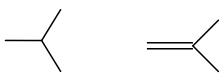

We will call the first vertex, vertex of type 1 and the second, vertex of type 2.

The free vector space spanned by closed G_2 webs will be denoted by $\mathcal{FS}p(G_2)$. We then denote by $\mathcal{S}p(G_2)$, the quotient of $\mathcal{FS}p(G_2)$ by the following local relations[1] [3]:

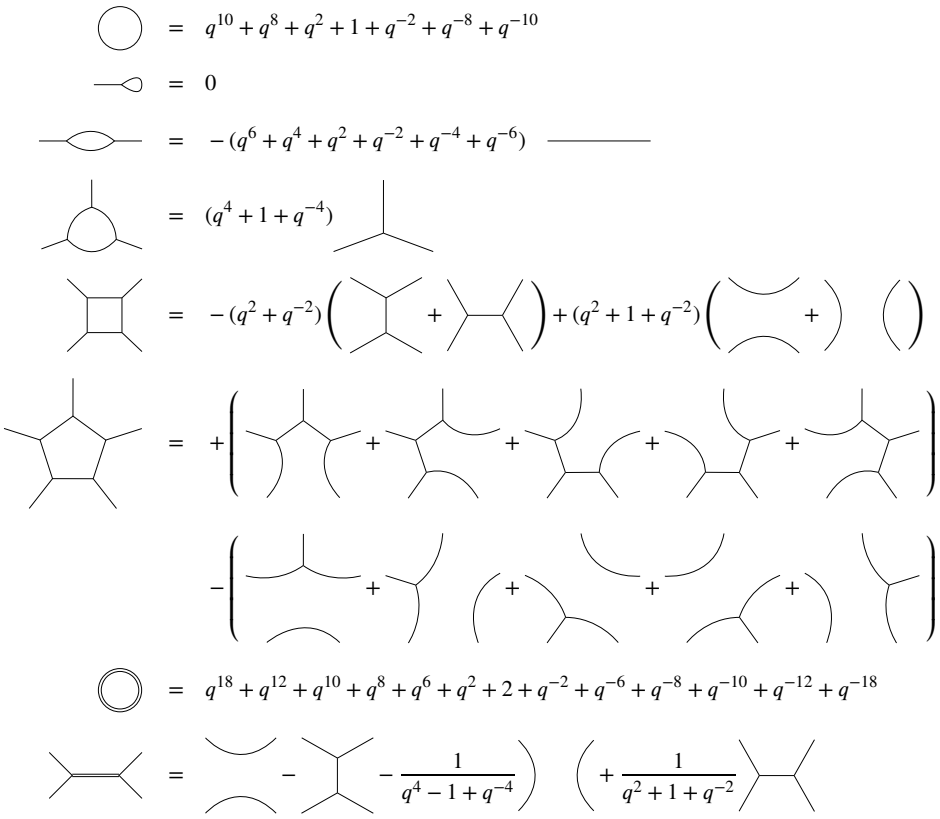

A number can be assigned unambiguously to any closed G_2 web thanks to these relations. Indeed, it is a result of [3] that any closed web is proportional to the empty one. For a G_2 web G, we call the proportionality factor the *Kuperberg weight* of G and denote it by $w_{\mathrm{K}}(G)$. Moreover, it is a result of [30] that relations (13a)-(13f) are sufficient to reduce unambiguously a closed G_2 web made of simple edges only to the empty one. We call such a web a *simple* G_2 web. An easy argument to see why any simple web can be reduced is the following. If a web contains a loop or a face surrounded by $n \leq 5$ edges, then it can be reduced in terms of smaller webs. If this always happens, the result follows by induction. Suppose it is not the case for a given web. Denote by F, E and V the number of faces, edges and vertices of this web. By the hand-shake lemma and Euler relation, we have that $2E = 3V$ and $F - E + V = 2$. Thus $F - \frac{1}{2}V = 2$. The assumption that all faces are of degree at least six means that $6F \leq 2E$, using the hand-shake lemma on the dual graph, so inserting we get $12 + 3V \leq 2E = 3V$, a contradiction.

We denote by $\mathcal{FS}p'(G_2)$, the free vector space generated by closed simple webs. The quotient of this space by relations (13a)-(13f) will be called $\mathcal{S}p'(G_2)$.

4.2. Definition of the models

We now define the G_2 web models on the hexagonal lattice $\mathbb{H}$. Configurations are given by closed simple G_2 webs embedded in $\mathbb{H}$. We will denote the configuration space by $\mathcal{K}$. We assign fugacities x to bonds and fugacities y to vertices. The product of the local fugacities and the non local weight given by the Kuperberg weight defines the Boltzmann weight of a configuration. The partition function then reads:

$$Z_{G_2} = \sum_{G \in \mathcal{K}} x^N y^M w_{\mathrm{K}}(G) \tag{14}$$

where N is the number of bonds and M is the number of vertices appearing in a given configuration. Remark that a trivalent graph has an even number of vertices, thus the partition function is independent of the sign of y.

One could also define a G_2 web model using both simple and double edge webs and two types of vertices. In this paper, we chose to focus on the simple case only.

[1] Note that our conventions differ from [3] by $q \leftrightarrow q^{\frac{1}{2}}$.

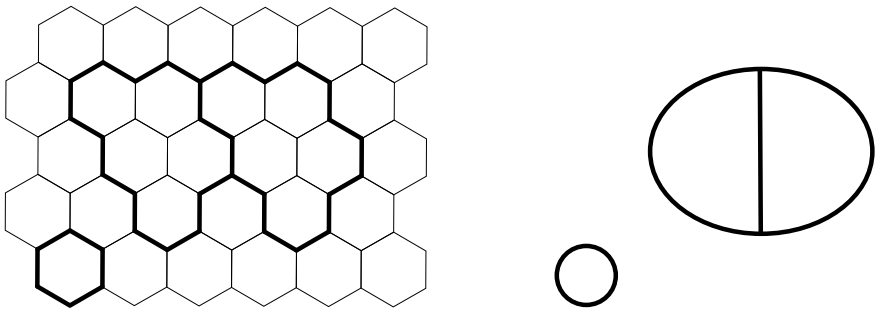

Fig. 3. Left panel: A configuration on $\mathbb{H}$ of weight $-x^{35}y^2(q^6+q^4+q^2+q^{-2}+q^{-4}+q^{-6})(q^{10}+q^8+q^2+1+q^{-2}+q^{-8}+q^{-10})^2$. Right panel: The same configuration drawn as a web.

4.3. Relation with an S_3 spin model

We can formulate an S_3 spin model defined on $\mathbb{T}$ in terms of its domain walls.[2] Consider spins $\{\sigma_i,\ i\in\mathbb{T}\}$ taking values in $\mathbb{Z}_3=\{0,1,2\}$. We define nearest neighbours interactions $x_{|\sigma_i-\sigma_j|}$ for a pair $\langle ij\rangle$ of neighbourings nodes. Here $|\sigma_i-\sigma_j|$ is to be understood modulo 3 and we normalise interactions such that $x_0=1$. Hence, this interaction depends only on one parameter x_1 that we rename x in the following. We also define a 3-site interaction for each plaquette $\langle ijk\rangle$ as

$$p_{\sigma_i,\sigma_j,\sigma_k}=\delta_{\sigma_i=\sigma_j=\sigma_k}+\sqrt{2}y\delta_{\sigma_i\neq\sigma_j\neq\sigma_k\neq\sigma_i}+\delta_{\sigma_i\neq\sigma_j=\sigma_k}+\delta_{\sigma_j\neq\sigma_k=\sigma_i}+\delta_{\sigma_k\neq\sigma_i=\sigma_j}\,. \tag{15}$$

Notice that this interaction is now invariant under any permutation of the three colours, so the corresponding model has an S_3 colour symmetry. The partition function of the model reads

$$Z_{S_3}=\sum_{\sigma}\left(\prod_{\langle ij\rangle}x_{|\sigma_i-\sigma_j|}\right)\left(\prod_{\langle ijk\rangle}p_{\sigma_i,\sigma_j,\sigma_k}\right). \tag{16}$$

We now reformulate the partition functions in terms of its domain walls. For two neighbouring spins σ_i and σ_j, if $|\sigma_i-\sigma_j|=1$, we draw a simple bond on the link of $\mathbb{H}$ separating the two spins whereas if $|\sigma_i-\sigma_j|=0$ we let the link empty. We obtain in this way a closed simple G_2 web G embedded in $\mathbb{H}$. The mapping is many to one and onto. The number of spin configurations having G as their domain wall is given by the number of proper 3-colourings of the dual graph $\hat{G}$. Denoting the chromatic polynomial with Q colours of $\hat{G}$ by $\chi_{\hat{G}}(Q)$, we have that

$$Z_{S_3}=\sum_{G\in\mathcal{K}}x^N(\sqrt{2}y)^M\chi_{\hat{G}}(3), \tag{17}$$

where N denotes the number of bonds, while M is the number of vertices of G. As an example, Fig. 3 corresponds to $\chi_{\hat{G}}(Q)=Q(Q-1)^2(Q-2)$.

We will now show that Z_{S_3} is equal to the partition function of the G_2 web model, up to an overall multiplicative constant, when

$$q=e^{i\frac{\pi}{6}}\quad\text{or}\quad q=e^{i\frac{5\pi}{6}}. \tag{18}$$

Remark that the product of the vertex fugacities and the Kuperberg weight do not depend on the embedding of the web into $\mathbb{H}$. Given a closed simple web G, rewriting the product of vertex fugacities as

$$y^M=(\sqrt{2}y)^M\left(\frac{1}{\sqrt{2}}\right)^M,$$

we call the product $\left(\frac{1}{\sqrt{2}}\right)^M w_{\mathrm{K}}(G)$, the *topological* weight of the web, $w_{\mathrm{top}}(G)$. Similarly as in the A_2 case, it can be computed thanks to modifications of the relations (13) in order to incorporate the vertex fugacity in the reduction process. This can be seen as a rescaling of the vertices of webs:

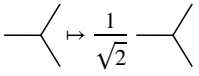

(19)

The relations to compute the topological weight of a simple web at either of the points (18) are thus

[2] Remark that this model is in general different than the one defined in Section 3.3.

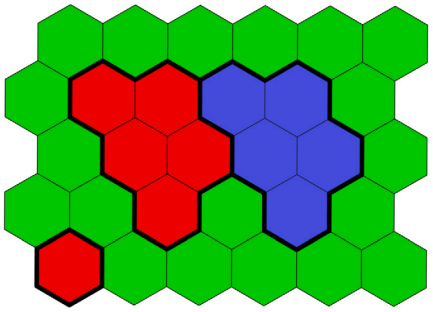

Fig. 4. A spin configuration, with the colours {red, blue, green} representing the spin values $\mathbb{Z}_3 := \{0, 1, 2\}$.

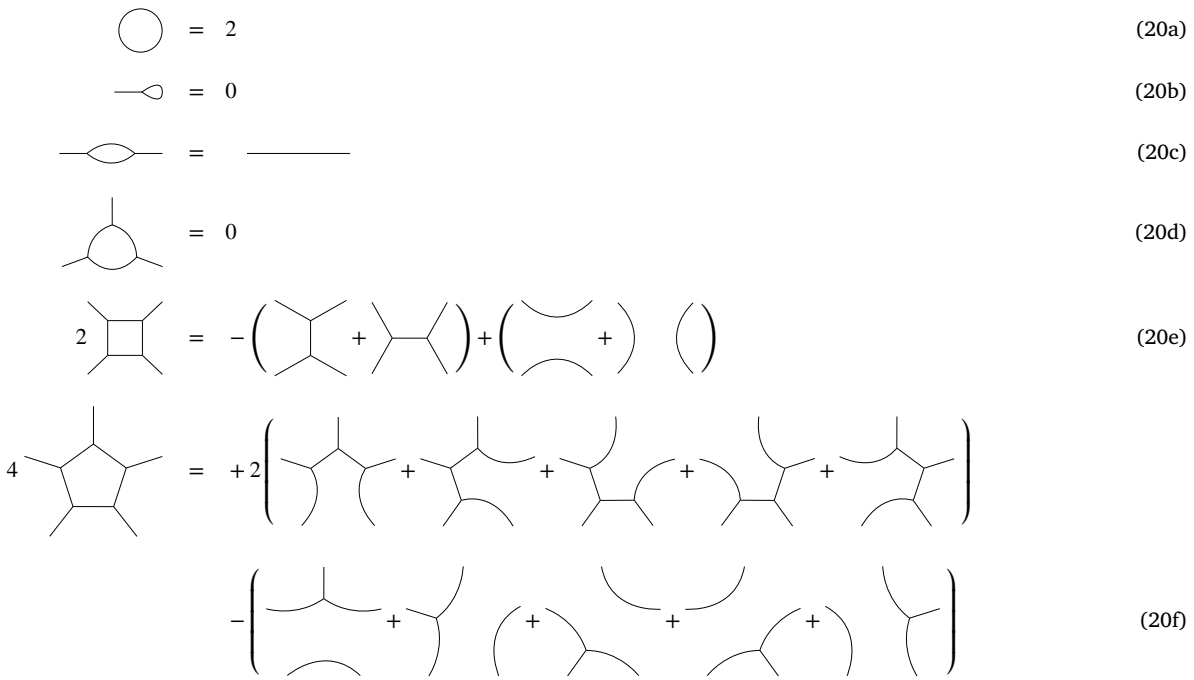

We will now show that, for any closed simple web G, $\chi_{\hat{G}}(3) = 3w_{\text{top}}(G)$. We begin by sketching a simple intuitive argument and below present a more formal variant using the chromatic algebra. See also Fig. 4.

We want to show that relations (20) hold true for domain walls in a 3-colouring problem. To this end we assign colours to the external faces of each relation and check the agreement between weights on the left- and right-hand sides of each relation. Consider, as an example, relation (20e). Encircling the whole diagram we encounter four domain walls, so the colours on one or both pairs of opposite external faces have to coincide. In the first case, there is no available colour for the central face on the left-hand side, so this side vanishes. On the right-hand side, one of the diagrams in the first parenthesis equals 1 and is compensated by one of the diagrams in the second parenthesis, while the other two diagrams vanish. In the second case, the left-hand side equals 2, while on the right-hand side both diagrams in the first parenthesis vanish, while each of the diagrams in the second parenthesis equals 1. The other relations are derived similarly.

Now, we move to the more formal argument using the chromatic algebra [31]. It will be sufficient to consider the chromatic algebra of degree 0, denoted $\mathcal{C}_0$, which is defined as follows. Consider the free vector space $\mathcal{F}_0$, spanned by planar graphs possibly containing closed loops, embedded in some simply connected domain. No edges are adjacent to the boundary of the domain, which is the meaning of "degree 0". $\mathcal{C}_0$ is defined to be the quotient of $\mathcal{F}_0$ by the following local relations:

(1) If e is an edge of a graph G which is not a loop, then $G = G/e - G \setminus e$, where G/e denotes the graph obtained from G by the contraction of e.
(2) If G contains a loop-edge e (i.e., an edge that connects a vertex to itself[3]), then $G = (Q-1)G \setminus e$.
(3) If G contains a 1-valent vertex then $G = 0$.

[3] The standard name for "loop-edge" in graph theory is simply *loop*, but we already use "loop" for what graph theorists would call a *cycle*.

Contrarily to webs, we do not consider graphs containing loops without vertices in $\mathcal{C}_0$. The chromatic algebra $\mathcal{C}_0$ depends on a parameter Q which has to be thought as a number of colours. Indeed, it was shown in [31] (Proposition 3.4) that a graph G in $\mathcal{C}_0$ is proportional to the empty graph:

$$G = Q^{-1}\chi_{\hat{G}}(Q)\emptyset \tag{21}$$

For completeness, we recall here the elements of the proof of Proposition 3.4 of [31]. Let e be an edge of G. Consider $\hat{e}$, the edge crossing e in the dual graph $\hat{G}$. Then, one has $\widehat{G/e} = \hat{G} \setminus \hat{e}$ and $\widehat{G \setminus e} = \hat{G}/\hat{e}$. Relation (1) is then translated to $\hat{G} = \hat{G} \setminus \hat{e} - \hat{G}/\hat{e}$ for the dual graph. This the deletion-contraction relation for the chromatic polynomial—a special case of a similar relation for the Q-state Potts model. Relation (3) follows as a 1-valent vertex in G corresponds to a loop in $\hat{G}$ and there are no proper Q-colourings of a graph containing loops. Finally, relation (2) follows because a loop whose interior trivially intersects G corresponds to a 1-valent vertex v in $\hat{G}$ and the number of Q-colourings of $\hat{G}$ is $Q-1$ times the number of Q-colourings of $\hat{G} \setminus \{v\}$. For a loop whose interior does not intersect G trivially, one can use relation (1) and (3) to reduce the interior of the loop to obtain a collection of nested loops. The interior of innermost of these loops then intersects G trivially. The overall factor of Q^{-1} in (21) corresponds to the fact that the dual graph of a mere vertex, which has Q ways to be coloured, is the empty graph.

Let us define a map g that sends a web in $\mathcal{FS}p'(G_2)$ to the chromatic algebra of degree 0, $\mathcal{C}_0$. This map simply identifies any web with its graph in $\mathcal{C}_0$, possibly adding a vertex to a loop if it is one of the components of a web. It is then extended by linearity. We will now show that this map factors through the quotient defined by relations (20a)-(20f), i.e. all these relations are satisfied in $\mathcal{C}_0$. The first 3 relations follow straightforwardly from the relations of $\mathcal{C}_0$. The fourth one is satisfied as there is clearly no 3 colouring of the dual graph of a graph containing the subgraph of the left hand side. The fifth one follows from repeated application of the relations of $\mathcal{C}_0$. To show that the last one is satisfied, we first remark that the left hand side is zero in $\mathcal{C}_0$ as there is no 3 colouring of the dual graph of a graph containing the left hand side as a subgraph. On the other hand, by repeated application of the relations of $\mathcal{C}_0$, one has that

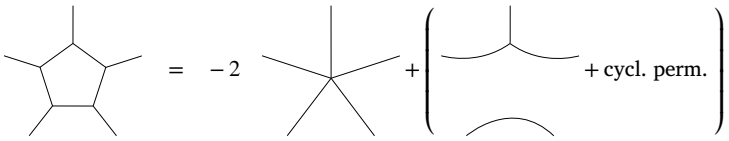

(22)

where by cycl(ic) perm(utations) we mean the 4 graphs obtained by discrete rotations, as in (20f). This linear combination is thus zero in $\mathcal{C}_0$. Applying the relations to the right hand side of (20f), we obtain

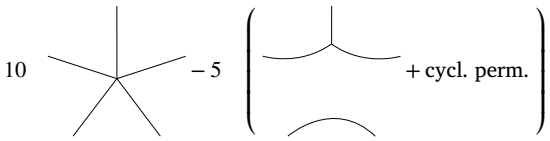

(23)

which is then vanishing as well in $\mathcal{C}_0$. Hence (20f) holds in $\mathcal{C}_0$.

We have thus shown that g defines a well defined linear map $\tilde{g}$ from $\mathcal{S}p'(G_2)$ to $\mathcal{C}_0$. We have then

$$\tilde{g}(G) = w_{\text{top}}(G)\,\emptyset \tag{24}$$

$$= 3^{-1}\chi_{\hat{G}}(3)\,\emptyset \tag{25}$$

leading to $\chi_{\hat{G}}(3) = 3w_{\text{top}}(G)$ as claimed.

We thus conclude that:

$$Z_{S_3} = 3Z_{G_2} \tag{26}$$

where domain walls of spin configurations are mapped to webs.

4.4. Relation with spanning trees

In the previous subsection, we define a S_3 symmetric spin model on the triangular lattice with nearest-neighbour and plaquette interactions. Let us focus for a moment on the S_Q symmetric spin model, or Q-state Potts models, with nearest-neighbour interactions only. The partition function reads

$$Z_{\text{Potts}} = \sum_{\sigma} \prod_{\langle ij \rangle} (x + (1-x)\delta_{\sigma_i \sigma_j}) \tag{27}$$

where $\sigma : \mathbb{T} \to \{1, \ldots, Q\}$. This model is known to be critical when [32]

$$Q = v^3 + 3v^2 \tag{28}$$

$$v = x^{-1} - 1$$

We can again express the partition function in terms of the domain walls between spin clusters. These subgraphs of $\mathbb{H}$ are again understood as simple G_2 webs. We thus obtain

$$Z_{\text{Potts}} = \sum_{G\in\mathcal{K}} x^N \chi_{\hat{G}}(Q)$$

where N denotes the number of bonds. The naive limit $Q=0$ is not interesting, as $\chi_{\hat{G}}(0)=0$ for any non-empty graph. Instead, we can focus on the polynomial

$$\kappa_{\hat{G}}(Q) = Q^{-1}\chi_{\hat{G}}(Q) \tag{29}$$

Then the limit

$$Z_{\text{tree}} = \lim_{Q\to 0} Q^{-1} Z_{\text{Potts}} = \sum_{G\in\mathcal{K}} x^N \kappa_{\hat{G}}(0) \tag{30}$$

defines a model of spanning trees on $\mathbb{T}$ [33]. The uniform probability measure on the set of spanning trees is obtained at $x=1$ and is critical by (28). We will now show that Z_{tree} is a special case of the G_2 web models for

$$q = i\,, \qquad y = i\,.$$

The proof is entirely analogous to the one for the S_3 spin model. First, we incorporate the vertex fugacity y into the Kuperberg relations to obtain a topological weight given by the modified relations

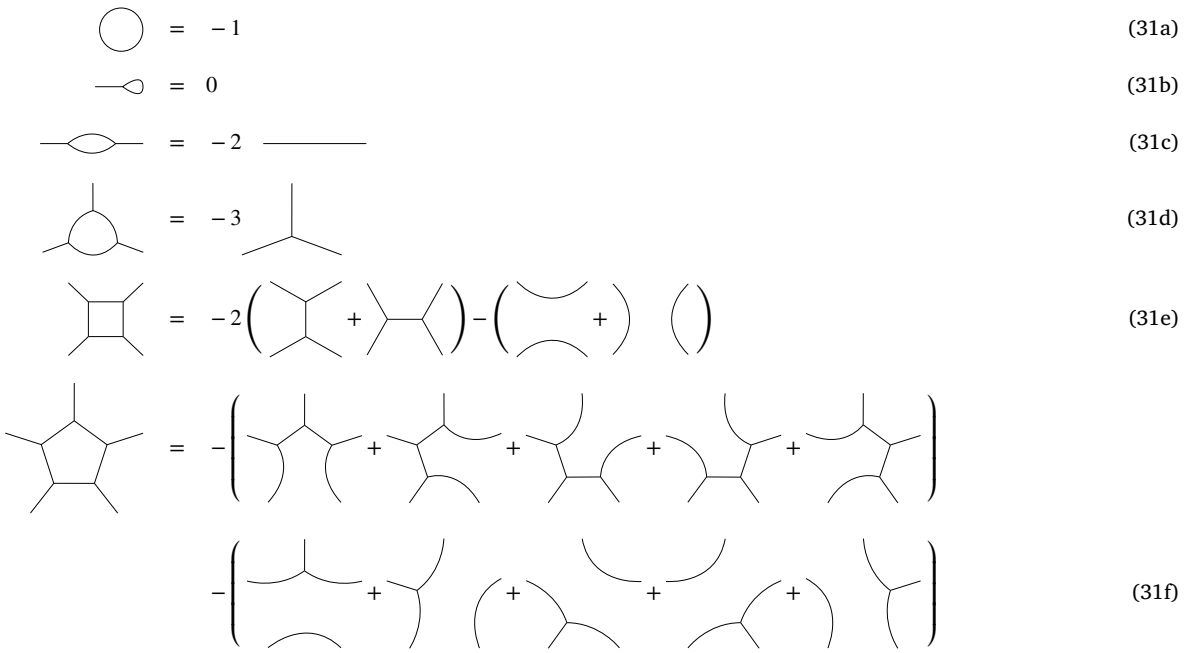

(31a) (31b) (31c) (31d) (31e) (31f)

Straightforward computations show that all the above relations hold in C_0 for $Q=0$. Hence the topological weight of G is nothing but $\kappa_{\hat{G}}(0)$ and we obtain

$$Z_{\text{tree}} = Z_{G_2} \tag{32}$$

5. The B_2 web models

For the last spider, the B_2 one, we can define two kinds of web models and establish relations with two kinds of spin models.

5.1. The B_2 spider relations

B_2 webs are planar graphs embedded in a simply connected domain whose connected components are either closed loops or graphs with trivalent vertices inside the domain or univalent vertices connected to the boundary of the domain. We again denote by open webs, the ones that possess univalent vertices connected to the boundary of the domain and closed webs, otherwise. Edges come again in two types and are called simple and double edges, depicted respectively as

Any trivalent vertex is required to be of the form

(33)

The free vector space spanned by closed B_2 webs will be called $\mathcal{FS}p(B_2)$. Then, $\mathcal{S}p(B_2)$ is the quotient of $\mathcal{FS}p(B_2)$ by the following local relations[4] [3]:

$$= \quad -(q^4+q^2+q^{-2}+q^{-4}) \tag{34a}$$

$$= \quad q^6+q^2+1+q^{-2}+q^{-6} \tag{34b}$$

$$= \quad 0 \tag{34c}$$

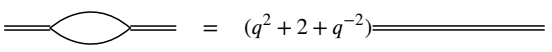

(34d)

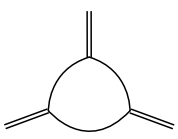

$$= \quad 0 \tag{34e}$$

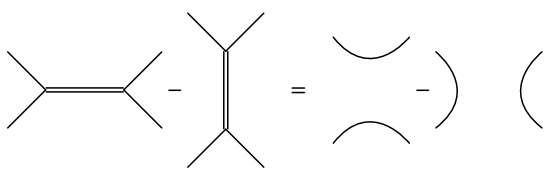

(34f)

A number can be assigned unambiguously to any closed B_2 web thanks to these relations. Indeed, it is a result of [3] that any closed web is proportional to the empty one. For a B_2 web G, we call the proportionality factor, the Kuperberg weight of G and denote it by $w_{\mathrm{K}}(G)$.

5.2. Definition of the models on the hexagonal lattice $\mathbb{H}$

The configuration space $\mathcal{K}$ is given by B_2 webs embedded in $\mathbb{H}$. We say a bond is *simple* (respectively *double*) when it is covered by a simple edge (respectively double). To a configuration G, we give a weight (or fugacity) $x_{t;1}$ (respectively $x_{v;1}$) to any tilted (respectively vertical) simple bond and a weight $x_{t;2}$ (respectively $x_{v;2}$) to any tilted (respectively vertical) double bond. We also give a fugacity y to any vertex. This determines the local part of the weight of G. The non local part is given by the Kuperberg weight $w_{\mathrm{K}}(G)$.

The partition function then reads:

$$Z_{B_2} = \sum_{G\in\mathcal{K}} x_{t;1}^{N_{t;1}} x_{v;1}^{N_{v;1}} x_{t;2}^{N_{t;2}} x_{v;2}^{N_{v;2}} y^{N_V} w_{\mathrm{K}}(G) \tag{35}$$

where $N_{t;1}$ (resp. $N_{v;1}$) is the number of tilted (resp. vertical) simple bonds, $N_{t;2}$ (resp. $N_{v;2}$) is the number of tilted (resp. vertical) double bonds and N_V is the number of vertices.

5.3. Definition of the models on the square lattice $\mathbb{S}$

Here we define B_2 web models on the square lattice. Their definition is motivated by connections with spin models that will be exposed in section 5.4.2.

First, let us augment $\mathcal{FS}p(B_2)$ by allowing 4-valent vertices whose adjacent edges are all simple. Let us denote the vector space spanned by such graphs by $\mathcal{FS}p'(B_2)$. We then quotient this space by the original B_2 relations (34) as well as:

[4] Note that our conventions differ from [3] by $q \leftrightarrow q^{\frac{1}{2}}$ and a rescaling of vertices by i.

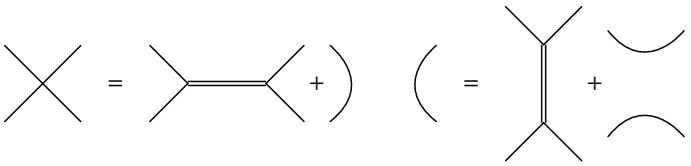

(36)

where the second equality is just a repetition of the defining relation (34f). This four-valent vertex was originally defined by Kuperberg [3]; notice that (34f) guarantees that it is indeed invariant under rotations through $\pm\frac{\pi}{2}$. The quotient space will be denoted by $\mathcal{S}p'(B_2)$.

First define a configuration on $\mathbb{S} \cup \mathcal{E}_b$ to be the replacement of each of its nodes by any of the following local states with the corresponding Boltzmann weights $b_1, \ldots, b_{14}$

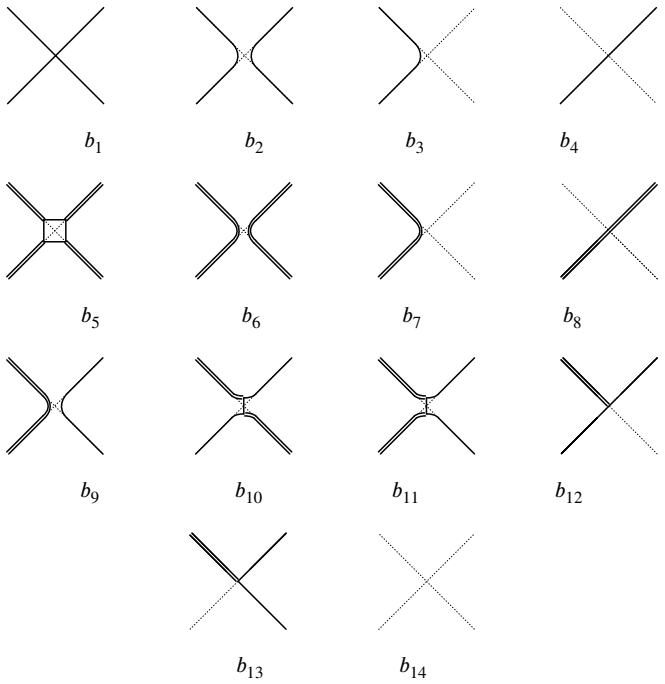

where we show only states up to rotations and reflections (the Boltzmann weights are taken to be invariant under these transformations). Moreover, each configuration is subject to the constraints that any link in $\mathcal{E}_b$ is empty and that any link has the same occupancy (empty, simple or double) with respect to each of the two nodes of $\mathbb{S}$ on which it is incident. Then delete from a given configuration the set of empty links. The result is a graph having only trivalent vertices of the type (33) and four-valent vertices surrounded by simple edges. In other words, it is a graph in $\mathcal{F}\mathcal{S}p'(B_2)$.

The weight of a configuration G is again the product of a local and a non-local part. The local part is a product of the local Boltzmann weights b_i. The non-local part is again $w_{\mathrm{K}}(G)$. It is computed by using the relations (34) once all 4-valent vertices, i.e. the ones with local weight b_1, have been resolved thanks to (36).

The partition function then reads:

$$Z_{B_2} = \sum_{G \in \mathcal{K}} \left(\prod_{i=1}^{14} b_i^{N_i} \right) w_{\mathrm{K}}(G) \tag{37}$$

where N_i is the number of local patterns of weight b_i.

Remark that we could have introduced models on the square lattice for the A_2 and G_2 cases as well. Here we consider only the hexagonal lattice for the latter as the integrable solutions described below contain the hexagonal lattice models with *isotropic* local weights. In contrast, this is not the case in the B_2 case which is why we defined the model on the hexagonal lattice with bond fugacities depending on the bond orientation. We can however define the above square lattice model with isotropic local weights for which there are integrable points. Finally, note that the local weights in the square lattice model are less constrained than in the hexagonal lattice case where they factorise in terms of bond and vertex fugacities. We could have defined the b_is as products of bond and vertex fugacities but, again, the more general non-factorised local weights b_i are needed in order for the model to contain integrable points.

5.4. Relation with S_3 and D_4 spin models

In this section, we show how the B_2 web models for some specific values of q are equivalent, at the level of partition functions, to three- and four-state spin models with global symmetries S_3 and D_4, respectively. In both cases the webs are identified with the corresponding spin clusters.

5.4.1. B_2 webs in $\mathbb{H}$ and the D_4 spin model

Consider the lattice dual to $\mathbb{H}$ embedded in the strip (respectively the cylinder), that is, a triangular lattice $\mathbb{T}$ with one (respectively two) point at infinity.

We begin by formulating the D_4 spin model in terms of its domain walls. Consider spins $\{\sigma_i,\ i \in \mathbb{T}\}$ taking values in $\mathbb{Z}_4 \cong \{0,1,2,3\}$. We define nearest neighbours interactions $x_{v,|\sigma_i-\sigma_j|}$ (respectively $x_{t,|\sigma_i-\sigma_j|}$) for two neighbouring sites i and j horizontally separated (respectively diagonally separated). Here $|\sigma_i - \sigma_j|$ is to be understood modulo 4 and we normalise interactions such that $x_0 = 1$. Hence, the nearest neighbour interaction term contains four parameters $x_{t;1}$, $x_{v;1}$, $x_{t;2}$ and $x_{v;2}$. We also add a plaquette interaction term

$$p_{\sigma_i,\sigma_j,\sigma_k} = 1 + y\left(\delta_{\sigma_i,\sigma_j\pm1}\delta_{\sigma_j,\sigma_k\pm1}\delta_{\sigma_k,\sigma_i\pm2} + \delta_{\sigma_i,\sigma_j\pm1}\delta_{\sigma_j,\sigma_k\pm2}\delta_{\sigma_k,\sigma_i\pm1} + \delta_{\sigma_i,\sigma_j\pm2}\delta_{\sigma_j,\sigma_k\pm1}\delta_{\sigma_k,\sigma_i\pm1} - 1\right)$$

which preserves D_4 symmetry. The partition function of the model reads

$$Z_{D_4} = \sum_{\sigma}\left(\prod_{\langle ij\rangle^t} x_{t,|\sigma_i-\sigma_j|}\right)\left(\prod_{\langle ij\rangle^v} x_{v,|\sigma_i-\sigma_j|}\right)\left(\prod_{\langle ijk\rangle} p_{\sigma_i,\sigma_j,\sigma_k}\right) \tag{38}$$

where $\langle ij\rangle^t$ (respectively $\langle ij\rangle^v$) denotes nearest neighbour pairs of sites diagonally separated (respectively horizontally separated).

Now we will rewrite the partition function in terms of its domain walls. Consider a spin configuration $\{\sigma_i,\ i \in \mathbb{T}\}$. For two neighbouring spins σ_i and σ_j, if $|\sigma_i - \sigma_j| = 1$, we draw a simple bond on the link of $\mathbb{H}$ separating the two spins. If $|\sigma_i - \sigma_j| = 2$, we draw a double bond, whereas if $|\sigma_i - \sigma_j| = 0$ we let the link empty. We obtain this way a Kuperberg B_2 web G embedded in $\mathbb{H}$, i.e. $G \in \mathcal{K}$. Clearly, the mapping is onto and many to one. That is, any $G \in \mathcal{K}$ is reached as a domain wall but different spin configurations may have the same set of domain walls G. Note that G contains, not only the information about domain walls between different spins but also what type of difference there is between spins, i.e. a difference of ±1 or ±2.

All configuration having the same domain wall G has the same weight. Hence, in order to write the partition function, it suffices to count how many spin configurations have the same domain walls. For later convenience we define this number in the following way. For a graph G whose connected components can be closed loops, such that all of its edges (or loops) are simple or double edges, consider the graph dual to G having its edges labelled by 1 (respectively 2) if they cross simple edges (respectively double edges). We say that its edges are of type 1 or type 2. We call such graphs *decorated*. Remark that G could be a B_2 web here, but it can be a more general graph with 4-valent vertices for instance. We will denote the dual graph of G by $\hat{G}$ and we stress that we consider $\hat{G}$ as a decorated graph. We call a *proper colouring* of a decorated graph H, a colouring of its vertices with colours in $\mathbb{Z}_4$ such that two colours connected by an edge of type 1 (respectively type 2) differ by ±1 modulo 4 (respectively ±2 modulo 4). We denote the number of proper colourings of H by ψ_H.

It is clear that, given a domain wall configuration $G \in \mathcal{K}$, the number of spin configurations that have G as its domain wall configuration is equal to $\psi_{\hat{G}}$. Hence the partition function of the spin model can be written as:

$$Z_{D_4} = \sum_{G\in\mathcal{K}} x_{t;1}^{N_{t;1}} x_{v;1}^{N_{v;1}} x_{t;2}^{N_{t;2}} x_{v;2}^{N_{v;2}} y^{N_V} \psi_{\hat{G}} \tag{39}$$

We will now show that $\psi_{\hat{G}} = 4w_{\mathrm{K}}(G)$ when $q = e^{i\frac{\pi}{4}}$, establishing the claimed equivalence. First, observe that we can extend by linearity the map ψ to $\mathcal{F}Sp(B_2)$ obtaining a linear form. We now claim that this map factors through the relations (34) to a well defined map on $Sp(B_2)$. For $q = e^{i\frac{\pi}{4}}$, the B_2 relations read:

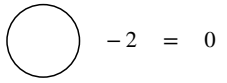

(40a)

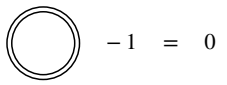

(40b)

(40c)

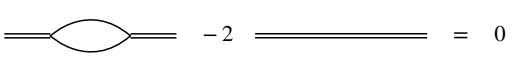

(40d)

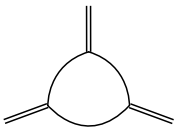
= 0 (40e)

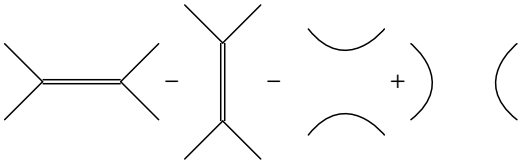
= 0 (40f)

We must verify that, for all relations, the left hand side is in the kernel of ψ. It is clear that this holds for the first 5 relations. To show that it holds for the last one, we can extend the definition of ψ to $\mathcal{F}Sp'(B_2)$ and show that it factors to a well defined map on $Sp'(B_2)$. We thus have to show that the linear combinations

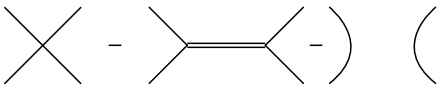
(41a)

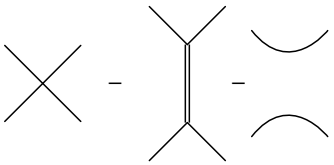
(41b)

are in the kernel of ψ. The proof being similar for the two expressions, let us detail it for the first one. Consider three webs G_1, G_2, G_3 that are the same except inside a disk where they look like:

$G_1 =$ 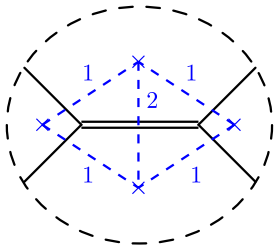

(42a)

$G_2 =$ 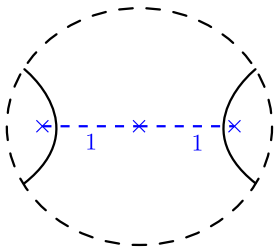

(42b)

$G_3 =$ 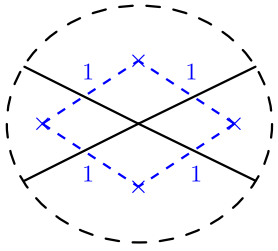

(42c)

where we have drawn in blue the parts of the dual graphs $\hat{G}_1$, $\hat{G}_2$ and $\hat{G}_3$ that are totally contained inside the disk. It is understood that there could be blue edges connecting vertices inside the disk to vertices outside the disk. It is clear that the number of proper colourings of $\hat{G}_3$ is the sum of the number of proper colourings where the top and bottom vertices are the same and the number of proper colourings where the vertices are different. Here, different implies differing by ± 2, hence we have $\psi_{\hat{G}_3} = \psi_{\hat{G}_1} + \psi_{\hat{G}_2}$. This shows that (41) is inside the kernel of ψ.

Since ψ is a well defined linear form on $Sp'(B_2)$ and every web G is proportional to the empty web by a factor $w_{\mathrm{K}}(G)$, we have that

$$\psi_{\hat{G}} = w_{\mathrm{K}}(G)\psi_{\hat{\emptyset}} = 4w_{\mathrm{K}}(G) \tag{43}$$

We thus have that

$$Z_{D_4} = 4Z_{B_2} \tag{44}$$

where domain walls and webs are identified in the mapping.

5.4.2. B_2 webs in $\mathbb{S}$, a D_3 and a D_4 spin model

Let us define a D_n spin model, with $n = 3$ or 4, on the lattice $\mathbb{S}^*$ dual to the square lattice $\mathbb{S}$. The local Boltzmann weights $p_{\sigma_i,\sigma_j,\sigma_k,\sigma_l}$ of the model depend of the values of the spins σ_i, σ_j, σ_k, $\sigma_l \in \mathbb{Z}_n$ (clockwise) cyclically ordered around a plaquette $\langle ijkl\rangle$, in the following way

$$\begin{aligned}
p_{\sigma_i,\sigma_j,\sigma_k,\sigma_l} =& b_1\delta_{\sigma_i,\sigma_j\pm1}\delta_{\sigma_j,\sigma_k\pm1}\delta_{\sigma_k,\sigma_l\pm1}\delta_{\sigma_l,\sigma_i\pm1}\\
&+ b_2\delta_{\sigma_i,\sigma_j\pm1}\delta_{\sigma_j,\sigma_k\pm1}\delta_{\sigma_k,\sigma_l\pm1}\delta_{\sigma_l,\sigma_i\pm1}(\delta_{\sigma_i,\sigma_k}+\delta_{\sigma_j,\sigma_l})\\
&+ b_3(\delta_{\sigma_i,\sigma_j}\delta_{\sigma_j,\sigma_k}\delta_{\sigma_k,\sigma_l\pm1}\delta_{\sigma_l,\sigma_i\pm1} + \delta_{\sigma_i,\sigma_j\pm1}\delta_{\sigma_j,\sigma_k}\delta_{\sigma_k,\sigma_l}\delta_{\sigma_l,\sigma_i\pm1}\\
&+ \delta_{\sigma_i,\sigma_j\pm1}\delta_{\sigma_j,\sigma_k\pm1}\delta_{\sigma_k,\sigma_l}\delta_{\sigma_l,\sigma_i} + \delta_{\sigma_i,\sigma_j}\delta_{\sigma_j,\sigma_k\pm1}\delta_{\sigma_k,\sigma_l\pm1}\delta_{\sigma_l,\sigma_i})\\
&+ b_4(\delta_{\sigma_i,\sigma_j\pm1}\delta_{\sigma_j,\sigma_k}\delta_{\sigma_k,\sigma_l\pm1}\delta_{\sigma_l,\sigma_i} + \delta_{\sigma_i,\sigma_j}\delta_{\sigma_j,\sigma_k\pm1}\delta_{\sigma_k,\sigma_l}\delta_{\sigma_l,\sigma_i\pm1})\\
&+ 2b_5\delta_{\sigma_i,\sigma_j\pm2}\delta_{\sigma_j,\sigma_k\pm2}\delta_{\sigma_k,\sigma_l\pm2}\delta_{\sigma_l,\sigma_i\pm2}\\
&+ b_6\delta_{\sigma_i,\sigma_j\pm2}\delta_{\sigma_j,\sigma_k\pm2}\delta_{\sigma_k,\sigma_l\pm2}\delta_{\sigma_l,\sigma_i\pm2}(\delta_{\sigma_i,\sigma_k}+\delta_{\sigma_j,\sigma_l})\\
&+ b_7(\delta_{\sigma_i,\sigma_j}\delta_{\sigma_j,\sigma_k}\delta_{\sigma_k,\sigma_l\pm2}\delta_{\sigma_l,\sigma_i\pm2} + \delta_{\sigma_i,\sigma_j\pm2}\delta_{\sigma_j,\sigma_k}\delta_{\sigma_k,\sigma_l}\delta_{\sigma_l,\sigma_i\pm2}\\
&+ \delta_{\sigma_i,\sigma_j\pm2}\delta_{\sigma_j,\sigma_k\pm2}\delta_{\sigma_k,\sigma_l}\delta_{\sigma_l,\sigma_i} + \delta_{\sigma_i,\sigma_j}\delta_{\sigma_j,\sigma_k\pm2}\delta_{\sigma_k,\sigma_l\pm2}\delta_{\sigma_l,\sigma_i})\\
&+ b_8(\delta_{\sigma_i,\sigma_j\pm2}\delta_{\sigma_j,\sigma_k}\delta_{\sigma_k,\sigma_l\pm2}\delta_{\sigma_l,\sigma_i} + \delta_{\sigma_i,\sigma_j}\delta_{\sigma_j,\sigma_k\pm2}\delta_{\sigma_k,\sigma_l}\delta_{\sigma_l,\sigma_i\pm2})\\
&+ b_9(\delta_{\sigma_i,\sigma_j\pm1}\delta_{\sigma_j,\sigma_k\pm1}\delta_{\sigma_k,\sigma_l\pm2}\delta_{\sigma_l,\sigma_i\pm2}\delta_{\sigma_i,\sigma_k} + \delta_{\sigma_i,\sigma_j\pm2}\delta_{\sigma_j,\sigma_k\pm1}\delta_{\sigma_k,\sigma_l\pm1}\delta_{\sigma_l,\sigma_i\pm2}\delta_{\sigma_j,\sigma_l}\\
&+ \delta_{\sigma_i,\sigma_j\pm2}\delta_{\sigma_j,\sigma_k\pm2}\delta_{\sigma_k,\sigma_l\pm1}\delta_{\sigma_l,\sigma_i\pm1}\delta_{\sigma_i,\sigma_k} + \delta_{\sigma_i,\sigma_j\pm1}\delta_{\sigma_j,\sigma_k\pm2}\delta_{\sigma_k,\sigma_l\pm2}\delta_{\sigma_l,\sigma_i\pm1}\delta_{\sigma_j,\sigma_l})\\
&+ b_{10}(\delta_{\sigma_i,\sigma_j\pm1}\delta_{\sigma_j,\sigma_k\pm2}\delta_{\sigma_k,\sigma_l\pm1}\delta_{\sigma_l,\sigma_i\pm2}\delta_{\sigma_i,\sigma_k\pm1} + \delta_{\sigma_i,\sigma_j\pm1}\delta_{\sigma_j,\sigma_k\pm2}\delta_{\sigma_k,\sigma_l\pm1}\delta_{\sigma_l,\sigma_i\pm2}\delta_{\sigma_j,\sigma_l\pm1}\\
&+ \delta_{\sigma_i,\sigma_j\pm2}\delta_{\sigma_j,\sigma_k\pm1}\delta_{\sigma_k,\sigma_l\pm2}\delta_{\sigma_l,\sigma_i\pm1}\delta_{\sigma_i,\sigma_k\pm1} + \delta_{\sigma_i,\sigma_j\pm2}\delta_{\sigma_j,\sigma_k\pm1}\delta_{\sigma_k,\sigma_l\pm2}\delta_{\sigma_l,\sigma_i\pm1}\delta_{\sigma_j,\sigma_l\pm1})\\
&+ b_{11}(\delta_{\sigma_i,\sigma_j\pm1}\delta_{\sigma_j,\sigma_k\pm1}\delta_{\sigma_k,\sigma_l\pm2}\delta_{\sigma_l,\sigma_i\pm2}\delta_{\sigma_j,\sigma_l\pm1} + \delta_{\sigma_i,\sigma_j\pm2}\delta_{\sigma_j,\sigma_k\pm1}\delta_{\sigma_k,\sigma_l\pm1}\delta_{\sigma_l,\sigma_i\pm2}\delta_{\sigma_i,\sigma_k\pm1}\\
&+ \delta_{\sigma_i,\sigma_j\pm2}\delta_{\sigma_j,\sigma_k\pm2}\delta_{\sigma_k,\sigma_l\pm1}\delta_{\sigma_l,\sigma_i\pm1}\delta_{\sigma_j,\sigma_l\pm1} + \delta_{\sigma_i,\sigma_j\pm1}\delta_{\sigma_j,\sigma_k\pm2}\delta_{\sigma_k,\sigma_l\pm2}\delta_{\sigma_l,\sigma_i\pm1}\delta_{\sigma_i,\sigma_k\pm1})\\
&+ b_{12}(\delta_{\sigma_i,\sigma_j\pm1}\delta_{\sigma_j,\sigma_k}\delta_{\sigma_k,\sigma_l\pm1}\delta_{\sigma_l,\sigma_i\pm2} + \delta_{\sigma_i,\sigma_j\pm2}\delta_{\sigma_j,\sigma_k\pm1}\delta_{\sigma_k,\sigma_l}\delta_{\sigma_l,\sigma_i\pm1}\\
&+ \delta_{\sigma_i,\sigma_j\pm1}\delta_{\sigma_j,\sigma_k\pm2}\delta_{\sigma_k,\sigma_l\pm1}\delta_{\sigma_l,\sigma_i} + \delta_{\sigma_i,\sigma_j}\delta_{\sigma_j,\sigma_k\pm1}\delta_{\sigma_k,\sigma_l\pm2}\delta_{\sigma_l,\sigma_i\pm1})\\
&+ b_{13}(\delta_{\sigma_i,\sigma_j\pm1}\delta_{\sigma_j,\sigma_k\pm1}\delta_{\sigma_k,\sigma_l}\delta_{\sigma_l,\sigma_i\pm2} + \delta_{\sigma_i,\sigma_j\pm2}\delta_{\sigma_j,\sigma_k\pm1}\delta_{\sigma_k,\sigma_l\pm1}\delta_{\sigma_l,\sigma_i}\\
&+ \delta_{\sigma_i,\sigma_j}\delta_{\sigma_j,\sigma_k\pm2}\delta_{\sigma_k,\sigma_l\pm1}\delta_{\sigma_l,\sigma_i\pm1} + \delta_{\sigma_i,\sigma_j\pm1}\delta_{\sigma_j,\sigma_k}\delta_{\sigma_k,\sigma_l\pm2}\delta_{\sigma_l,\sigma_i\pm1}\\
&+ \delta_{\sigma_i,\sigma_j}\delta_{\sigma_j,\sigma_k\pm1}\delta_{\sigma_k,\sigma_l\pm1}\delta_{\sigma_l,\sigma_i\pm2} + \delta_{\sigma_i,\sigma_j\pm2}\delta_{\sigma_j,\sigma_k}\delta_{\sigma_k,\sigma_l\pm1}\delta_{\sigma_l,\sigma_i\pm1}\\
&+ \delta_{\sigma_i,\sigma_j\pm1}\delta_{\sigma_j,\sigma_k\pm2}\delta_{\sigma_k,\sigma_l}\delta_{\sigma_l,\sigma_i\pm1} + \delta_{\sigma_i,\sigma_j\pm1}\delta_{\sigma_j,\sigma_k\pm1}\delta_{\sigma_k,\sigma_l\pm2}\delta_{\sigma_l,\sigma_i}\\
&+ b_{14}\delta_{\sigma_i,\sigma_j}\delta_{\sigma_j,\sigma_k}\delta_{\sigma_k,\sigma_l}\delta_{\sigma_l,\sigma_i}
\end{aligned}$$

One may check that $p_{\sigma_i,\sigma_j,\sigma_k,\sigma_l}$ respects D_4 symmetry. Note that the factor 2 in front of b_5 is due to the two ways of colouring the inside of the square in the corresponding plaquette.

The partition function then reads

$$Z_{D_4} = \sum_{\{\sigma\}} \prod_{<ijkl>} p_{\sigma_i,\sigma_j,\sigma_k,\sigma_l} \tag{45}$$

where the usual nearest-neighbour interactions have now been absorbed into the b_i. When $n = 4$, each summand in $p_{\sigma_i,\sigma_j,\sigma_k,\sigma_l}$ can be graphically expressed thanks to the corresponding web in Section 5.3 where simple (respectively double) bonds separate spins differing by ±1 (respectively ±2). Thus, the only non vanishing summands in the product over all plaquettes $\prod_{<ijkl>} p_{\sigma_i,\sigma_j,\sigma_k,\sigma_l}$ are

given by webs embedded in $\mathbb{S}$ as in Section 5.3. Given such a web G, the corresponding summand will be equal to, after summing over spin configurations,

$$\left(\prod_{i=1}^{14} b_i^{N_i}\right)\psi_{\hat{G}}$$

When $q = e^{i\frac{\pi}{4}}$, we have seen in (43) that $\psi_{\hat{G}} = 4w_{\mathrm{K}}(G)$, hence

$$Z_{D_4} = 4Z_{B_2} \tag{46}$$

When $n = 3$, summands in $p_{\sigma_i,\sigma_j,\sigma_k,\sigma_l}$ do not determine uniquely a web as $\sigma \pm 1 = \sigma \pm 2$. Yet, if we forbid double-edge configurations by setting

$$b_i = 0\,, \text{ for } i \in [\![5, 13]\!]\,, \tag{47}$$

there is again a one-to-one correspondence. The corresponding webs involve only simple edges. Denote by $\mathcal{K}'$ the corresponding set of webs embedded in $\mathcal{S}$. We have that

$$Z_{D_3} = \sum_{G\in\mathcal{K}'}\left(b_{14}^{N_{14}}\prod_{i=1}^{4} b_i^{N_i}\right)\chi_{\hat{G}}(3) \tag{48}$$

We will now show that $\chi_{\hat{G}}(3) = 3w_{\mathrm{K}}(G)$ when $q = e^{i\frac{\pi}{3}}$.

We define a morphism from $\mathcal{S}p'(B_2)$ at $q = e^{i\frac{\pi}{3}}$ to the chromatic algebra C_0 whose definition was given in Section 4.3. Consider first the map f that sends a web G in $\mathcal{F}\mathcal{S}p'(B_2)$ to the graph in C_0 obtained by forgetting the information of edges being simple or double, possibly adding a vertex to a loop if present. Extend f by linearity to $\mathcal{F}\mathcal{S}p'(B_2)$. We want to show that f factors through the quotient of B_2 relations (34) and (36) to a map $\tilde{f}$ from $\mathcal{S}p'(B_2)$ to C_0. We then need to show that the following linear combinations are in the kernel of f:

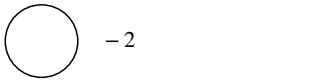

(49a)

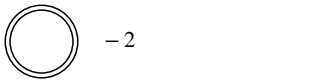

(49b)

(49c)

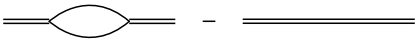

(49d)

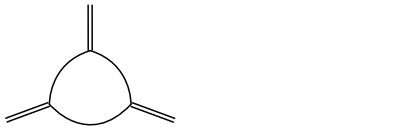

(49e)

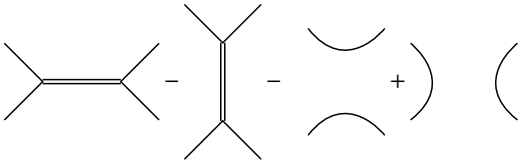

(49f)

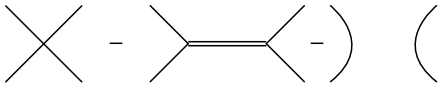

(49g)

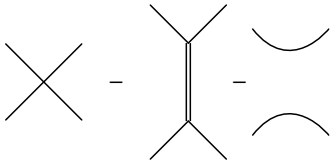

(49h)

This follows from a straightforward application of the relations of C_0. Hence, for a given web G we have that

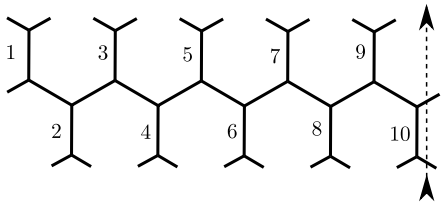

Fig. 5. The row to row transfer matrix in the case of periodic boundary conditions with $2L = 10$.

$$\tilde{f}(G) = w_{\mathrm{K}}(G)\,\emptyset = 3^{-1}\chi_{\hat{G}}(3)\,\emptyset \tag{50}$$

leading to $\chi_{\hat{G}}(3) = 3w_{\mathrm{K}}(G)$.

Thus, we have

$$Z_{D_3} = 3Z_{B_2} \tag{51}$$

6. Transfer matrices

From now on, we add to the discussion the A_1 case, as it will serve as a simpler and well-known example, the dilute loop model, which will guide the discussion of the rank 2 web models. Let X denote one of our algebras of interest, A_1, A_2, G_2 or B_2. As in [2], we define local transfer matrices thanks to the identification given by the spiders between diagrams and intertwiners of quantum group representations [3]. To each link of the lattice is associated a local space of state $\mathcal{H}_X$ that carries a particular representation of the quantum group, a direct sum of trivial and fundamental representations. The trivial representation $\mathbb{C}$ corresponds to the link not being covered by a web. We denote the vacuum vector $1 \in \mathbb{C}$ by $|\,\rangle$. Let us build the row to row transfer matrices by composing smaller, local transfer matrices.

In the hexagonal lattice $\mathbb{H}$ case, we shall call node of type 1 (respectively type 2) a node situated at the bottom (respectively top) of a vertical link. Denote by $t^X_{(k)}$ the local transfer matrices propagating through a node of type $k \in \{1,2\}$. They are linear maps:

$$t^X_{(1)} : \mathcal{H}_X \otimes \mathcal{H}_X \to \mathcal{H}_X\,, \tag{52a}$$

$$t^X_{(2)} : \mathcal{H}_X \to \mathcal{H}_X \otimes \mathcal{H}_X\,, \tag{52b}$$

and we use their pictorial notation  and  , respectively, in Fig. 5. We will show how to obtain these linear maps in the next sections. Their composition $t^X = t^X_{(2)} t^X_{(1)}$ is a linear map from $\mathcal{H}_X \otimes \mathcal{H}_X$ to itself (i.e., an endomorphism of $\mathcal{H}_X \otimes \mathcal{H}_X$).[5] We index the copies t^X_i of these operators by their position i in a row as in Fig. 5. The square lattice case is analogous but local transfer matrices are now defined as operators from $\mathcal{H}_X \otimes \mathcal{H}_X$ to itself from the beginning.

In case of open boundary conditions the row-to-row[6] transfer matrix then reads

$$T_X = \left(\prod_{k=0}^{L-1} t^X_{2k+1}\right)\left(\prod_{k=1}^{L-1} t^X_{2k}\right). \tag{53}$$

It is an endomorphism of $\mathcal{H}_X^{\otimes 2L}$. On appropriate lattices, the partition functions are then recovered as the vacuum expectation values of powers of the transfer matrix:

$$Z_X = \left\langle T_X^M \right\rangle. \tag{54}$$

By the vacuum expectation value, we mean the matrix element from $|\,\rangle^{\otimes 2L}$ to itself. To be precise, the right-hand-side of (54) expresses the partition function Z_X on a hexagonal lattice with $2M-2$ rows, because while T_X^M builds configurations on a lattice with $2M$ rows, the vertices in the first and last row and their adjacent edges are all constrained to be empty due to our choice of vacuum state.

However, when the web model is embedded in the cylinder we need twisted periodic boundary conditions to give the correct weights to webs that wrap the periodic direction [2]. In the A_1 and A_2 cases this is obtained by the action of a twist operator

$$S_X = q^{2H_\rho} \tag{55}$$

leading to the following modified transfer matrix [2]

[5] Remark that t^X corresponds to summing over the state of a vertical link, so that a pair of vertices on $\mathbb{H}$ is effectively transformed into a single vertex on a (tilted) square lattice.

[6] Note that with our definition, the row-to-row transfer matrix propagates states through *two* rows of the lattice.

$$T_X = \left(\prod_{k=0}^{L-1} t^X_{2k+1}\right)\left(\prod_{k=1}^{L-1} t^X_{2k}\right) S_X t^X_{2L} S_X^{-1}\,, \tag{56}$$

where S_X acts non-trivially on site 1 only.

In the G_2 and B_2 cases, the transfer matrix is still given by (56), but the twist operator is now

$$S_X = (-1)^{2H_{\rho^\vee}} q^{2H_\rho} \tag{57}$$

where $\boldsymbol{\rho}$ and $\boldsymbol{\rho}^\vee$ denote the Weyl vector and the dual Weyl vector respectively (see Appendix B).

Remark that the twist operator could also be chosen differently from (55) and (57); see [1]. This is useful in order to define modified partition functions that are lattice analogs of two-point functions of electric operators in Coulomb Gas conformal field theories.

6.1. A reminder on the dilute loop model

Before going on the discussion of web models, let us remind the well known and similar case of the dilute loop model on the hexagonal lattice. The local transfer matrices of the model can be written graphically as

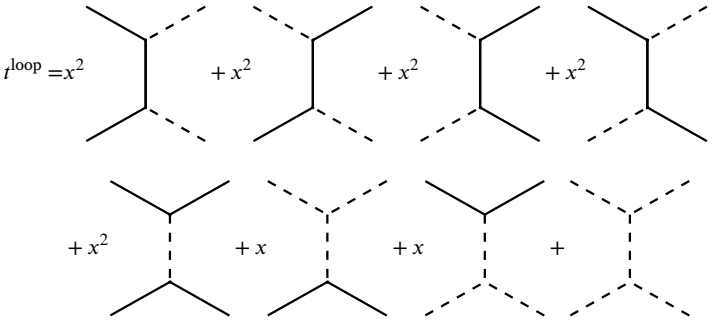

(58)

where the dashed line represents an empty link and x is the bond fugacity, i.e., the local weight assigned to a link covered by a loop.

Each diagram can be understood as an intertwiner of $U_{-q}(A_1)$ representations if we set the loop weight to $[2]_q$. These diagrams are called (dilute) Temperley-Lieb (TL) diagrams. The local space of states of the loop model is given by $\mathcal{H}_{A_1} = \mathbb{C} \oplus V_1$ where V_1 denotes the fundamental representation. Any diagram can be expressed by concatenating vertically and horizontally juxtaposing the following elementary diagrams (and possibly identity strands joining the top and bottom boundaries)

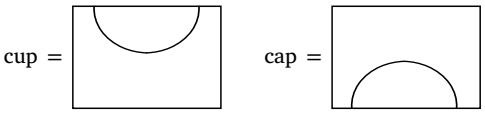

where cup and cap are embedded in the lattice as, respectively, the second- and third-last diagram of (58).

We use a general convention that these 'string' diagrams are read from bottom to top, the strings are labelled by the fundamental representation V_1 and the empty source/target of a diagram corresponds to the trivial representation $\mathbb{C}$. For example, the above cap diagram is an intertwiner $V_1 \otimes V_1 \to \mathbb{C}$ that can be the best described in a basis. Let $\{e_1, e_2\}$ denote the standard basis of V_1, and $\{f_1, f_2\}$ be its dual. Then, the corresponding intertwiners are

$$\begin{aligned} \text{cup}: \quad & \mathbb{C} \to V_1 \otimes V_1 \\ & 1 \mapsto e_1 \otimes e_2 + q^{-1} e_2 \otimes e_1 \\ \text{cap} = \; & q f_1 \otimes f_2 + f_2 \otimes f_1 \end{aligned}$$

where in the last equality we used the obvious identification of $V_1^* \otimes V_1^*$ with the space of linear maps $V_1 \otimes V_1 \to \mathbb{C}$. The maps cup and cap were obtained by calculation of $U_{-q}(A_1)$ invariant vectors in $V_1 \otimes V_1$ and in its dual space. That is, we find a vector annihilated by the action of E and F given by the coproduct (118).

We furthermore remark that the invariant vectors, and thus the corresponding maps, are defined up to a multiplicative constant that can be fixed in the following way. The maps cup and cap are assumed to satisfy the zigzag rules

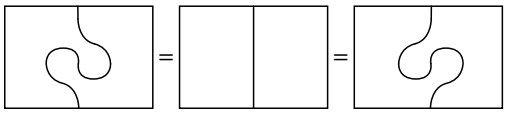

(59)

which reflect the fact that our diagrams are considered up to an isotopy, or equivalently, this is an implication of the Temperley-Lieb relations. These rules reduce the choices of constants to one "gauge" degree of freedom: one may multiply the cup intertwiner by some factor η and the cap intertwiner by η^{-1}. In the expressions above we have chosen a definite value of the gauge factor η.

6.2. The A_2 case

Let V_1 be the fundamental representation of $U_{-q}(A_2)$ of highest weight $\boldsymbol{w_1}$. In V_1, pick a highest weight vector, u_1. Then we obtain a basis $\{u_i, i \in [\![1,3]\!]\}$ by applying lowering operators:

$$u_2 = F_1 u_1 \tag{60a}$$

$$u_3 = F_2 F_1 u_1 \tag{60b}$$

The action of the quantum group generators in our bases is given in appendix D.

Let V_2 be the fundamental representation of $U_{-q}(A_2)$ of highest weight $\boldsymbol{w_2}$. In V_2, pick a highest weight vector, v_1. Then we obtain a basis $\{v_i, i \in [\![1,3]\!]\}$ by applying lowering operators:

$$v_2 = F_2 v_1 \tag{61a}$$

$$v_3 = F_1 F_2 v_1 \tag{61b}$$

Let $\{e_i, i \in [\![1,7]\!]\} = \{u_1, u_2, u_3, v_1, v_2, v_3, 1\}$ be a basis of $\mathcal{H}_{A_2} = V_1 \oplus V_2 \oplus \mathbb{C}$.

Any A_2 web can be expressed as the vertical concatenation and horizontal juxtaposition of the following elementary webs (and possibly identity strands connecting the bottom and top boundaries)

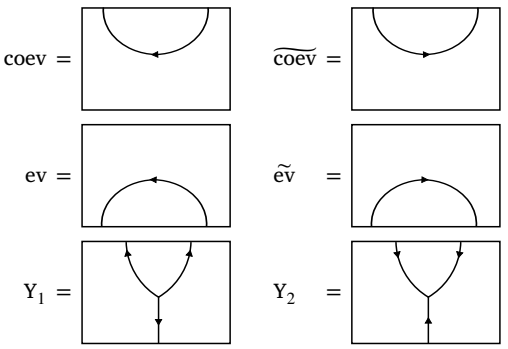

(62)

Here is an illustration on how one can obtain any open web from the above set

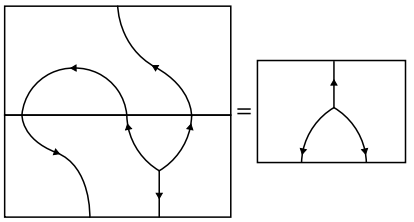

(63)

In the left hand side, the top diagram is a juxtaposition of ev and an identity strand whereas the bottom one is a juxtaposition of an identity strand and Y_1. By concatenating them vertically, we get the web on the right hand side.

These webs represent the following intertwiners:

$$\text{coev}: \quad \mathbb{C} \to V_1 \otimes V_2$$
$$e_7 \mapsto q e_1 \otimes e_6 + e_2 \otimes e_5 + q^{-1} e_3 \otimes e_4$$

$$\widetilde{\text{coev}}: \quad \mathbb{C} \to V_2 \otimes V_1$$
$$e_7 \mapsto q^{-1} e_6 \otimes e_1 + e_5 \otimes e_2 + q e_4 \otimes e_3$$

$$\text{ev} = q^{-1} e_6^* \otimes e_1^* + e_5^* \otimes e_2^* + q e_4^* \otimes e_3^*$$

$$\widetilde{\text{ev}} = q e_1^* \otimes e_6^* + e_2^* \otimes e_5^* + q^{-1} e_3^* \otimes e_4^*$$

$$Y_1: \quad V_2 \to V_1 \otimes V_1$$
$$e_4 \mapsto e_1 \otimes e_2 + q^{-1} e_2 \otimes e_1$$

$$e_5 \mapsto e_1 \otimes e_3 + q^{-1} e_3 \otimes e_1$$
$$e_6 \mapsto e_2 \otimes e_3 + q^{-1} e_3 \otimes e_2$$

$$\mathrm{Y}_2 : \quad V_1 \to V_2 \otimes V_2$$
$$e_1 \mapsto q e_4 \otimes e_5 + e_5 \otimes e_4$$
$$e_2 \mapsto q e_4 \otimes e_6 + e_6 \otimes e_4$$
$$e_3 \mapsto q e_5 \otimes e_6 + e_6 \otimes e_5$$

Horizontal juxtaposition of webs corresponds to taking the tensor product of intertwiners and vertical concatenation corresponds to composition. For instance the web in (63) represents the following intertwiner:

$$\left(\mathrm{ev} \otimes \mathrm{Id}_{V_1}\right) \circ \left(\mathrm{Id}_{V_2} \otimes \mathrm{Y}_1\right)$$

Similarly to the $U_{-q}(A_1)$ case, the maps ev and coev are defined up to multiplicative scalars from an invariant vector in $V_1 \otimes V_2$, i.e. a vector in $V_1 \otimes V_2$ that is annihilated by the action of E_1, E_2, F_1 and F_2 using the coproduct defined in (118) from Appendix C. Similarly, $\widetilde{\mathrm{ev}}$ and $\widetilde{\mathrm{coev}}$ are defined up to multiplicative scalars from an invariant vector in $V_2 \otimes V_1$. The freedom on multiplicative scalars is reduced to one degree of freedom once we impose that the maps satisfy the loop rule as well as the zigzag rules

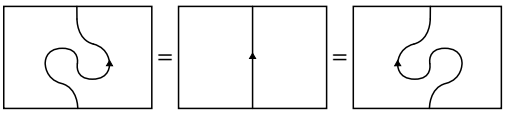

(64)

To construct Y_1, one looks for a highest weight vector v of weight $\boldsymbol{w}_2$ inside $V_1 \otimes V_1$ using the actions of E_1, E_2 determined by the coproduct (118). Note that this specifies v only up to a multiplicative scalar. The map Y_1 is then defined as mapping e_4 to v, e_5 to $F_2 v$ and e_6 to $F_1 F_2 v$ where the actions of F_1, F_2 on $V_1 \otimes V_1$ are again determined by the coproduct. This defines Y_1 up to a multiplicative scalar. Similarly, one defines Y_2 up to a multiplicative scalar. Asking that the maps satisfy the digon and square rules reduce the freedom to one degree of freedom. So, in total we have two free parameters that we have chosen to fix to some values.

The local transfer matrices of the A_2 web model are then given by

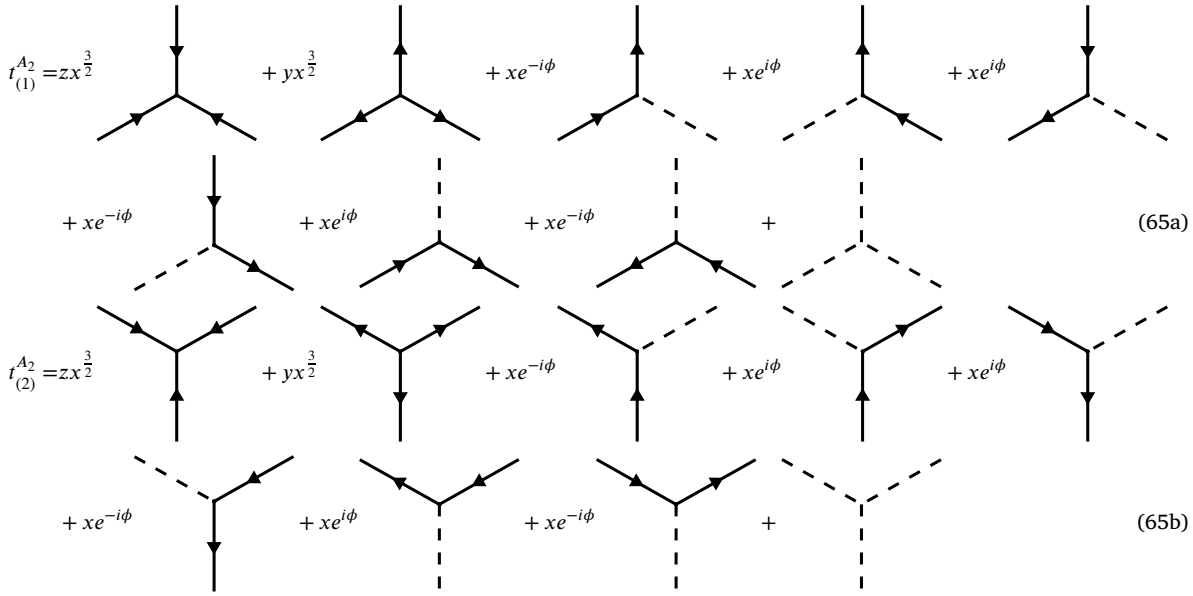

(65a)

(65b)

Above, diagrams must be understood as webs when dashed lines are forgotten. For instance in the expression of $t^{A_2}_{(1)}$, the first term is defined by (63), while the third to the sixth therms are given by identity lines. The seventh and eighth terms are given by ev and $\widetilde{\mathrm{ev}}$ respectively, and the ninth one is the empty web, i.e., the identity on the trivial representation $\mathbb{C}$.

6.3. The G_2 case

Let V be the fundamental representation of $U_q(G_2)$ of highest weight $\boldsymbol{w}_1$. In V, pick a highest weight vector, e_1. Then we obtain a basis $\{e_i, i \in [\![1,7]\!]\}$ by applying lowering operators:

$$e_2 = F_1 e_1 \qquad e_3 = F_2 F_1 e_1$$
$$e_4 = F_1 F_2 F_1 e_1 \qquad e_5 = F_1^2 F_2 F_1 e_1$$
$$e_6 = F_2 F_1^2 F_2 F_1 e_1 \qquad e_7 = F_1 F_2 F_1^2 F_2 F_1 e_1$$

Denote by $\{f_i, i \in [\![1,7]\!]\}$, the dual basis in V^*. Any G_2 web can be expressed as the vertical concatenation and horizontal juxtaposition of the following elementary webs (and possibly identity strands)

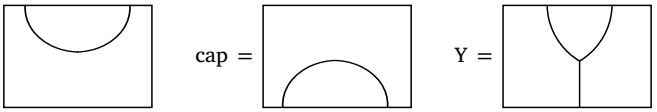

(66)

These webs represent the following intertwiners:

$$\text{cup} : \mathbb{C} \to V \otimes V$$
$$1 \mapsto e_7 \otimes e_1 + q^{10} e_1 \otimes e_7 - q e_6 \otimes e_2 - q^9 e_2 \otimes e_6 + q^4 e_5 \otimes e_3 + q^6 e_3 \otimes e_5 - q^6 e_4 \otimes e_4$$

$$\text{cap} = q^{-10} f_7 \otimes f_1 + f_1 \otimes f_7 - q^{-9} f_6 \otimes f_2 - q^{-1} f_2 \otimes f_6 + q^{-6} f_5 \otimes f_3 + q^{-4} f_3 \otimes f_5 - q^{-6} f_4 \otimes f_4$$
$$\text{Y} : V \to V \otimes V$$

$$e_1 \mapsto q^6 e_1 \otimes e_4 - e_4 \otimes e_1 - [2]_q q^4 e_2 \otimes e_3 + [2]_q q e_3 \otimes e_2$$
$$e_2 \mapsto -q^4 e_2 \otimes e_4 + q^2 e_4 \otimes e_2 + q^5 e_1 \otimes e_5 - e_5 \otimes e_1$$
$$e_3 \mapsto -q^4 e_3 \otimes e_4 + q^2 e_4 \otimes e_3 + q^5 e_1 \otimes e_6 - e_6 \otimes e_1$$
$$e_4 \mapsto (q^2 - q^4) e_4 \otimes e_4 - q^2 e_3 \otimes e_5 + q^2 e_5 \otimes e_3$$
$$+ q^5 e_2 \otimes e_6 - q^{-1} e_6 \otimes e_2 + q^4 e_1 \otimes e_7 - e_7 \otimes e_1$$
$$e_5 \mapsto q^2 e_5 \otimes e_4 - q^4 e_4 \otimes e_5 + [2]_q q^5 e_2 \otimes e_7 - [2]_q e_7 \otimes e_2$$
$$e_6 \mapsto q^2 e_6 \otimes e_4 - q^4 e_4 \otimes e_6 + [2]_q q^5 e_3 \otimes e_7 - [2]_q e_7 \otimes e_3$$
$$e_7 \mapsto -e_7 \otimes e_4 + q^6 e_4 \otimes e_7 + q e_6 \otimes e_5 - q^4 e_5 \otimes e_6$$

Horizontal juxtaposition of webs corresponds to taking the tensor product of intertwiners and vertical concatenation corresponds to composition. The above maps were obtained similarly as in the A_2 case.

The local transfer matrices of the G_2 web model are then given by

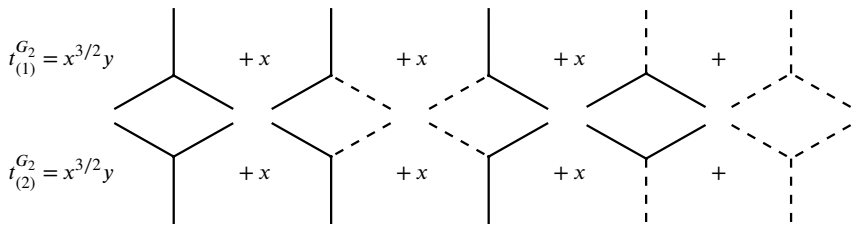

(67a)

(67b)

6.4. The B_2 case

Let V_1 and V_2 be the fundamental representations of $U_q(B_2)$ of highest weights $\boldsymbol{w_1}$ and $\boldsymbol{w}_2$ respectively. In V_1, pick a highest weight vector, e_1. Then we obtain a basis $\{e_i, i \in [\![1,4]\!]\}$ by applying lowering operators:

$$e_2 = F_1 e_1 \tag{68a}$$
$$e_3 = F_2 F_1 e_1 \tag{68b}$$
$$e_4 = F_1 F_2 F_1 e_1 \tag{68c}$$

Denote by $\{f_i, i \in [\![1,4]\!]\}$, the dual basis in V_1^*.

In V_2, pick a highest weight vector, v_1. Then we obtain a basis $\{v_i, i \in [\![1,5]\!]\}$ by applying lowering operators:

$$v_2 = F_2 v_1 \tag{69a}$$
$$v_3 = F_1 F_2 v_1 \tag{69b}$$

$$v_4 = F_1^2 F_2 v_1 \tag{69c}$$

$$v_5 = F_2 F_1^2 F_2 v_1 \tag{69d}$$

Denote by $\{g_i, i \in [\![1,5]\!]\}$, the dual basis in V_2^*.

Any B_2 web can be expressed as the vertical concatenation and horizontal juxtaposition of the following elementary webs (and possibly identity strands)

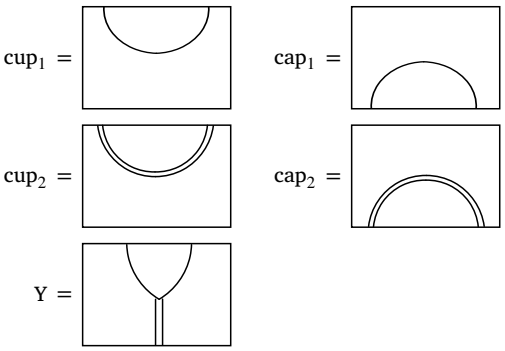

(70)

These webs represent the following intertwiners:

$$\begin{aligned}
\mathrm{cup}_1 &: \mathbb{C} \to V \otimes V \\
&1 \mapsto e_4 \otimes e_1 - q^4 e_1 \otimes e_4 - q e_3 \otimes e_2 + q^3 e_2 \otimes e_3
\end{aligned}$$

$$\mathrm{cap}_1 = f_1 \otimes f_4 - q^{-4} f_4 \otimes f_1 - q^{-1} f_2 \otimes f_3 + q^{-3} f_3 \otimes f_2$$

$$\begin{aligned}
\mathrm{cup}_2 &: \mathbb{C} \to V \otimes V \\
&1 \mapsto v_5 \otimes v_1 + q^6 v_1 \otimes v_5 - q^2 v_4 \otimes v_2 - q^4 v_2 \otimes v_4 + q^4 v_3 \otimes v_3
\end{aligned}$$

$$\mathrm{cap}_2 = g_1 \otimes g_5 + q^{-6} g_5 \otimes g_1 - q^{-2} g_2 \otimes g_4 - q^{-4} g_4 \otimes g_2 + q^{-4} g_3 \otimes g_3$$

$$\begin{aligned}
\mathrm{Y} &: V_2 \to V_1 \otimes V_1 \\
&v_1 \mapsto iq e_1 \otimes e_2 - i e_2 \otimes e_1 \\
&v_2 \mapsto iq e_1 \otimes e_3 - i e_3 \otimes e_1 \\
&v_3 \mapsto iq e_2 \otimes e_3 - iq^{-1} e_3 \otimes e_2 + i e_1 \otimes e_4 - i e_4 \otimes e_1 \\
&v_4 \mapsto i[2]_q q e_2 \otimes e_4 - i[2]_q e_4 \otimes e_2 \\
&v_5 \mapsto i[2]_q q e_3 \otimes e_4 - i[2]_q e_4 \otimes e_3
\end{aligned}$$

Horizontal juxtaposition of webs corresponds to taking the tensor product of intertwiners and vertical concatenation corresponds to composition. The above maps were obtained similarly as in the A_2 case.

The local transfer matrices of the B_2 web model are then given by

$$\begin{aligned}
t^{B_2}_{(1)} = {} & x_{t;1} x_{v;2}^{1/2} y + x_{t;1}^{1/2} x_{v;1}^{1/2} x_{t;2}^{1/2} y + x_{t;1}^{1/2} x_{v;1}^{1/2} x_{t;2}^{1/2} y \\
& + + x_{t;2}^{1/2} x_{v;2}^{1/2} + x_{t;2}^{1/2} x_{v;2}^{1/2} + x_{t;2} \\
& + x_{t;1}^{1/2} x_{v;1}^{1/2} + x_{t;1}^{1/2} x_{v;1}^{1/2} + x_{t;1} +
\end{aligned} \tag{71a}$$

Table 1
Big and small quantum groups.

Case	$U_t(\tilde{X})$	$U_q(X)$	$\tilde{X}$, X
1	$U_t(A_2^{(2)})$	$U_{t^4}(A_1)$	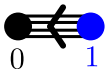
2	$U_t(G_2^{(1)})$	$U_{t^3}(A_2)$	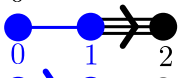
3	$U_t(D_4^{(3)})$	$U_t(G_2)$	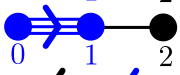
4	$U_t(A_4^{(2)})$	$U_{t^2}(B_2)$	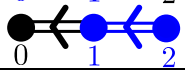

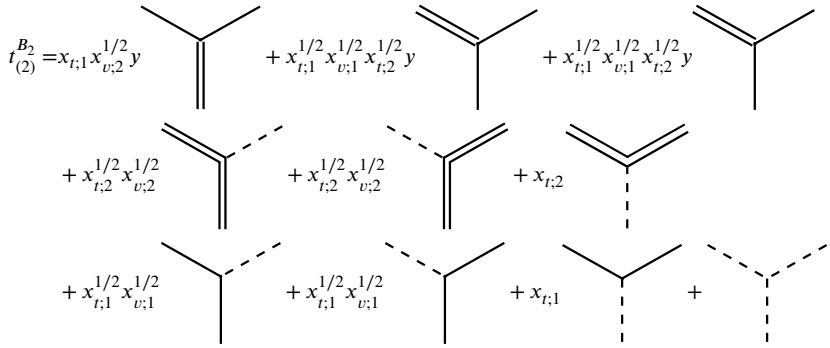

(71b)

The local transfer matrices for the square lattice case can be defined analogously. That is, they are linear operators in $\mathrm{End}(\mathcal{H}_X \otimes \mathcal{H}_X)$ given by the linear combination of diagrams (and their reflections and rotations) from below (36) weighted by the corresponding factors b_i's. Each diagram is again understood as a linear operator.

7. Integrability

In this section, we exhibit integrable manifolds in the parameter spaces of web models. Let us first give the steps of the general strategy we follow.

- First, we look for an affine Dynkin diagram $\tilde{X}$ that reduces to the finite type Dynkin diagram X when we erase one of its nodes n_0. This implies that the Hopf subalgebra $U_t(\tilde{X})$ generated by the Chevalley generators E_i, F_i, H_i, $i \neq n_0$ is isomorphic to $U_q(X)$ for some $q(t)$. We will call $U_t(\tilde{X})$ and $U_q(X)$ the "big" and "small" quantum groups respectively.[7]
  Here we list the big and small quantum groups we will consider[8]:
  The definitions of these quantum groups are recalled in Appendix C, with the corresponding Cartan matrices given in Appendix B.
- We then look for an irreducible "evaluation"[9] representation V_u, $u \in \mathbb{C}^*$ of $U_t(\tilde{X})$ that decomposes under the subalgebra $U_q(X)$ as the local space of states $\mathcal{H}_X$, independently of the evaluation, or spectral, parameter u. We will denote the representation map $\rho_u : U_t(\tilde{X}) \to \mathrm{End}(V_u)$.
- We then follow Jimbo's strategy [34] to find a solution of the spectral parameter dependant Yang Baxter equation. Let us recall it. Suppose that the tensor product $\rho_u \otimes \rho_v$, $u, v \in \mathbb{C}^*$ is irreducible. We are looking for an operator $\check{R}(u,v)$ intertwining $\rho_u \otimes \rho_v$ and $\rho_v \otimes \rho_u$, i.e.

$$\check{R}(u,v)(\rho_u \otimes \rho_v)(a) = (\rho_v \otimes \rho_u)(a)\check{R}(u,v), \quad a \in U_t(\tilde{X}) \tag{72}$$

  Because $\rho_u \otimes \rho_v$ is irreducible, if (72) admits a non-zero solution, it is unique up to a multiplicative constant. Moreover, since $U_t(\tilde{X})$ has a universal R matrix [35,36], it follows that $\check{R}(u,v)$ is non-zero and satisfies the spectral parameter dependent Yang-Baxter equation:

$$\check{R}_{23}(u,v)\check{R}_{12}(u,w)\check{R}_{23}(v,w) = \check{R}_{12}(v,w)\check{R}_{23}(u,w)\check{R}_{12}(u,v) \quad \text{on } V_u \otimes V_v \otimes V_w \tag{73}$$

  where the subscript in $\check{R}_{ij}$ indicates that it acts as $\check{R}$ on the ith and jth tensor factors and as identity elsewhere.

[7] It should not be confused with Lusztig's small quantum group, defined at roots of unity.
[8] Given X, there might be several choices for $\tilde{X}$ and n_0. For instance, if $X = B_2$, $\tilde{X} = A_4^{(2)}$, then $n_0 = 0$ and $n_0 = 2$ are both valid. The second step actually fixes such choices.
[9] Strictly speaking, evaluation representations might not exist because the evaluation morphism on the quantum group level exists for A_n types only.

In order to find $\check{R}(u,v)$, we first notice that, under the small quantum group

$$V_u \otimes V_v \cong V_v \otimes V_u \cong \mathcal{H}_X \otimes \mathcal{H}_X$$

Thus, we can expand $\check{R}(u,v)$ as a sum of intertwiners of $U_q(X)$ from $\mathcal{H}_X \otimes \mathcal{H}_X$ to itself

$$\check{R}(u,v) = \sum_i a_i(u,v) W_i \tag{74}$$

where the sum is taken over an index set of the web basis $\{W_i\}$ of $\mathrm{End}_{U_q(X)}(\mathcal{H}_X \otimes \mathcal{H}_X)$ and $a_i(u,v)$ are unknown functions. The system (72) is then reduced to a system of linear equations on the unknowns $a_i(u,v)$

$$\check{R}(u,v)(\rho_u \otimes \rho_v)(a) = (\rho_v \otimes \rho_u)(a)\check{R}(u,v), \quad a = E_{n_0}, F_{n_0} \tag{75}$$

which is much simpler to solve than the cubic Yang-Baxter equations (73).
In the case the representation $\mathcal{H}_X$ of the small quantum group $U_q(X)$ is irreducible and $\mathcal{H}_X \otimes \mathcal{H}_X$ is a direct sum of irreducible representations of multiplicity 1, techniques have been developed to solve (72) [37–39]. However, this is not our case because $\mathcal{H}_X$ is reducible and multiplicities are sometimes higher than 1. Instead, we solve the linear system (75) directly by using software.

- Finally, we identify values (u_0, v_0) of the spectral parameters (u,v) such that

$$a_i(u_0, v_0) = 0$$

for all i corresponding to webs W_i that do not appear in the local transfer matrix of the given web model. We then reach the local transfer matrix by making a gauge transformation

$$t^X_{(2)} t^X_{(1)} = \left(D_2^{-1} \otimes D_1^{-1}\right) \check{R}(u_0, v_0) \left(D_1 \otimes D_2\right)$$

for some diagonal matrices D_1 and D_2 commuting with $U_q(X)$ on $\mathcal{H}_X$.

In the case of A_2 and G_2, the evaluation representations we consider were previously studied in a different context [25,26]. They are given respectively in appendices D.1.2 and D.2.2. However, in the case of B_2, the two evaluation representations of $U_t(A_4^{(2)})$ defined in D.3.2 and D.3.3 are new to the best of our knowledge.

7.1. A reminder on the dilute loop model

Consider the quantum affine algebra $U_t(A_2^{(2)})$ (see Appendix C for definitions) with Cartan matrix

$$\begin{pmatrix} 2 & -4 \\ -1 & 2 \end{pmatrix}$$

There is a 3-dimensional evaluation representation V_u given by the following matrices in the basis $\{1, e_1, e_2\}$, where $\{1\}$ (respectively $\{e_1, e_2\}$) denotes the basis of the trivial (respectively fundamental) representation of $U_{-q}(A_1)$

$$E_0 = u\begin{bmatrix} 0 & \sqrt{[2]_t} & 0 \\ 0 & 0 & 0 \\ \sqrt{[2]_t} & 0 & 0 \end{bmatrix} \qquad E_1 = \begin{bmatrix} 0 & 0 & 0 \\ 0 & 0 & 1 \\ 0 & 0 & 0 \end{bmatrix}$$

$$F_0 = \frac{1}{u}\begin{bmatrix} 0 & 0 & \sqrt{[2]_t} \\ \sqrt{[2]_t} & 0 & 0 \\ 0 & 0 & 0 \end{bmatrix} \qquad F_1 = \begin{bmatrix} 0 & 0 & 0 \\ 0 & 0 & 0 \\ 0 & 1 & 0 \end{bmatrix}$$

$$H_0 = \begin{bmatrix} 0 & 0 & 0 \\ 0 & -2 & 0 \\ 0 & 0 & 2 \end{bmatrix} \qquad H_1 = \begin{bmatrix} 0 & 0 & 0 \\ 0 & 1 & 0 \\ 0 & 0 & -1 \end{bmatrix}$$

$U_t(A_2^{(2)})$ contains a $U_{t^4}(A_1)$ Hopf subalgebra generated by E_1, F_1 and H_1. Setting $q = -t^4$, we have that $V_u = \mathbb{C} \oplus V_1$ as representations of this $U_{t^4}(A_1)$ subalgebra. We can write a basis of $\mathrm{End}_{U_{t^4}(A_1)}\left((\mathbb{C} \oplus V_1)^2\right)$ in terms of the TL diagrams defined above. The R-matrix can then be decomposed as

$\check{R}(u,v) = a_1(u,v)$ $+ a_2(u,v)$ $+ a_3(u,v)$

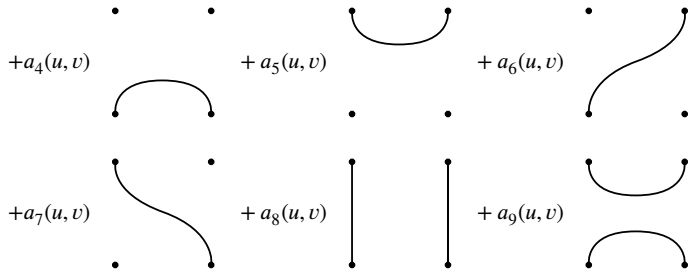

(76)

Asking that the R-matrix commute with the 0th labelled generators gives a system of linear equations for the coefficients $a_i(u,v)$. From the spectral parameter dependence of the representatives of the 0th labelled generators, we see that the coefficients depend only on the ratio $s=\frac{u}{v}$ and we write $a_i(u,v)=a_i(s)$. The unique solution, up to a multiplicative constant, is given by

$$a_1(s) = t^8 - t^2 s^4 + (t-1)(t+1)\left(t^8 - t^4 + 1\right) s^2 \tag{77a}$$
$$a_2(s) = \left(t^4 - 1\right) s \left(t^6 + s^2\right) \tag{77b}$$
$$a_3(s) = \left(t^4 - 1\right) s \left(t^6 + s^2\right) \tag{77c}$$
$$a_4(s) = t^2 \left(t^4 - 1\right) s \left(s^2 - 1\right) \tag{77d}$$
$$a_5(s) = -t^4 \left(t^4 - 1\right) s \left(s^2 - 1\right) \tag{77e}$$
$$a_6(s) = -t^2 \left(s^2 - 1\right) \left(t^6 + s^2\right) \tag{77f}$$
$$a_7(s) = -t^2 \left(s^2 - 1\right) \left(t^6 + s^2\right) \tag{77g}$$
$$a_8(s) = \left(t^4 - s^2\right) \left(t^6 + s^2\right) \tag{77h}$$
$$a_9(s) = -t^4 \left(s^2 - 1\right) \left(t^2 + s^2\right) \tag{77i}$$

It was originally found in [23].

We see that, if we want to recover (58), we need to tune the spectral parameter such that $a_8(s)=0$ and $a_i(s)\neq 0$ for $i\neq 8$. This happens for $s=-t^2$. Then, by renormalising the R matrix and taking the following gauge transformation

$$D = \mathrm{Diag}(1,\alpha,\alpha)$$
$$\check{R}(s) \mapsto \left(D^{-1}\otimes D^{-1}\right)\check{R}(s)(D\otimes D) \tag{78}$$

for well chosen α, we recover (58) with

$$q = -e^{4i\psi} \tag{79a}$$
$$x = \frac{1}{2\sin(\psi)} \tag{79b}$$

Remark that, after a gauge transformation, the R-matrix still satisfies the Yang-Baxter equation. The gauge transformation is equivalent to the choice of multiplicative constant in defining the cup and cap maps.

In the next sections, we will employ the same strategy for the rank 2 web models.

7.2. The A_2 web model

We now consider the second line of the Table 1. Let V_u, $u\in\mathbb{C}^*$, be the representation of $U_t(G_2^{(1)})$ given in Appendix D.1.2 which is actually isomorphic to the one considered in [25]. We are looking for an operator $\check{R}(u,v)$ intertwining $V_u\otimes V_v$ and $V_v\otimes V_u$. Remark that, in $U_t(G_2^{(1)})$, E_i, F_i and H_i for $i=0,1$ generate a Hopf subalgebra isomorphic to $U_{t^3}(A_2)$. Under the action of this subalgebra, V_u decomposes as:

$$V_u = V_1 \oplus V_2 \oplus \mathbb{C} \tag{80}$$

which can be seen from the explicit matrix expressions given in section D.1.1 after some relabelling of the nodes in the Dynkin diagram.

Hence $\check{R}(u,v)$ will decompose as a sum of $U_{t^3}(A_2)$ intertwiners:

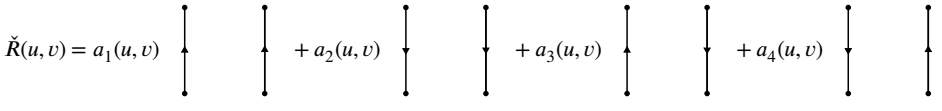

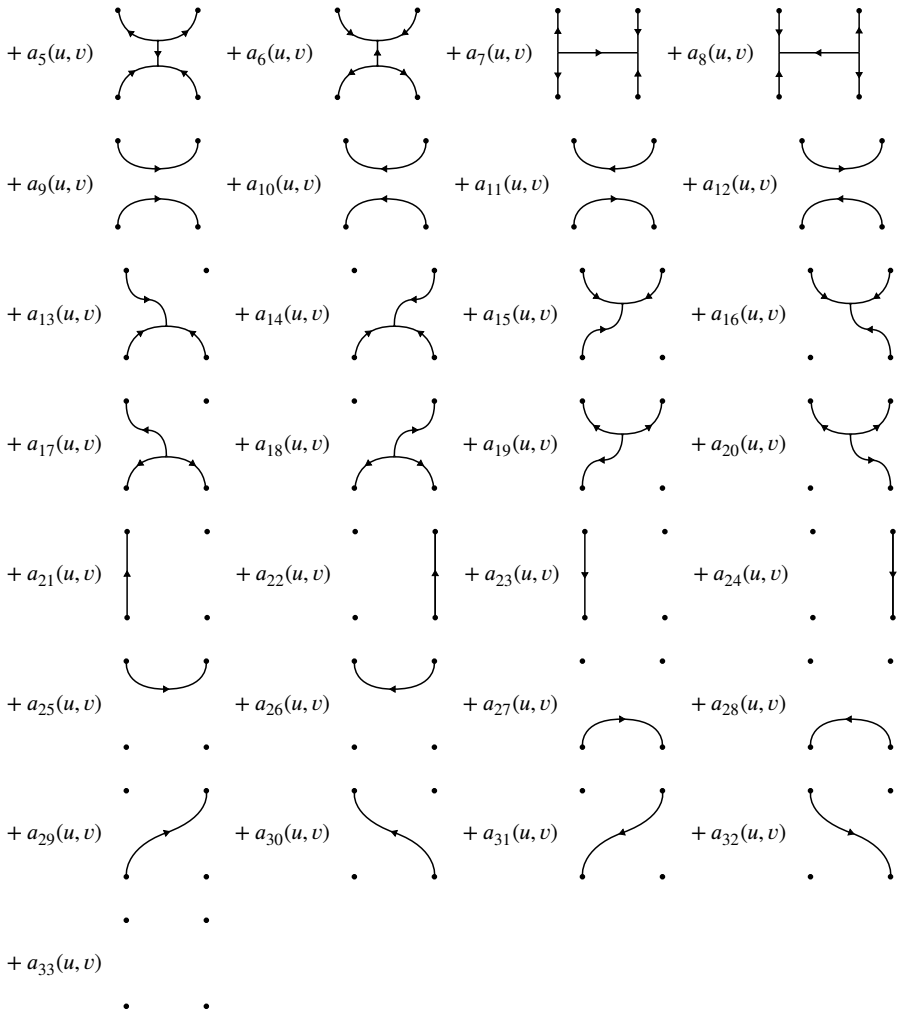

(81)

where $a_i(u,v)$ are some coefficients and the corresponding webs span the space of intertwiners $\mathrm{End}_{U_{t^3}(A_2)}\left((V_1 \oplus V_2 \oplus \mathbb{C})^2\right)$. Indeed, elements of the latter are in bijection with invariants of $(V_1 \oplus V_2 \oplus \mathbb{C})^4$, so upon expanding we get products of V_1 and V_2 of length 0 up to 4. Invariants on these spaces were classified by Kuperbergs [3], our webs are basis elements of them.

Asking for $\check{R}(u,v)$ to commute with the remaining generators of $U_t(G_2^{(1)})$, we see that it may depend only on the ratio $s = \frac{u}{v}$. We find

$$a_1(s) = -\frac{\left(t^2-s^3\right)\left(t^8-s^3\right)}{t^2\sqrt{\frac{1}{t}+t}\left(-1+t^2\right)s^2\left(-1+s^3\right)} \qquad a_2(s) = -\frac{\left(t^2-s^3\right)\left(t^8-s^3\right)}{t^2\sqrt{\frac{1}{t}+t}\left(-1+t^2\right)s^2\left(-1+s^3\right)}$$

$$a_3(s) = \frac{-t^8+s^3}{t^2\sqrt{\frac{1}{t}+t}\left(-1+s^3\right)} \qquad a_4(s) = \frac{-t^8+s^3}{t^2\sqrt{\frac{1}{t}+t}\left(-1+s^3\right)}$$

$$a_5(s) = \frac{\sqrt{\frac{1}{t}+t}\left(t^6-t^2s^3\right)}{\left(-1+t^4\right)s^2} \qquad a_6(s) = \frac{\sqrt{\frac{1}{t}+t}\left(t^6-t^2s^3\right)}{\left(-1+t^4\right)s^2}$$

$$a_7(s) = \frac{\sqrt{\frac{1}{t}+t}\left(t^8-s^3\right)}{\left(-1+t^4\right)s^2} \qquad a_8(s) = \frac{\sqrt{\frac{1}{t}+t}\left(t^8-s^3\right)}{\left(-1+t^4\right)s^2}$$

$$a_9(s) = \frac{t^2\left(t^4-s^3\right)\left(t^{10}-s^3\right)}{\sqrt{\frac{1}{t}+t}\left(-1+t^2\right)s^2\left(t^{12}-s^3\right)} \qquad a_{10}(s) = \frac{t^2\left(t^4-s^3\right)\left(t^{10}-s^3\right)}{\sqrt{\frac{1}{t}+t}\left(-1+t^2\right)s^2\left(t^{12}-s^3\right)}$$

$$a_{11}(s) = \frac{t^8\left(-t^4+s^3\right)}{\sqrt{\frac{1}{t}+t}\left(t^{12}-s^3\right)} \qquad a_{12}(s) = \frac{t^4\left(-t^4+s^3\right)}{\sqrt{\frac{1}{t}+t}\left(t^{12}-s^3\right)}$$

$$a_{13}(s)=1 \qquad a_{14}(s)=\frac{-t^2}{s}$$

$$a_{15}(s)=\frac{-t}{s} \qquad a_{16}(s)=\frac{1}{t}$$

$$a_{17}(s)=\frac{t^5}{s} \qquad a_{18}(s)=-t^3$$

$$a_{19}(s)=-t^2 \qquad a_{20}(s)=\frac{t^4}{s}$$

$$a_{21}(s)=\frac{\sqrt{\frac{1}{t}+t}\left(-t^2+t^4-t^6+s^3\right)}{t\left(-1+s^3\right)} \qquad a_{22}(s)=\frac{-t^8+s^3+t^6\left(-1+s^3\right)}{t^2\sqrt{\frac{1}{t}+ts}\left(-1+s^3\right)}$$

$$a_{23}(s)=\frac{-t^8+s^3+t^6\left(-1+s^3\right)}{t^2\sqrt{\frac{1}{t}+ts}\left(-1+s^3\right)} \qquad a_{24}(s)=\frac{\sqrt{\frac{1}{t}+t}\left(-t^2+t^4-t^6+s^3\right)}{t\left(-1+s^3\right)}$$

$$a_{25}(s)=\frac{-t^{11}(1+t^2)+t(1+t^6)s^3}{\sqrt{\frac{1}{t}+ts}(t^{12}-s^3)} \qquad a_{26}(s)=\frac{t^2\sqrt{\frac{1}{t}+t}(-t^6+t^8-t^{10}+s^3)}{t^{12}-s^3}$$

$$a_{27}(s)=\frac{t^4\sqrt{\frac{1}{t}+t}(-t^6+t^8-t^{10}+s^3)}{t^{12}-s^3} \qquad a_{28}(s)=\frac{-t^{13}(1+t^2)+t^3(1+t^6)s^3}{\sqrt{\frac{1}{t}+ts}(t^{12}-s^3)}$$

$$a_{29}(s)=\frac{t^6-s^3}{\sqrt{\frac{1}{t}+t}(-1+t^2)s^2} \qquad a_{30}(s)=\frac{t^6-s^3}{\sqrt{\frac{1}{t}+t}(-1+t^2)s^2}$$

$$a_{31}(s)=\frac{t^6-s^3}{\sqrt{\frac{1}{t}+t}(-1+t^2)s^2} \qquad a_{32}(s)=\frac{t^6-s^3}{\sqrt{\frac{1}{t}+t}(-1+t^2)s^2}$$

$$a_{33}(s)=-\frac{\left(t^2-s\right)\left(t^4+t^2s+s^2\right)\left(t^2\left(t^{12}+\left(t^{14}-2t^{12}+t^8-2t^6+t^4-2\right)s^3+s^6\right)+s^3\right)}{t^2\sqrt{t+\frac{1}{t}}\left(t^2-1\right)s^2\left(s^3-1\right)\left(t^{12}-s^3\right)}$$

by plugging the linear system for the functions $a_i(s)$ into MATHEMATICA (or some other formal calculus software). One can then show, again using MATHEMATICA, that the corresponding operator $\check{R}(s)$ satisfies the multiplicative spectral-parameter dependant Yang-Baxter equation.

We can obtain a manifestly PT-invariant R-matrix[10] by using the following gauge transformation

$$D=\mathrm{Diag}(\alpha,\alpha,\alpha,\beta,\beta,\beta,1)$$
$$\check{R}(s)\to\left(D^{-1}\otimes D^{-1}\right)\check{R}(s)\left(D\otimes D\right) \tag{82}$$

The form of D corresponds to rescaling subrepresentations of V in (80) independently. Renormalising the R-matrix, we obtain

$$a_1(s)=a_2(s)=-\frac{\left(t^2-s^3\right)\left(t^8-s^3\right)}{t\left(t^2-1\right)s^2\left(s^3-1\right)}$$

$$a_3(s)=\frac{t^8-s^3}{ts-ts^4}$$

$$a_4(s)=s\frac{t^8-s^3}{ts-ts^4}$$

$$a_5(s)=a_6(s)=\frac{t^6-t^2s^3}{\left(t^2-1\right)s^2}$$

$$a_7(s)=a_8(s)=\frac{t^8-s^3}{\left(t^2-1\right)s^2}$$

$$a_9(s)=a_{10}(s)=\frac{t^3\left(t^4-s^3\right)\left(t^{10}-s^3\right)}{\left(t^2-1\right)s^2\left(t^{12}-s^3\right)}$$

[10] We here understand PT-symmetry as the invariance under the rotation of the diagrams through an angle π.

$$a_{11}(s) = t^9 \frac{t^4 - s^3}{s^4 - t^{12} s}$$

$$a_{12}(s) = t^5 s \frac{t^4 - s^3}{s^4 - t^{12} s}$$

$$a_{13}(s) = a_{16}(s) = a_{18}(s) = a_{19}(s) = -it^2 \sqrt{t + \frac{1}{t}}$$

$$a_{14}(s) = a_{15}(s) = a_{17}(s) = a_{20}(s) = \frac{it^4 \sqrt{t + \frac{1}{t}}}{s}$$

$$a_{21}(s) = a_{24}(s) = \frac{-t^8 + t^2 \left(s^3 - 1\right) + s^3}{t \left(s^3 - 1\right)}$$

$$a_{22}(s) = a_{23}(s) = \frac{t^8 - \left(t^6 + 1\right) s^3 + t^6}{t \left(s - s^4\right)}$$

$$a_{25}(s) = a_{28}(s) = \frac{t^3 \left(t^{12} + t^{10} - \left(t^6 + 1\right) s^3\right)}{s^4 - t^{12} s}$$

$$a_{26}(s) = a_{27}(s) = \frac{t^3 \left(\left(t^2 + 1\right) s^3 - t^6 \left(t^6 + 1\right)\right)}{t^{12} - s^3}$$

$$a_{29}(s) = a_{30}(s) = a_{31}(s) = a_{32}(s) = \frac{t \left(t^6 - s^3\right)}{\left(t^2 - 1\right) s^2}$$

$$a_{33}(s) = -\frac{\left(t^2 - s\right) \left(t^4 + t^2 s + s^2\right) \left(t^2 \left(t^{12} + \left(t^{14} - 2t^{12} + t^8 - 2t^6 + t^4 - 2\right) s^3 + s^6\right) + s^3\right)}{t \left(t^2 - 1\right) s^2 \left(s^3 - 1\right) \left(t^{12} - s^3\right)}$$

It is apparent that by setting the spectral parameter $s = t^{\frac{8}{3}}$, $\check{R}(s)$ will be decomposed only in terms of webs appearing in the local transfer matrix of the A_2 web model. In order to put it in the form of (65), we renormalise the PT-invariant R-matrix so as to recover the local transfer matrix (65) with the following parametrisation, setting $t = e^{i\psi}$:

$$q = -e^{3i\psi} \tag{83a}$$

$$x = \frac{1}{2\sin(\psi)} \tag{83b}$$

$$y = z = \sqrt{2\sin(2\psi)} \tag{83c}$$

$$e^{i\phi} = i e^{i\frac{\psi}{3}} \tag{83d}$$

Remark that points related by $\psi \to \pi - \psi$ satisfy

$$q \to -q^{-1} \tag{84a}$$

$$x \to x \tag{84b}$$

$$y \to iy \tag{84c}$$

$$z \to iz \tag{84d}$$

$$e^{i\phi} \to e^{-i\phi} \tau \tag{84e}$$

with $\tau^3 = 1$. Moreover the points related by $\psi \to -\psi$ satisfy

$$q \to q^{-1} \tag{85a}$$

$$x \to -x \tag{85b}$$

$$y \to iy \tag{85c}$$

$$z \to iz \tag{85d}$$

$$e^{i\phi} \to -e^{-i\phi} \tau \tag{85e}$$

These transformations are combinations of the symmetries mentioned in section 3.2. They imply that it suffices to focus on the interval $\psi \in [0, \frac{\pi}{2}]$.

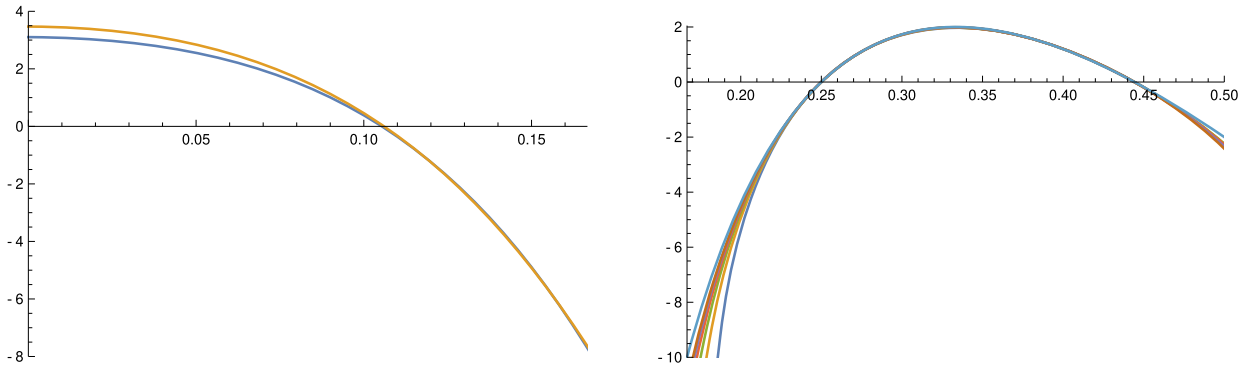

Fig. 6. Two-point fits $c_L(\psi)$ for the central charge in the A_2 web model, plotted against $\frac{\psi}{\pi}$. Regime 2 (left panel) is for $\psi \in [0, \frac{\pi}{6}[$, using sizes $\{L, L-3\}$ with $L=6$ (dark blue) and $L=9$ (orange). Regime 1 (right panel) is for $\psi \in]\frac{\pi}{6}, \frac{\pi}{2}]$, using sizes $\{L, L-1\}$ with $L=4,5,\dots,9$. The smallest size corresponds to the lowest curve (dark blue). The topmost curve (light blue) is the exact analytical result.

7.2.1. Central charge and phase diagram

We have numerically diagonalised the transfer matrix for cylinders of circumference of sizes $L=3,4,\dots,9$. Estimates c_L for the central charge can then be extracted from the finite-size scaling of the largest eigenvalue for two different sizes. The computations were made for 100 equally-spaced values of $\psi \in [0, \frac{\pi}{2}]$, and we show here the curves $c_L(\psi)$ obtained by applying MATHEMATICA's interpolation function to these values.

As shown in Fig. 6 we find two different regimes, defined as follows:

$$\begin{aligned} &\text{Regime 1:} \quad \psi \in]\tfrac{\pi}{6}, \tfrac{\pi}{2}]\,, \\ &\text{Regime 2:} \quad \psi \in [0, \tfrac{\pi}{6}]\,. \end{aligned} \tag{86}$$

The central charge throughout Regime 1 is shown in the right panel of the figure. A Coulomb gas computation, which will be published elsewhere [28], gives the exact result

$$c(\psi) = 2 - 24\frac{(1-g)^2}{g}\,, \qquad g = \frac{3\psi}{\pi}\,, \tag{87}$$

where g is the Coulomb gas coupling constant. The agreement between the numerical values $c_L(\psi)$ and the analytical result $c(\psi)$ is seen to be excellent.

We define two distinct phases inside Regime 1:

$$\begin{aligned} &\text{Dense phase:} \quad \psi \in]\tfrac{\pi}{6}, \tfrac{\pi}{3}]\,, \quad \tfrac{1}{2} < g \le 1\,, \\ &\text{Dilute phase:} \quad \psi \in [\tfrac{\pi}{3}, \tfrac{\pi}{2}]\,, \quad 1 \le g \le \tfrac{3}{2}\,. \end{aligned} \tag{88}$$

The physical motivation for the names *dense* and *dilute* comes from properties of the full phase diagram in the two-dimensional space of bond and vertex fugacities (x and $y=z$ respectively), for a fixed value of ψ (or q). This is discussed in more detail in [2], but we recall here the salient features. Starting from the trivial empty phase, upon increasing the density of bonds and vertices one first hits a critical line—a one-dimensional critical sub-manifold of the parameter space—on which the model is in the dilute universality class. The fraction of links which are covered by a bond is zero. The whole dilute critical line is governed by an attractive renormalisation-group fixed point. We believe that the integrable point in the dilute phase—which, we recall, is for the A_2 model modified by the inclusion of bending weights, but we think that bending is unlikely to change the critical behaviour—is in the same universality class as this dilute fixed point. Increasing further the density of bonds and vertices one enters a critical region—a two-dimensional critical sub-manifold of the parameter space—throughout which the model is in the dense universality class. The fraction of links which are covered by a bond is now finite, and the whole critical region is governed by a certain fixed point. We believe that the integrable point in the dense phase is in the same universality class as this dense fixed point.

The central charge is given by the same analytic function of g throughout Regime 1, and the same holds true for each critical exponent [28]. This is why the two phases are grouped within the same regime. The dense and dilute phases intersect in the point $\psi = \frac{\pi}{3}$, for which the central charge is $c=2$, the rank of the A_2 algebra. At this point the field theory is a CFT of two free bosons.

We do not yet have an analytic understanding of Regime 2. Our numerical results for $c_L(\psi)$ are shown in the left panel of Fig. 6. It is clear that $c(\psi)$ cannot be given by the same analytic expression as (87), so we are indeed in a different regime. The numerical results clearly show that the ground state sector—then one determining c—is only present for L a multiple of 3. This is a hint of a higher symmetry, as is the fact, that c takes larger values than in Regime 1. We have indeed $c \gtrapprox 3$ for small ψ, and possibly even $c(\psi) \to 4$ for $\psi \to 0$. It seems possible that the limit $c(\psi \to \frac{\pi}{6}^-)$ is equal to $c(\psi \to \frac{\pi}{6}^+) = -10$, obtained from (87). In any case, it is obvious that the finite-size effects are much larger in Regime 2 than in Regime 1. Such slow convergence is usually the hallmark of a non-compact continuum limit. Notice that in the A_1 loop model there is indeed a regime III for which the continuum limit has one

compact and on non-compact boson. This leads us to conjecture that Regime 2 of the A_2 web model has one or two non-compact bosons.

Further investigations of Regime 2 would require the access to larger sizes. This could be achieved, e.g., by setting up the Bethe Ansatz equations and studying them numerically or even analytically. We leave such developments for future work.

7.2.2. Special points

We now discuss a number of points of particular interest.

Case of $q = e^{\pm i\frac{\pi}{4}}$ These are the values of q for which one has a mapping to a 3-state Potts models (see Section 3.3). The corresponding integrable points are given by

ψ	$\frac{\pi}{4}$	$\frac{5\pi}{12}$	$\frac{11\pi}{12}$
x	$\frac{1}{\sqrt{2}}$	$\sqrt{2-\sqrt{3}}$	$\sqrt{\sqrt{3}+2}$
$y=z$	$\sqrt{2}$	1	i
$e^{i\phi}$	$e^{i\frac{7\pi}{12}}$	$e^{i\frac{23\pi}{36}}$	$e^{i\frac{29\pi}{36}}$
c	0	$\frac{4}{5}$	≈ 1.5

The point $\psi = \frac{5\pi}{12}$ in the dilute phase of Regime 1 is likely to be in the same universality class as the analogous point in the dilute phase of the A_2 web models considered in [2]. It was argued there that this point is in the ferromagnetic 3-state Potts model class. Recall that the work in [2] did not include the bending weight ϕ, but we do not think this changes the universality class. Indeed $c(\psi = \frac{5\pi}{12}) = \frac{4}{5}$ from (87) as expected.

It seems worth pointing out that the integrable 3-state Potts model described in this paper is not the same as the one considered in [40], although both include plaquette interactions.

Similarly, we believe that the point $\psi = \frac{\pi}{4}$ in the dense phase of Regime 1 is in the universality class of the analogous point of [2], which can in turn be identified with the infinite-temperature 3-state Potts model. The latter has obviously $c_{\text{eff}} = 0$, in agreement with $c(\psi = \frac{\pi}{4}) = 0$ from (87).

Finally we identify the point $\psi = \frac{11\pi}{12}$ of the above table with the point $\psi = \frac{\pi}{12}$, due to the symmetry (84). For the latter, our numerical results are $c_6 \simeq 1.367$ from sizes $L = 3, 6$, and $c_9 \simeq 1.516$ from sizes $L = 6, 9$. To our best knowledge, no previous study has found such a high value of c for a 3-state spin model.

For completeness we mention that yet other universality classes of a 3-state Potts model on the triangular lattice have been reported in [41].

Case of $q = \pm i$ When $q = \pm i$, $[2]_q = 0$, so that any web containing a digon has weight 0. Actually any web that is not a collection of loops has vanishing weight. This can be shown by induction on the number of vertices. It is clearly true for webs with 2 vertices. Without loss of generality, consider a web that does not contain loops with V vertices, E edges and F faces. Suppose the statement is true for webs with strictly less than V vertices. By the Euler relation and the hand shake lemma we have

$$F - E + V = 2$$

$$2E = 3V$$

If the web contains a digon, its weight is 0. If not, any face is surrounded by at least 4 edges and

$$2E \geq 4F$$

This implies a lower bound on the number of vertices

$$V \geq 8$$

If we now reduce the web by the square rule, i.e. the only rule applicable, we get a linear combination of webs with a number of vertices $V' = V - 4 > 0$. By the induction hypothesis their weights are 0 hence also is the weight of the original web.

We thus obtained a model of oriented loops of topological weight $[3]_q = -1$. If we sum over orientation taking into account the fugacities corresponding to the bendings of web edges we obtain the familiar $O(N)$ model of unoriented loops with contractible loop weight

$$N = -e^{6i\phi} - e^{-6i\phi} = e^{2i\psi} + e^{-2i\psi},$$

non contractible loop weight -2 and bond fugacity

$$x = \frac{1}{2\sin(\psi)}.$$

$q = \pm i$ is attained for the following values of ψ

$$\psi = \frac{\pi}{6}, \frac{\pi}{2}$$

The first point gives $N = 1$ and $x = 1$. These values correspond to site percolation on the triangular lattice, a point in the dense phase of the loop model. Since the non contractible loop weight is equal to -2, the effective central charge is given by $-\infty$, which is certainly different from the analytical result $c(\psi \to \frac{\pi}{6}^+) = -10$, and possibly also incompatible with the numerical result $c(\psi \to \frac{\pi}{6}^-)$ for Regime 2. In any case, there is a discontinuity at the junction between Regimes 1 and 2.

The second point, $\psi = \frac{\pi}{2}$, gives $N = -2$ and $x = \frac{1}{2}$. This value corresponds to the loop-erased random walk, in agreement with the value $c = -2$ from (87).

Case of $\psi = 0$ From Fig. 6 this is the most remarkable point in Regime 2, so we investigate here its lattice realisation in some more detail. For $\psi = 0$, one obtains $y = z = 0$ and $x \to \infty$. To make sense of the model, one needs to first renormalise the local transfer matrices (65) by $\frac{1}{x}$ and then send ψ to zero. One then obtains

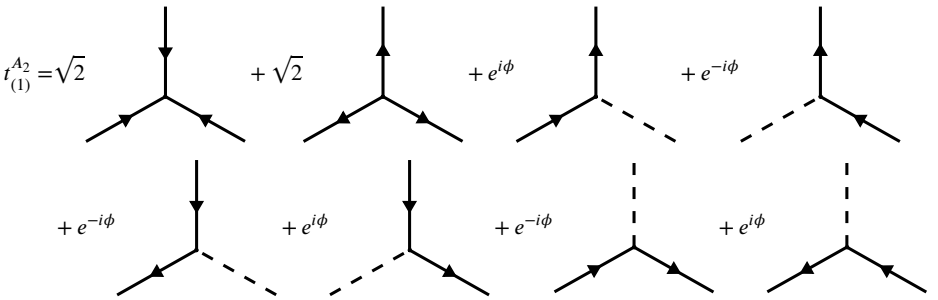

(89a)

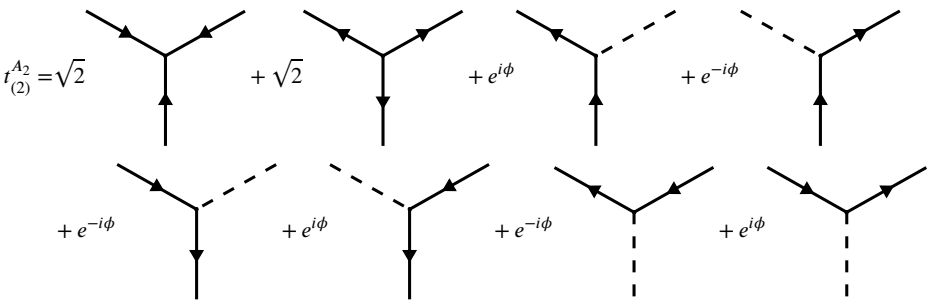

(89b)

with $q = -1$ and $e^{i\phi} = i$. It is not clear to us at present why this lattice model has the special properties (slow convergence and the largest central charge) that we observe numerically.

7.3. The G_2 web model

We now consider the third line of Table 1. Let V_u, $u \in \mathbb{C}^*$, be the representation of $U_q(D_4^{(3)})$ given in Appendix D which is actually isomorphic to the one considered in [26].[11] We are looking for an operator $\check{R}(u, v)$ intertwining $V_u \otimes V_v$ and $V_v \otimes V_u$. Remark that, in $U_q(D_4^{(3)})$, E_i, F_i and H_i for $i = 0, 1$ generate a Hopf subalgebra isomorphic to $U_q(G_2)$. Under the action of this subalgebra, V_u decomposes as:

$$V_u = \mathbb{C} \oplus V \tag{90}$$

Hence $\check{R}(u, v)$ will decompose as a sum of $U_q(G_2)$ intertwiners:

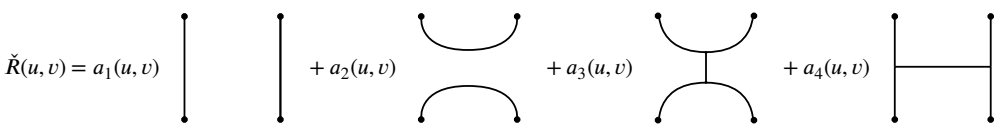

[11] Beware of a typo in the representation matrices of [26].

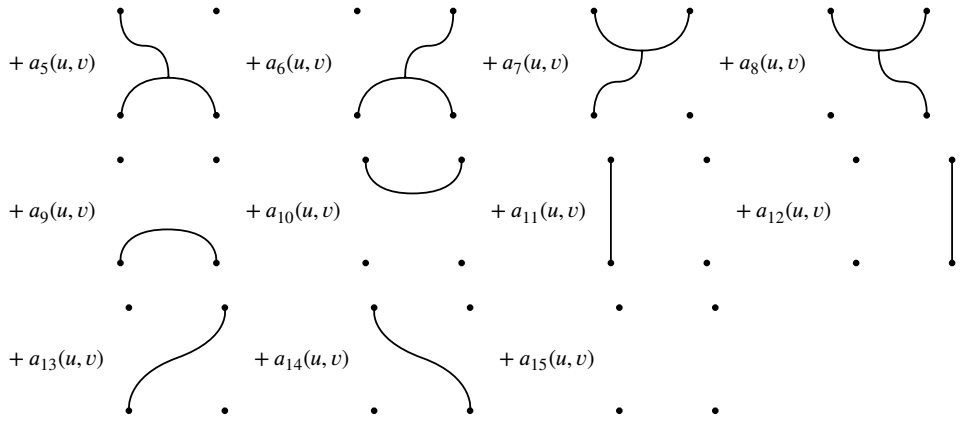

(91)

where $a_i(u,v)$ are some coefficients and the webs span the space of intertwiners $\mathrm{End}_{U_q(G_2)}\left((\mathbb{C}\oplus V)^2\right)$.

Asking for $\check{R}(u,v)$ to commute with the remaining generators, we see that it depends only on the ratio $s=\frac{u}{v}$. Plugging this linear system for the functions $a_i(s)$ into Mathematica, we find

$$
\begin{aligned}
a_1(s) &= \frac{s^3-q^{12}}{q^4(s-1)}\\
a_2(s) &= \frac{q^8-q^2s^3}{q^6-s}\\
a_3(s) &= q^4+q^2s+s^2\\
a_4(s) &= \frac{q^8+q^4s+s^2}{q^2}\\
a_5(s) &= q^4\sqrt{[3]_q}\left(q^2-1\right)s\\
a_6(s) &= q^4\sqrt{[3]_q}\left(q^2-1\right)s\\
a_7(s) &= -\frac{\sqrt{[3]_q}\left(q^2-1\right)s}{q^2}\\
a_8(s) &= -\frac{\sqrt{[3]_q}\left(q^2-1\right)s}{q^2}\\
a_9(s) &= \frac{q^8\left(q^6-1\right)s(s+1)}{q^6-s}\\
a_{10}(s) &= \frac{\left(q^6-1\right)s(s+1)}{q^4\left(q^6-s\right)}\\
a_{11}(s) &= -\frac{\left(q^6-1\right)s\left(q^6+s\right)}{q^4(s-1)}\\
a_{12}(s) &= -\frac{\left(q^6-1\right)s\left(q^6+s\right)}{q^4(s-1)}\\
a_{13}(s) &= q^6+q^4(s+1)+\frac{s^2}{q^2}+s^2+s\\
a_{14}(s) &= q^6+q^4(s+1)+\frac{s^2}{q^2}+s^2+s\\
a_{15}(s) &= q^{14}-q^8+q^6+q^4s+q^4+\frac{1}{q^4}+\left(\frac{1}{q^2}+1\right)s^2-q^2+\frac{1-q^{12}}{q^4(s-1)}+\frac{q^8-q^{20}}{q^6-s}+s
\end{aligned}
$$

One can then show, using for instance Mathematica, that the corresponding operator $\check{R}(s)$ satisfies the multiplicative spectral parameter dependant Yang-Baxter equation. Using the following gauge transformation (which is just an elementary rescaling of the irreducible components in the decomposition (90))

$$
\begin{aligned}
D &= \mathrm{Diag}(1,\alpha,\alpha,\alpha,\alpha,\alpha,\alpha,\alpha)\\
\check{R}(s) &\to \left(D^{-1}\otimes D^{-1}\right)\check{R}(s)(D\otimes D)
\end{aligned}
\tag{92}
$$

for well chosen α, we obtain

$$
\begin{aligned}
a_1(s) =& \frac{s^3 - q^{12}}{q^4(s-1)} \\
a_2(s) =& \frac{q^8 - q^2 s^3}{q^6 - s} \\
a_3(s) =& q^4 + q^2 s + s^2 \\
a_4(s) =& \frac{q^8 + q^4 s + s^2}{q^2} \\
a_5(s) =& a_6(s) = a_7(s) = a_8(s) = -iq\sqrt{[3]_q}\left(q^2 - 1\right) s \\
a_9(s) =& a_{10}(s) = -\frac{q^2\left(q^6 - 1\right) s(s+1)}{q^6 - s} \\
a_{11}(s) =& a_{12}(s) = -\frac{\left(q^6 - 1\right) s\left(q^6 + s\right)}{q^4(s-1)} \\
a_{13}(s) =& a_{14}(s) = q^6 + q^4(s+1) + \frac{s^2}{q^2} + s^2 + s \\
a_{15}(s) =& q^{14} - q^8 + q^6 + q^4 s + q^4 + \frac{1}{q^4} + \left(\frac{1}{q^2} + 1\right) s^2 - q^2 + \frac{1 - q^{12}}{q^4(s-1)} + \frac{q^8 - q^{20}}{q^6 - s} + s
\end{aligned}
$$

It is apparent that by setting the spectral parameter $s = e^{-\frac{2i\pi}{3}} q^4$, $\check{R}(s)$ will be decomposed only in terms of webs appearing in the local transfer matrix of the G_2 web model. By renormalising the R-matrix, we recover the local transfer matrix (67) with the following parametrisation, setting $q = e^{i\gamma}$:

$$
x = \frac{1}{2\cos\left(2\gamma + \frac{2\pi}{3}\right)} \tag{93a}
$$

$$
y = 2\cos\left(\gamma - \frac{\pi}{6}\right)\sqrt{\frac{2\cos\left(2\gamma + \frac{2\pi}{3}\right)}{[3]_q}} \tag{93b}
$$

Note that points related by $\gamma \to \gamma + \pi$ have the same bond fugacity but a vertex fugacity related by $y \to -y$. They are equivalent as the partition function only depends on y^2 and q^2. We could focus for instance on the interval $\gamma \in [0, \pi]$. The Kuperberg weight only depends on $\pm 2\gamma$ and for each value of the former, there are exactly two integrable points. Hence, the model describes two phases.

7.3.1. Central charge and phase diagram

Also for the G_2 web model have we numerically diagonalised the transfer matrix on cylinders of circumference L. Recall that for the A_2 case we found L mod 3 parity effects in one of the regimes. For the G_2 model such effects are found to depend on L mod 2, so in this case we perform the diagonalisation for sizes $L = 2, 4, 6, 8$, from which estimates for the central charge c_L can be extracted. The computations were made for 50 equally-spaced values of $\gamma \in [0, \pi]$ and we show again curves $c_L(\gamma)$ obtained from extrapolation of these values.

The number of regimes is now larger. The numerical results, shown in Fig. 7, combined with analytical considerations on the weights (see below) lead us to define four regimes:

$$
\begin{aligned}
&\text{Regime 1:} \quad \gamma \in [\tfrac{\pi}{6}, \tfrac{\pi}{3}], \\
&\text{Regime 2:} \quad \gamma \in [\tfrac{\pi}{3}, \tfrac{\pi}{2}], \\
&\text{Regime 3:} \quad \gamma \in [\tfrac{\pi}{2}, \tfrac{2\pi}{3}], \\
&\text{Regime 4:} \quad \gamma \in [\tfrac{2\pi}{3}, \tfrac{7\pi}{8}].
\end{aligned} \tag{94}
$$

The numerical results alone suggest that Regime 1 might have a larger extent, $\gamma =]\frac{\pi}{8}, \frac{\pi}{3}]$, but in any case the point $\gamma = \frac{\pi}{8}$ is special (see below) and should be excluded. The remaining two pieces of the interval $[0, \pi]$ do not allow for convincing numerical results for $c_L(\gamma)$, and since γ is defined modulo π it is not clear whether these pieces should be considered one or two extra regimes. In the following we shall focus only on Regimes 1–4.

7.3.2. Special points

We discuss again a number of points of special interest.

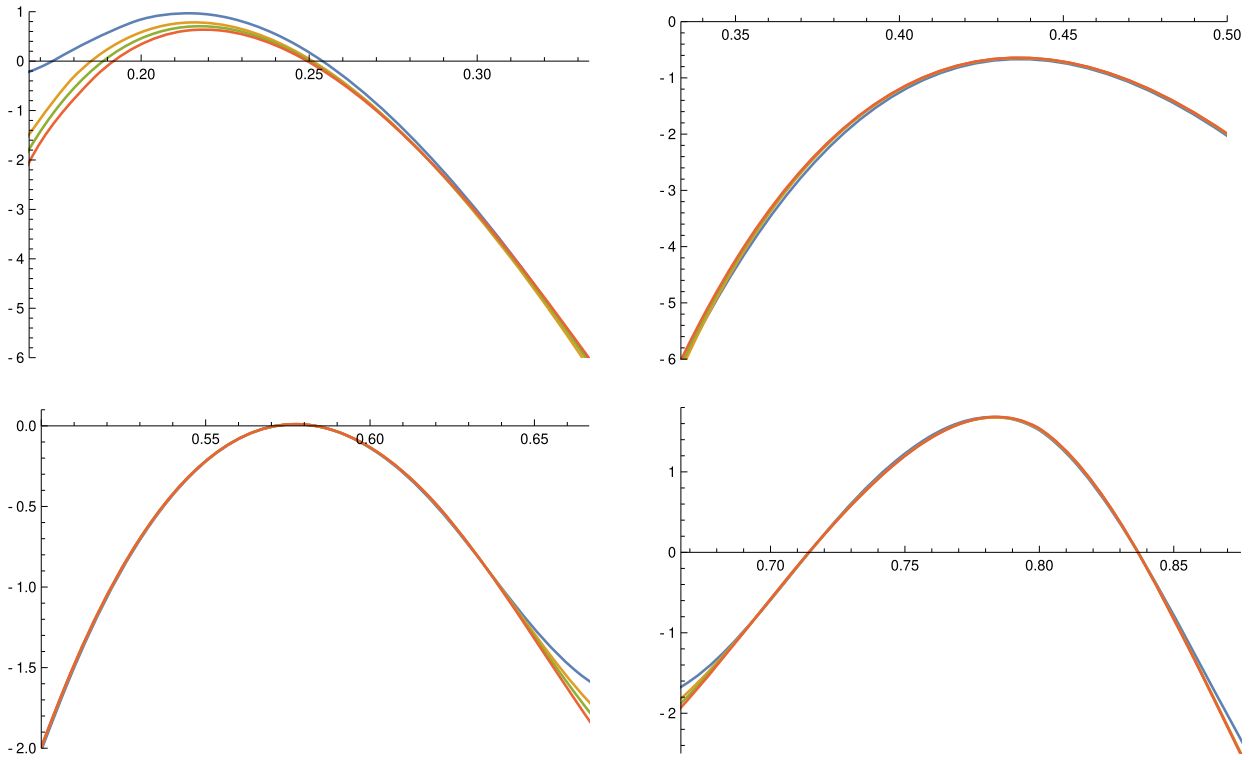

Fig. 7. Fits $c_L(\gamma)$ for the central charge in the G_2 web model, plotted against $\frac{\gamma}{\pi}$. We show two-point fits using sizes $\{L, L-2\}$ with $L=4$ (blue), $L=6$ (orange) and $L=8$ (green), as well as a three-point fit using sizes $\{L, L-2, L-4\}$ with $L=8$ (red). Regime 1 (upper left panel) is for $\gamma \in [\frac{\pi}{6}, \frac{\pi}{3}]$, Regime 2 (upper right panel) is for $\gamma \in [\frac{\pi}{3}, \frac{\pi}{2}]$, Regime 3 (lower left panel) is for $\gamma \in [\frac{\pi}{2}, \frac{2\pi}{3}]$, and finally Regime 4 (lower right panel) is for $\gamma \in [\frac{2\pi}{3}, \frac{7\pi}{8}]$.

Case of $\gamma = \frac{\pi}{6}, \frac{5\pi}{6}$ For these values of γ, we have described in Section 4.3 a mapping to the 3-state Potts model on the dual triangular lattice. We obtain the following integrable points:

γ	$\frac{\pi}{6}$	$\frac{5\pi}{6}$
x	$-\frac{1}{2}$	1
y	$2i$	$-\frac{1}{\sqrt{2}}$

The point $\gamma = \frac{5\pi}{6}$ corresponds to the infinite-temperature limit of the 3-state Potts model, with bond fugacity $x=1$. This identification is consistent with the observed value $c(\frac{5\pi}{6}) = 0$ in Regime 4. On the other hand, the numerical results for $\gamma = \frac{\pi}{6}$ in Regime 1 lead us to conjecture that $c(\frac{\pi}{6}) = -2$, which is an unusual and presently unexplained result for a 3-state model. Notice that the weight of each web configuration depends on y via the combination y^2. The fact that both x and y^2 are negative in this case is presumably at the root of the observed unusual behaviour.

Case of $\gamma = \frac{\pi}{2}$ For this value of γ, one has $x=1$ and $y=i$. As shown in Section 4.4, this web model describes the uniform probability measure on spanning trees of the dual lattice. This is known to have $c=-2$, in perfect agreement with the numerical results at the boundary between Regimes 2 and 3.

Case of $\gamma = \frac{2\pi}{3}$ For these values of γ, we have $y=0$ and the model becomes simply the $O(N)$ loop model. For this value, we have $N=-2$ and $x=\frac{1}{2}$, which corresponds to the dilute phase of the loop model, hence to loop-erased random walks. Also this point is known to have $c=-2$, a value that agrees perfectly with the numerical results at the boundary between Regimes 3 and 4.

Case of $\gamma = \frac{5\pi}{12}, \frac{11\pi}{12}$ For these values of γ, the bond fugacity is infinite. By renormalising the weights, we obtain the following local transfer matrices

$t^{G_2}_{(1)} = (-1 \pm \sqrt{3})$ 

and similarly for $t_{(2)}^{G_2}$. The + sign in $(-1 \pm \sqrt{3})$ corresponds to $\gamma = \frac{5\pi}{12}$, and the − sign to $\gamma = \frac{11\pi}{12}$. For the first case, $\gamma = \frac{5\pi}{12}$, the numerical results in Regime 2 lend strong credence to the conjecture $c(\frac{5\pi}{12}) = -\frac{4}{5}$, but we have no theoretical understanding of this value. The second case, $\gamma = \frac{11\pi}{12}$, is outside the four regimes defined above, and we refrain from giving any numerical estimate for c.

Case of vanishing digon weight We now look at values of γ such that the digon factor $-(q^6 + q^4 + q^2 + q^{-2} + q^{-4} + q^{-6})$ vanishes. This happens for $\gamma = \frac{\pi}{3}, \frac{2\pi}{3}, \frac{\pi}{8}, \frac{3\pi}{8}, \frac{5\pi}{8}, \frac{7\pi}{8}$.

For $\gamma = \frac{\pi}{3}$, the vertex fugacity is infinite, whereas the bond fugacity stays finite—and is in fact trivial up to a sign ($x = -1$). Hence the model contains only one configuration, the hexagonal lattice being completely covered by the web. The numerical results in Regime 2 give strong support for the conjecture $c(\frac{\pi}{3}) = -6$. This is again an unusual value for which we have presently no analytical explanation.

The case $\gamma = \frac{2\pi}{3}$ was treated above.

For the other four values of γ, we have a loop weight of $N = -1$ and a bond fugacity

$$x = \left(\epsilon_1 \sqrt{2 + \epsilon_2 \sqrt{3}}\right)^{-1}$$

for some signs ϵ_1, ϵ_2. Moreover, when the digon factor is 0, all webs that are not a collection of loops have vanishing Kuperberg weight. This can be shown along the lines of the analogous situation for A_2 webs, by induction on the number of vertices. It is clearly true for a web having 2 vertices. Let V be the number of vertices of a given web G and suppose that the statement is true for webs having less than V vertices. Without loss of generality, we may assume that G does not contain any loop. Suppose that G does not contain digons either. We then have, thanks to the Euler relation and the hand-shake lemma,

$$V \geq 4\,.$$

Suppose there is a trigon, then G is proportional to a web with $V - 2$ vertices. If there is no trigon, we have the better bound

$$V \geq 8\,.$$

Then we can use the square or pentagon rule and obtain a linear combination of webs. In all cases, we have that G can be written as a linear combination of webs with a strictly smaller, yet non-vanishing number of vertices and the induction hypothesis applies.

The resulting models are in fact $O(-1)$ loops in their dense ($\epsilon_2 = -1$) or dilute ($\epsilon_2 = 1$) phase. The case $\gamma = \frac{\pi}{8}$ is outside of the four regimes for which we have good numerical results. In fact, the numerical evidence alone is in favour of Regime 1 having extent $]\frac{\pi}{8}, \frac{\pi}{3}]$, but assuming this, the numerical results indicate that $c(\gamma) \to -\infty$ as $\gamma \to \frac{\pi}{8}^+$. This is not compatible with the analytical result $c = -\frac{3}{5}$ for the dilute $O(-1)$ model, so at least the point $\frac{\pi}{8}$ cannot be contained in the definition of Regime 1. For the case $\gamma = \frac{5\pi}{8}$, on the other hand, the numerical results in Regime 3 are in perfect agreement with $c = -\frac{3}{5}$.

It remains to discuss the two cases $\gamma = \frac{3\pi}{8}$ and $\frac{7\pi}{8}$ for which we should find a dense $O(-1)$ model with $c = -7$ by the above analytical reasoning. The first of these points, $\gamma = \frac{3\pi}{8}$, is inside Regime 2, while the other, $\gamma = \frac{7\pi}{8}$ is at the boundary of Regime 4. The numerical results are well-behaved in both cases, finding $c \simeq -2.33$ for the former and $c \simeq -2.50$ for the latter. We do not presently know how to reconcile this diagreement with the analytical result and suspect that some non-commutativity of limits might be at play. In any case, we stress that because of the very high dimension of the transfer matrix, the numerical results are obtained by interpolation from a set of 50 values of γ, and we did not examine the diagonalisation problem directly at the points $\gamma = \frac{3\pi}{8}$ and $\frac{7\pi}{8}$.

Case of $\gamma = \frac{\pi}{4}$ This point is situated inside Regime 1, and based on the numerical results we conjecture that $c(\frac{\pi}{4}) = 0$. We have, however, no analytical argument in support of this value.

7.4. The B_2 web model

We now consider the fourth line of Table 1. Let V_u, $u \in \mathbb{C}^*$, be the first representation of $U_t(A_4^{(2)})$ given in Appendix D.3.2. We are looking for an operator $\check{R}(u, v)$ intertwining $V_u \otimes V_v$ and $V_v \otimes V_u$. Remark that E_i, F_i and H_i for $i = 1, 2$ generate a Hopf subalgebra isomorphic to $U_{t^2}(B_2)$. Under the action of this subalgebra, V_u decomposes as:

$$V_u = \mathbb{C} \oplus V_1 \oplus V_2 \tag{95}$$

Hence $\check{R}(u, v)$ will decompose as a sum of $U_{t^2}(B_2)$ intertwiners:

$\check{R}(u,v) = a_1(u,v)$ $+ a_2(u,v)$  $+ a_3(u,v)$ 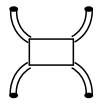 $+ a_4(u,v)$ 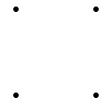

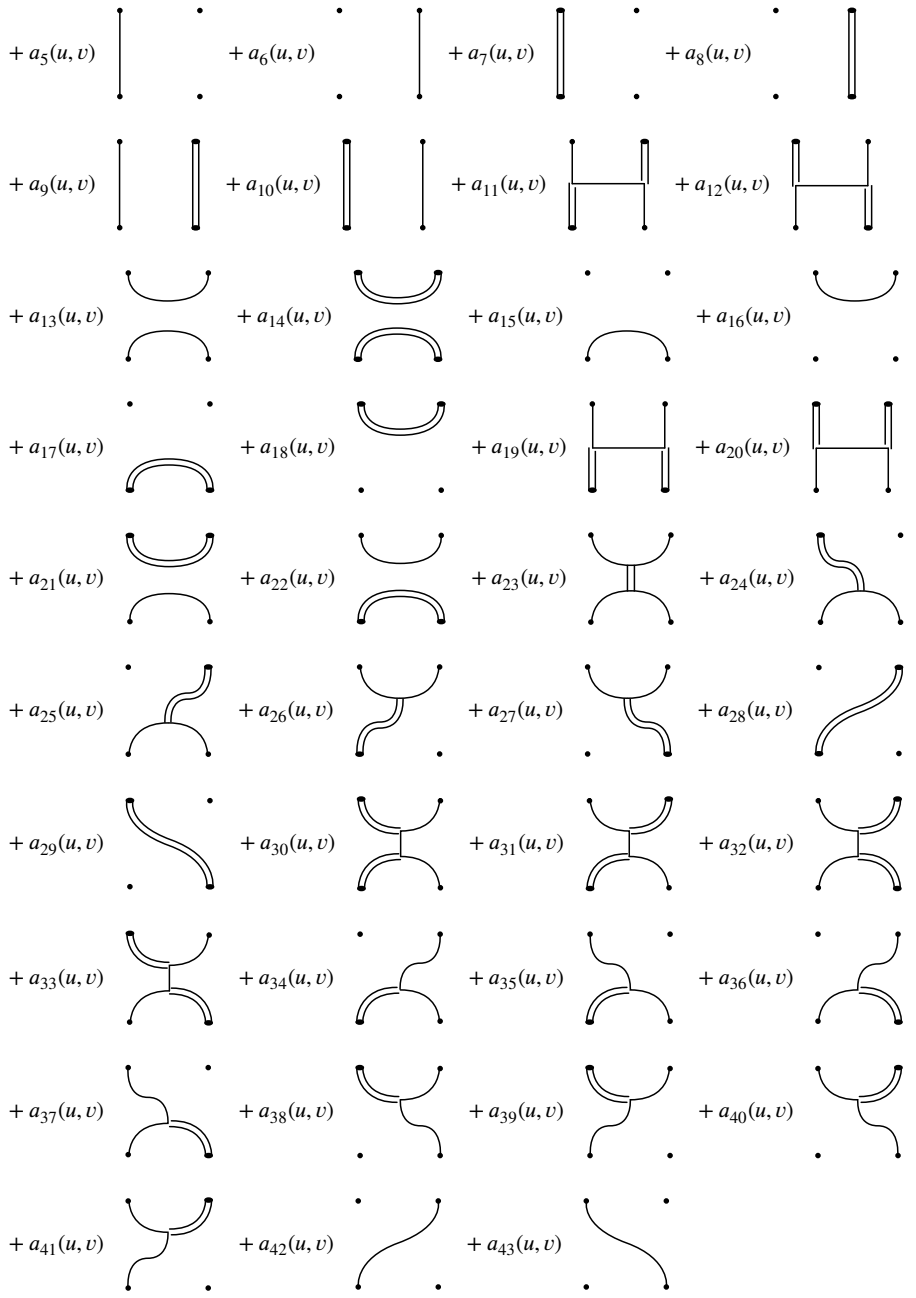

where $a_i(u,v)$ are some coefficients and the webs span the space of intertwiners $\mathrm{End}_{U_{i^2}(B_2)}\left((\mathbb{C}\oplus V_1\oplus V_2)^2\right)$.

Asking for $\check{R}(u,v)$ to commute with the remaining generators, we see that it depends only on the ratio $s=\frac{u}{v}$. Plugging this linear system for the functions $a_i(s)$ into Mathematica, we find

$$
\begin{aligned}
a_1(s) &= \left(t^4+1\right)^2\left(t^8-s^2\right)\left(t^{10}+s^2\right)\left(-t^8+t^2s^4-(t-1)(t+1)\left(t^8-t^4+1\right)s^2\right)\\
a_2(s) &= -\left(t^4+1\right)^2\left(t^2-s\right)\left(t^2+s\right)\left(t^8-s^2\right)\left(t^6+s^2\right)\left(t^{10}+s^2\right)\\
a_3(s) &= t^8\left(s^2-1\right)\left(t^8-s^2\right)\left(t^2+s^2\right)\left(t^{10}+s^2\right)\\
a_4(s) &= \left(t^4+1\right)^2\left[-t^{24}-t^4s^8-\left(t^4-t^2+1\right)\left(\left(t^{16}-4t^8-t^6+6t^4-t^2-4\right)t^8+1\right)s^4\right.\\
&\quad +\left(t^{14}-3t^{12}+t^{10}+3t^8-3t^6-t^4+3t^2-1\right)t^2s^6\\
&\quad \left.-\left(t^{14}-3t^{12}+t^{10}+3t^8-3t^6-t^4+3t^2-1\right)t^{12}s^2\right]\\
a_5(s) &= -\left(\left(t^{12}-t^{10}+t^8-t^4+t^2-1\right)s\left(t^{10}+s^2\right)\left(t^{12}-t^2s^4+\left(t^{14}+t^{10}+t^8-t^6-t^4-1\right)s^2\right)\right)
\end{aligned}
$$

$$a_6(s) = -\left(\left(t^{12}-t^{10}+t^8-t^4+t^2-1\right) s\left(t^{10}+s^2\right)\left(t^{12}-t^2s^4+\left(t^{14}+t^{10}+t^8-t^6-t^4-1\right)s^2\right)\right)$$
$$a_7(s) = -\left(\left(t^6-2t^4+2t^2-1\right)\left(t^6+t^4+t^2+1\right)^2 s^2\left(t^8-s^2\right)\left(t^{10}+s^2\right)\right)$$
$$a_8(s) = -\left(\left(t^6-2t^4+2t^2-1\right)\left(t^6+t^4+t^2+1\right)^2 s^2\left(t^8-s^2\right)\left(t^{10}+s^2\right)\right)$$
$$a_9(s) = -\left(\left(t^4-1\right)\left(t^4+1\right)^2 s\left(t^8-s^2\right)\left(t^6+s^2\right)\left(t^{10}+s^2\right)\right)$$
$$a_{10}(s) = -\left(\left(t^4-1\right)\left(t^4+1\right)^2 s\left(t^8-s^2\right)\left(t^6+s^2\right)\left(t^{10}+s^2\right)\right)$$
$$a_{11}(s) = -t^4\left(t^4+1\right)\left(s^2-1\right)\left(t^8-s^2\right)\left(t^6+s^2\right)\left(t^{10}+s^2\right)$$
$$a_{12}(s) = -t^4\left(t^4+1\right)\left(s^2-1\right)\left(t^8-s^2\right)\left(t^6+s^2\right)\left(t^{10}+s^2\right)$$
$$a_{13}(s) = t^8\left(t^4+1\right)\left(s^2-1\right)\left(t^2+s^2\right)\left(t^{12}-t^2s^4+\left(t^{14}-t^{12}+t^8-t^6+t^2-1\right)s^2\right)$$
$$a_{14}(s) = t^8\left(t^4+1\right)^2\left(s^2-1\right)\left(t^2-s\right)\left(t^2+s\right)\left(t^2+s^2\right)\left(t^6+s^2\right)$$
$$a_{15}(s) = t^8\left(t^4-1\right)\left(t^5-t^3+t\right)^2 s\left(s^2-1\right)\left(t^{12}-t^2s^4+\left(t^{14}+t^{10}+t^8-t^6-t^4-1\right)s^2\right)$$
$$a_{16}(s) = -\left(\left(t^4-1\right)\left(t^4+1\right)^2 s\left(s^2-1\right)\left(t^{12}-t^2s^4+\left(t^{14}+t^{10}+t^8-t^6-t^4-1\right)s^2\right)\right)$$
$$a_{17}(s) = t^{14}\left(t^2-1\right)\left(t^{10}+t^6+t^4+1\right)^2 s^2\left(s^2-1\right)\left(t^2+s^2\right)$$
$$a_{18}(s) = t^2\left(t^2-1\right)\left(t^6+t^4+t^2+1\right)^2 s^2\left(s^2-1\right)\left(t^2+s^2\right)$$
$$a_{19}(s) = -t^6\left(t^4-1\right)\left(t^4+1\right)^2 s\left(s^2-1\right)\left(t^8-s^2\right)\left(t^{10}+s^2\right)$$
$$a_{20}(s) = t^4\left(t^4-1\right) s\left(s^2-1\right)\left(t^8-s^2\right)\left(t^{10}+s^2\right)$$
$$a_{21}(s) = t^8\left(t^8-1\right) s\left(s^2-1\right)\left(t^4-s^2\right)\left(t^2+s^2\right)$$
$$a_{22}(s) = -t^{10}\left(t^4-1\right)\left(t^4+1\right)^3 s\left(s^2-1\right)\left(t^4-s^2\right)\left(t^2+s^2\right)$$
$$a_{23}(s) = -t^6\left(t^4+1\right)\left(s^2-1\right)\left(t^8-s^2\right)\left(t^2+s^2\right)\left(t^{10}+s^2\right)$$
$$a_{24}(s) = -it^6\left(t^8-t^6+t^2-1\right) s\left(s^2-1\right)\left(t^8-s^2\right)\left(t^{10}+s^2\right)$$
$$a_{25}(s) = -it^6\left(t^8-t^6+t^2-1\right) s\left(s^2-1\right)\left(t^8-s^2\right)\left(t^{10}+s^2\right)$$
$$a_{26}(s) = i\left(t^4-1\right)\left(t^5+t\right)^2 s\left(s^2-1\right)\left(t^8-s^2\right)\left(t^{10}+s^2\right)$$
$$a_{27}(s) = i\left(t^4-1\right)\left(t^5+t\right)^2 s\left(s^2-1\right)\left(t^8-s^2\right)\left(t^{10}+s^2\right)$$
$$a_{28}(s) = t^4\left(t^4+1\right)^2\left(s^2-1\right)\left(t^8-s^2\right)\left(t^2+s^2\right)\left(t^{10}+s^2\right)$$
$$a_{29}(s) = t^4\left(t^4+1\right)^2\left(s^2-1\right)\left(t^8-s^2\right)\left(t^2+s^2\right)\left(t^{10}+s^2\right)$$
$$a_{30}(s) = t^8\left(t^8-1\right) s\left(s^2-1\right)\left(t^2+s^2\right)\left(t^{10}+s^2\right)$$
$$a_{31}(s) = -t^8\left(t^4+1\right)\left(s^2-1\right)\left(t^4-s^2\right)\left(t^2+s^2\right)\left(t^{10}+s^2\right)$$
$$a_{32}(s) = t^8\left(t^8-1\right) s\left(s^2-1\right)\left(t^2+s^2\right)\left(t^{10}+s^2\right)$$
$$a_{33}(s) = -t^8\left(t^4+1\right)\left(s^2-1\right)\left(t^4-s^2\right)\left(t^2+s^2\right)\left(t^{10}+s^2\right)$$
$$a_{34}(s) = -it^{10}\left(t^{12}-t^{10}+t^8-t^4+t^2-1\right) s\left(s^2-1\right)\left(t^2+s^2\right)\left(t^{10}+s^2\right)$$
$$a_{35}(s) = -it^8\left(t^2-1\right)\left(t^4+1\right)\left(t^6+1\right)^2 s^2\left(s^2-1\right)\left(t^{10}+s^2\right)$$
$$a_{36}(s) = -it^8\left(t^2-1\right)\left(t^4+1\right)\left(t^6+1\right)^2 s^2\left(s^2-1\right)\left(t^{10}+s^2\right)$$
$$a_{37}(s) = -it^{10}\left(t^{12}-t^{10}+t^8-t^4+t^2-1\right) s\left(s^2-1\right)\left(t^2+s^2\right)\left(t^{10}+s^2\right)$$
$$a_{38}(s) = -it^4\left(t^8-1\right) s\left(s^2-1\right)\left(t^2+s^2\right)\left(t^{10}+s^2\right)$$
$$a_{39}(s) = -it^2\left(t^{14}+t^8-t^6-1\right) s^2\left(s^2-1\right)\left(t^{10}+s^2\right)$$
$$a_{40}(s) = -it^2\left(t^{14}+t^8-t^6-1\right) s^2\left(s^2-1\right)\left(t^{10}+s^2\right)$$
$$a_{41}(s) = -it^4\left(t^8-1\right) s\left(s^2-1\right)\left(t^2+s^2\right)\left(t^{10}+s^2\right)$$
$$a_{42}(s) = -t^4\left(t^4+1\right)\left(s^2-1\right)\left(t^{10}+s^2\right)\left(\left(t^4+1\right)s^4-t^{10}\left(t^4+1\right)+\left(t^{14}-2t^{12}+t^8-t^6+2t^2-1\right)s^2\right)$$
$$a_{43}(s) = -t^4\left(t^4+1\right)\left(s^2-1\right)\left(t^{10}+s^2\right)\left(\left(t^4+1\right)s^4-t^{10}\left(t^4+1\right)+\left(t^{14}-2t^{12}+t^8-t^6+2t^2-1\right)s^2\right)$$

One can then show, using for instance Mathematica, that the corresponding operator $\check{R}(s)$ satisfies the multiplicative spectral parameter dependant Yang-Baxter equation.

7.4.1. Integrable B_2 web model on the hexagonal lattice

It is apparent that by setting the spectral parameter $s = t^4$, $\check{R}(s)$ will be decomposed only in terms of webs appearing in the local transfer matrix of the B_2 web model on the hexagonal lattice. In order to put it in the form of (71), we renormalise the R matrix and take the following transformation

$$\begin{aligned} D &= \mathrm{Diag}(1,\alpha,\alpha,\alpha,\alpha,\beta,\beta,\beta,\beta,\beta) \\ \check{R}(s) &\to \left(D^{-1}\otimes D^{-1}\right)\check{R}(s)\,(D\otimes D) \end{aligned} \tag{96}$$

which is just an elementary rescaling of the irreducible components in the decomposition (95). For a well-chosen normalisation constant and parameters α, β, we recover the local transfer matrix (71) with the following parametrisation, setting $t = e^{i\psi}$:

$$q = e^{2i\psi} \tag{97a}$$

$$x_{t;1} = \frac{2\sin(\psi)}{4\sin^2(\psi)-1} \tag{97b}$$

$$x_{t;2} = \frac{1}{4\sin^2(\psi)-1} \tag{97c}$$

$$x_{v;1} = -\frac{1}{4\sin(\psi)\cos(2\psi)} \tag{97d}$$

$$x_{v;2} = 0 \tag{97e}$$

$$y = 1 \tag{97f}$$

7.4.2. Integrable B_2 web model on the square lattice

Let us now turn to the model on the square lattice. When one tunes the spectral parameter as $s = e^{i\frac{\pi}{4}}t^{\frac{5}{2}}$ and uses the gauge freedom (96), one obtains the B_2 web model on the square lattice defined in Section 5.3 with the following Boltzmann weights:

$$b_1 = -\frac{i(-1+t(t-i))(1+(t-1)t(t+1)(t-i))}{t^5+t}$$

$$b_2 = -\frac{1+t(t-i)\left(-2+t\left(t^3-t+i\right)(-2+t(t-i))\right)}{t^4}$$

$$b_3 = \frac{e^{i\frac{3\pi}{4}}(-1+t(t-i))\left(1+i\left(t^3-t+i\right)t^2\right)\left(-1+t(t-i)\left(1+(t-1)(t+1)\left(t^4+it+2\right)t^2\right)\right)}{t^{13/2}\left(t^4+1\right)}$$

$$b_4 = -\frac{i(-1+t(t-i))(1+(t-1)t(t+1)(t-i))\left(1+\left(t^6-2t^4+2it^3-2it-2\right)t^2\right)}{t^9+t^5}$$

$$b_5 = \frac{t\left(it^2+t-i\right)(1+(t-1)t(t+1)(t-i))}{\left(t^4+1\right)^2}$$

$$b_6 = 1$$

$$b_7 = -\frac{(t-i)^2\left(t^6-2t^4+2t^2-1\right)}{t^4}$$

$$b_8 = \frac{\left(it^2+t-i\right)(1+(t-1)t(t+1)(t-i))}{t^3}$$

$$b_9 = \frac{e^{i\frac{3\pi}{4}}(t-1)(t-i)(t+1)}{t^{3/2}}$$

$$b_{10} = -\frac{1+(t-1)t(t+1)(t-i)}{t^4+1}$$

$$b_{11} = \frac{e^{i\frac{\pi}{4}}(1+it)(t-1)(t+1)(1+(t-1)t(t+1)(t-i))}{t^{3/2}\left(t^4+1\right)}$$

$$b_{12} = \frac{\left(t^2-1\right)\left(t^3+i\right)^2(-1+t(t-i))(1+(t-1)t(t+1)(t-i))}{\left(t^5+t\right)\sqrt{t^{10}-t^8+t^6}}$$

$$b_{13} = \frac{e^{i\frac{\pi}{4}}(t-1)(t-i)(t+1)\sqrt{t^{10}-t^8+t^6}(1+(t-1)t(t+1)(t-i))}{t^{11/2}\left(t^4+1\right)}$$

$$b_{14} = -it^{-9}(-1+t(t-i))[1 + t(t-i)(-1+t((t-1)t(t+1)(-3+t(t(3+t(t-i)(-3+t((-2+t(t+i))t^3+2t-i)))-2i))-i))]$$

7.4.3. An integrable dilute BMW model

Another integrable solution for the B_2 web model on the square lattice can be obtained. This model is much simpler than the preceding one, since it uses only single lines. Let V'_u, $u \in \mathbb{C}^*$, be the second representation of $U_t(A_4^{(2)})$ given in Appendix D.3.3. We are looking for an operator $\check{R}(u,v)$ intertwining $V'_u \otimes V'_v$ and $V'_v \otimes V'_u$. Remark that E_i, F_i and H_i for $i = 1, 2$ generate a Hopf subalgebra isomorphic to $U_{t^2}(B_2)$. Under the action of this subalgebra, V'_u decomposes as:

$$V'_u = \mathbb{C} \oplus V_1 \tag{98}$$

Hence $\check{R}(u,v)$ will decompose as a sum of $U_{t^2}(B_2)$ intertwiners:

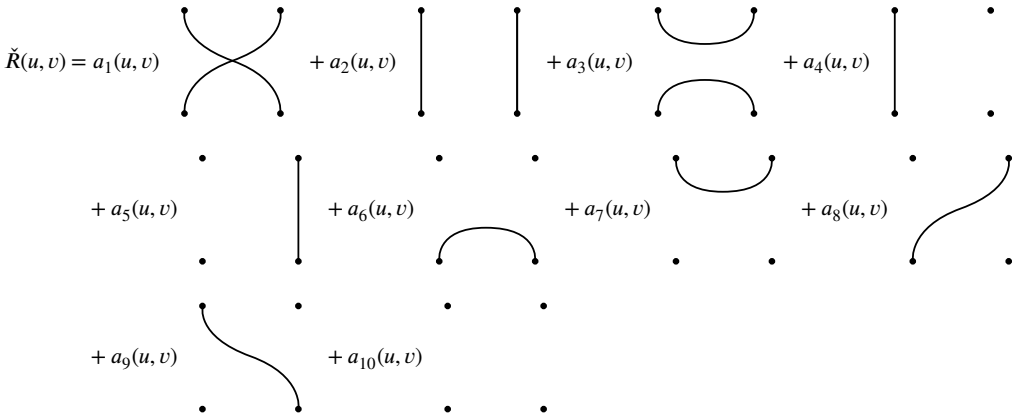

(99)

where $a_i(u,v)$ are some coefficients and the webs span the space of intertwiners $\mathrm{End}_{U_{t^2}(B_2)}\left((\mathbb{C} \oplus V_1)^2\right)$, with the first web defined in (36).[12]

Asking for $\check{R}(u,v)$ to commute with the remaining generators, we see that it depends only on the ratio $s = \frac{u}{v}$. Plugging this linear system for the functions $a_i(s)$ into Mathematica, we find

$$\begin{aligned}
a_1(s) &= \frac{(t^5 s^{-1} + t^{-5} s)(s - s^{-1})}{t^2 + t^{-2}} \\
a_2(s) &= (t^2 s^{-1} - t^{-2} s)(t^5 s^{-1} + t^{-5} s) \\
a_3(s) &= -(t^3 s^{-1} + t^{-3} s)(s - s^{-1}) \\
a_4(s) &= (t^2 - t^{-2})(t^5 s^{-1} + t^{-5} s) \\
a_5(s) &= (t^2 - t^{-2})(t^5 s^{-1} + t^{-5} s) \\
a_6(s) &= t^5 (t^2 - t^{-2})(s - s^{-1}) \\
a_7(s) &= -\frac{1}{t^5}(t^2 - t^{-2})(s - s^{-1}) \\
a_8(s) &= -(t^5 s^{-1} + t^{-5} s)(s - s^{-1}) \\
a_9(s) &= -(t^5 s^{-1} + t^{-5} s)(s - s^{-1}) \\
a_{10}(s) &= (t^5 + t^{-5})(t^2 - t^{-2}) - (t^5 s^{-1} + t^{-5} s)(s - s^{-1})
\end{aligned}$$

One can then show, using for instance Mathematica, that the corresponding operator $\check{R}(s)$ satisfies the multiplicative spectral parameter dependant Yang-Baxter equation.

Remark that the diagrams appearing in the decomposition of $\check{R}(u,v)$ are generators of the dilute BMW algebra once one considers the braiding operator [3]:

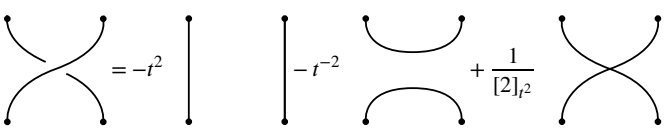

[12] Remark that this map is not the flip map.

The dilute BMW algebra has been baxterised [29] and the above integrable $\check{R}$-matrix (99) can then be recovered from [29, eq. (3.9)] (with the sign $\sigma = -1$ in the notations of that reference).

We now tune the spectral parameter as $s = -e^{i\frac{\pi}{4}} t^{\frac{5}{2}}$ and use the gauge freedom

$$D = \mathrm{Diag}(1, \alpha, \alpha, \alpha, \alpha)$$
$$\check{R}(s) \to \left(D^{-1} \otimes D^{-1}\right) \check{R}(s) (D \otimes D)$$

which is just an elementary rescaling, thanks to the decomposition (98). One then obtains the B_2 web model on the square lattice defined in Section 5.3 with the following Boltzmann weights:

$$\begin{aligned}
b_1 &= \frac{\cos^2(\frac{5}{2}\psi - \frac{\pi}{4})}{2\cos(2\psi)} \\
b_2 &= \sin\left(\frac{1}{2}\psi + \frac{\pi}{4}\right)\cos\left(\frac{5}{2}\psi - \frac{\pi}{4}\right) \\
b_3 &= -\sin(2\psi)\cos\left(\frac{5}{2}\psi - \frac{\pi}{4}\right) \\
b_4 &= -\cos^2(\frac{5}{2}\psi - \frac{\pi}{4}) \\
b_{14} &= \cos(5\psi)\sin(2\psi) - \cos^2(\frac{5}{2}\psi - \frac{\pi}{4}) \\
b_i &= 0 \qquad \text{for } i \in [\![5, 13]\!]
\end{aligned}$$

where we have parametrised as $t = e^{i\psi}$. Notice that the last condition on vanishing weights is the same as (47) that forbids double edges in the corresponding spin model.

8. Discussion

In this paper, we have defined web models as lattice models based on all the rank-two spiders introduced by Kuperberg in [3,30]. We have exhibited specific root-of-unity values of the deformation parameter q for which the weight of closed webs can be used to count the number of colourings of their dual graphs, possibly with some constraints. These combinatorial properties allowed us to relate the web models at these special values of q to three- and four-state spins model with certain plaquette interactions and specific global symmetries.

We have then used the central results of [3] which connect open webs with invariants of quantum group representations in order to write explicit local transfer matrices of the web models. Finally, we derived integrable R-matrices, which for a well-chosen value of their spectral parameter reproduce these transfer matrices. In particular, we have exhibited new integrable points for the spin models.

Although this paper begins with the definition of certain web models and then demonstrates how they are obtained from affine R-matrices of well-chosen integrable models, another point of view would be that the definitions of those particular models are motivated by their integrability. Once the integrable R-matrix has been expressed in terms of webs, we may then define a related web model on the lattice.

As in the well known case of loop models, the most convenient models are obtained on the square lattice or the hexagonal lattice. We have chosen to prioritise the simplest choice, which is the hexagonal lattice $\mathbb{H}$. The configurations are easily described as embeddings of webs in $\mathbb{H}$. Moreover, the local patterns around a vertex of $\mathbb{H}$ are so few that it is always possible to write rotationally invariant local Boltzmann weights in terms of local fugacities. The fugacities account for links or nodes to be covered by specific types of edges of a given web.

By contrast, the models on the square lattice $\mathbb{S}$ are a bit more involved, and the local patterns at each vertex are more complicated, decorated graph embeddings. In particular, we have chosen to define the B_2 web models on $\mathbb{S}$, because the integrable solutions on $\mathbb{H}$ are not rotational invariant. We might of course also have defined integrable A_2 and G_2 web models on $\mathbb{S}$. In the A_2 case, for instance, this would have led to interactions of the form

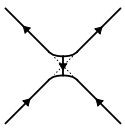

It is worth mentioning that the web models on $\mathbb{S}$ could potentially have a richer phase diagram than their counterparts on $\mathbb{H}$. For instance, the loop model on $\mathbb{S}$ presents three different integrable regimes [23], one of which has a non-compact continuum limit [9], but only one of those regimes survives the restriction of the model to the simpler lattice $\mathbb{H}$. Remarkably, our numerical work shows that the A_2 and G_2 web models defined on $\mathbb{H}$ have two and (at least) four regimes, respectively. The corresponding models defined on $\mathbb{S}$ might conceivably possess an even greater number of regimes.

We now discuss some possible directions for future work. First and foremost, one might solve the integrable web models by the Bethe ansatz. The fact that R-matrices are obtained from quantum group symmetries suggests the use of the algebraic Bethe ansatz. But even the more modest goal of setting up the Bethe ansatz equations might be worthwhile, since this would give access to larger system sizes than can be attained by exact diagonalisation of the transfer matrix.

Another direction is to study the geometrical nature of the excitations present in the spectra of the transfer matrices. This has been discussed in [2] for the A_2 case, where it was suggested that such excitations correspond to lattice precursors of electromagnetic operators in a Coulomb Gas description of the continuum limit. This A_2 Coulomb Gas will be defined in a future paper [28]. One might also hope to find analogous Coulomb Gas descriptions for the other G_2 and B_2 web models, although it seems more challenging when the relevant Dynkin diagram is not simply laced (see the discussion in [42]).

Some of the special points that we have identified in the phase diagrams of the web models are of particular interest. For instance, the dense G_2 web model at $q = e^{i\frac{5\pi}{6}}$ describes a three-colour analogue of percolation which has not been studied before, to our best knowledge (see Section 7.3.2). It is also interesting that some instances of the *loop* models, such as percolation or LERW, appear at specific points of the rank-2 *web* models (see Sections 7.2.2 and 7.3.2). These give access to operators which are not present in the rank-1 realisations of these models, and may hence provide new details about their critical behaviour. The challenge would then be to describe the geometrical interpretation of such operators.

Other special points indicate that the three-state Potts model with plaquette interactions can give rise to universality classes which are unusual for this model. For instance we have found cases of central charge $c = -2$ and $c \approx 1.5$. It would be interesting to study further the possible RG flows between these models, and in particular whether some of the flows are integrable.

We did not present here the numerical analysis of the B_2 models, due to the large dimension of its transfer matrix. We also did not study the special points of this model. However, by the structure of its symmetries at $q = i$, the B_2 web model is a good candidate for realising symplectic fermions at $c = -4$.

Finally, one can define discrete holomorphic observables from the intertwining relations (75) and give them a combinatorial formulation thanks to webs, as was already done in the loop model case [43–46]. One might hope that some of these observables would enable us to rigorously derive conformal invariance of the corresponding lattice models, analogously to what was already done for the Ising model in its dilute loop representation [47], or for percolation [48,49].

CRediT authorship contribution statement

Augustin Lafay: Conceptualization, Investigation, Software, Writing – original draft. **Azat M. Gainutdinov:** Conceptualization, Supervision, Writing – review & editing. **Jesper Lykke Jacobsen:** Conceptualization, Software, Supervision, Writing – review & editing.

Declaration of competing interest

The authors declare that they have no known competing financial interests or personal relationships that could have appeared to influence the work reported in this paper.

Data availability

No data was used for the research described in the article.

Acknowledgements

Part of this work was done when Augustin Lafay was affiliated with the LPENS. His research is now supported by the Academy of Finland grant number 340461, entitled “Conformal invariance in planar random geometry”. The work of Azat M. Gainutdinov was supported by the CNRS, and partially by the ANR grant JCJC ANR-18-CE40-0001. AMG is also grateful to LPENS, Paris for its kind hospitality in 2022 and 2023. This work of Jesper L. Jacobsen was supported by the French Agence Nationale de la Recherche (ANR) under grant ANR-21-CE40-0003 (project CONFICA).

Appendix A. Some symmetries of the A_2 web models

The Boltzmann weight of the A_2 web models is of the form $x^N (yz)^{N_V} e^{iM\phi} w_{\mathrm{K}}(G)$ for a given configuration G. Denote by $w_{\mathrm{loc}}(G) = x^N (yz)^{N_V} e^{iM\phi}$ the product of its local fugacities. We will show by induction on the number of edges that $N + N_V + M \equiv 0 \bmod 2$, $M \equiv 0 \bmod 3$.

Consider a web G embedded in the hexagonal lattice $\mathbb{H}$. If G is a collection of loops, the result is clear. Supose it is not the case. Let F be a face of G other than the exterior one that is not surrounded by a loop. Remove the edges surrounding F going clockwise around it and reverse the orientation of the others. It is clear that the resulting graph G' embedded in $\mathbb{H}$ is again a web. Moreover G' has strictly less edges and the induction hypothesis applies.

Around each node of $\mathbb{H}$ surrounding F, there are, up to rotations, 6 possibilities. We draw them below as well as their transformed counterparts, dotted lines meaning empty links.

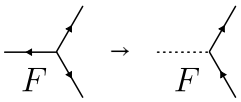

$$: \quad x^{3/2}y \to xe^{i\phi} \tag{100a}$$

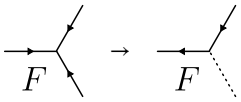

$$: \quad x^{3/2}z \to xe^{i\phi} \tag{100b}$$

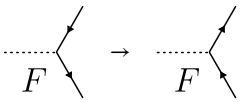

$$: \quad xe^{-i\phi} \to xe^{i\phi} \tag{100c}$$

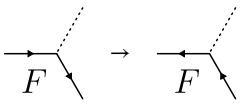

$$: \quad xe^{i\phi} \to xe^{-i\phi} \tag{100d}$$

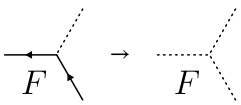

$$: \quad xe^{-i\phi} \to 1 \tag{100e}$$

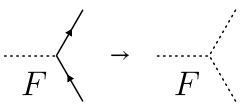

$$: \quad xe^{i\phi} \to 1 \tag{100f}$$

We also wrote the corresponding change in the contribution to the Boltzmann weight from local fugacities, understanding that the fugacity of a half bond is $x^{1/2}$. Denote by l the number of source/sink pairs surrounding F, by m_1 the number of nodes as in (100c), by m_2 the number of nodes as in (100d), by n_1 the number of nodes as in (100e) and by n_2 the number of nodes as in (100f).

We have that

$$\begin{aligned} w_{\mathrm{loc}}(G) =& (xyze^{i2\phi})^l (e^{i\phi})^{m_1} (e^{-i\phi})^{m_2} (xe^{i\phi})^{n_1} (xe^{-i\phi})^{n_2} w_{\mathrm{loc}}(G') \\ =& x^{l+n_1+n_2} (yz)^l (e^{i\phi})^{2l+2m_1-2m_2+n_1-n_2} w_{\mathrm{loc}}(G') \end{aligned}$$

As F is surrounded by an even number of edges,

$$2l + m_1 + m_2 + n_1 + n_2 \equiv 0 \bmod 2$$

from which it follows, using the induction hypothesis, that

$$N + N_V + M \equiv 0 \bmod 2$$

Moreover, one has that the number of nodes where F is locally convex minus the number of nodes where F is not is equal to 6. Thus

$$2l + m_2 + n_1 - m_1 - n_2 = 6 \equiv 0 \bmod 3$$

which implies that

$$2l + 2m_1 - 2m_2 + n_1 - n_2 \equiv 0 \bmod 3$$

and then, using the induction hypothesis, that

$$M \equiv 0 \bmod 3$$

Appendix B. Data and conventions for root systems

Here, we give Cartan matrix conventions for the quantum groups used in the main text, in the order that the big quantum group follows the small one, for instance, $G_2^{(1)}$ follows A_2. We describe also the symmetrisation of the Cartan matrix A_{ij} in terms of the relatively prime positive integers d_i such that $d_i A_{ij}$ is symmetric. We also give the fundamental weights in the non-affine cases.

B.1. A_2 web models

B.1.1. A_2

Let $\boldsymbol{\alpha}_1$ and $\boldsymbol{\alpha}_2$ be the two simple roots of A_2. We normalise them such that $(\boldsymbol{\alpha}_1 \boldsymbol{\alpha}_1) = 2$. The Cartan matrix is given by:

$$A_{ij} = 2\frac{(\boldsymbol{\alpha}_i, \boldsymbol{\alpha}_j)}{(\boldsymbol{\alpha}_i, \boldsymbol{\alpha}_i)} = \begin{pmatrix} 2 & -1 \\ -1 & 2 \end{pmatrix} \tag{101}$$

The simple coroots are given by

$$\boldsymbol{\alpha}_1^\vee = \boldsymbol{\alpha}_1 \tag{102a}$$

$$\boldsymbol{\alpha}_2^\vee = \boldsymbol{\alpha}_2 \tag{102b}$$

The fundamental weights are given by

$$\boldsymbol{w}_1 = \frac{2}{3}\boldsymbol{\alpha}_1 + \frac{1}{3}\boldsymbol{\alpha}_2 \tag{103a}$$

$$\boldsymbol{w}_2 = \frac{1}{3}\boldsymbol{\alpha}_1 + \frac{2}{3}\boldsymbol{\alpha}_2 \tag{103b}$$

The Weyl vector and dual Weyl vector are

$$\boldsymbol{\rho} = \boldsymbol{w}_1 + \boldsymbol{w}_2 = \boldsymbol{\alpha}_1 + \boldsymbol{\alpha}_2 \tag{104a}$$

$$\boldsymbol{\rho}^\vee = \boldsymbol{\rho} \tag{104b}$$

B.1.2. $G_2^{(1)}$

The Cartan matrix is given by:

$$A_{ij} = \begin{pmatrix} 2 & -1 & 0 \\ -1 & 2 & -1 \\ 0 & -3 & 2 \end{pmatrix} \tag{105}$$

$$d_1 = 3, \qquad d_2 = 3, \qquad d_3 = 1$$

B.2. G_2 *web models*

B.2.1. G_2

Let $\boldsymbol{\alpha}_1$ and $\boldsymbol{\alpha}_2$ be the two simple roots of G_2 with $\boldsymbol{\alpha}_1$ the smallest one. We normalise them such that $(\boldsymbol{\alpha}_1\boldsymbol{\alpha}_1) = 2$. The Cartan matrix is given by:

$$A_{ij} = 2\frac{(\boldsymbol{\alpha}_i, \boldsymbol{\alpha}_j)}{(\boldsymbol{\alpha}_i, \boldsymbol{\alpha}_i)} = \begin{pmatrix} 2 & -3 \\ -1 & 2 \end{pmatrix} \tag{106}$$

$$d_1 = 1, \qquad d_2 = 3$$

The simple coroots are given by

$$\boldsymbol{\alpha}_1^\vee = \boldsymbol{\alpha}_1 \tag{107a}$$

$$\boldsymbol{\alpha}_2^\vee = \frac{1}{3}\boldsymbol{\alpha}_2 \tag{107b}$$

The fundamental weights are given by

$$\boldsymbol{w}_1 = 2\boldsymbol{\alpha}_1 + \boldsymbol{\alpha}_2 \tag{108a}$$

$$\boldsymbol{w}_2 = 3\boldsymbol{\alpha}_1 + 2\boldsymbol{\alpha}_2 \tag{108b}$$

The Weyl vector and dual Weyl vector are

$$\boldsymbol{\rho} = \boldsymbol{w}_1 + \boldsymbol{w}_2 = 5\boldsymbol{\alpha}_1 + 3\boldsymbol{\alpha}_2 \tag{109a}$$

$$\boldsymbol{\rho}^\vee = 3\boldsymbol{\alpha}_1 + \frac{5}{3}\boldsymbol{\alpha}_2 \tag{109b}$$

B.2.2. $D_4^{(3)}$

The Cartan matrix is given by:

$$A_{ij} = \begin{pmatrix} 2 & -1 & 0 \\ -3 & 2 & -1 \\ 0 & -1 & 2 \end{pmatrix} \tag{110}$$

$$d_1 = 3, \qquad d_2 = 1, \qquad d_3 = 1$$

B.3. B_2 web models

B.3.1. B_2

Let $\boldsymbol{\alpha}_1$ and $\boldsymbol{\alpha}_2$ be the two simple roots of B_2 with $\boldsymbol{\alpha}_1$ the smallest one. We normalise them such that $(\boldsymbol{\alpha}_1\boldsymbol{\alpha}_1) = 2$. The Cartan matrix is given by:

$$A_{ij} = 2\frac{(\boldsymbol{\alpha}_i, \boldsymbol{\alpha}_j)}{(\boldsymbol{\alpha}_i, \boldsymbol{\alpha}_i)} = \begin{pmatrix} 2 & -2 \\ -1 & 2 \end{pmatrix} \tag{111}$$

$$d_1 = 1, \qquad d_2 = 2$$

The simple coroots are given by

$$\boldsymbol{\alpha}_1^\vee = \boldsymbol{\alpha}_1 \tag{112a}$$

$$\boldsymbol{\alpha}_2^\vee = \frac{1}{2}\boldsymbol{\alpha}_2 \tag{112b}$$

The fundamental weights are given by

$$\boldsymbol{w}_1 = \boldsymbol{\alpha}_1 + \frac{1}{2}\boldsymbol{\alpha}_2 \tag{113a}$$

$$\boldsymbol{w}_2 = \boldsymbol{\alpha}_1 + \boldsymbol{\alpha}_2 \tag{113b}$$

The Weyl vector and dual Weyl vector are

$$\boldsymbol{\rho} = \boldsymbol{w}_1 + \boldsymbol{w}_2 = 2\boldsymbol{\alpha}_1 + \frac{3}{2}\boldsymbol{\alpha}_2 \tag{114a}$$

$$\boldsymbol{\rho}^\vee = \frac{3}{2}\boldsymbol{\alpha}_1 + \boldsymbol{\alpha}_2 \tag{114b}$$

B.3.2. $A_4^{(2)}$

The Cartan matrix is given by:

$$A_{ij} = \begin{pmatrix} 2 & -2 & 0 \\ -1 & 2 & -2 \\ 0 & -1 & 2 \end{pmatrix} \tag{115}$$

$$d_1 = 1, \qquad d_2 = 2, \qquad d_3 = 4$$

Appendix C. Conventions for quantum groups

Let $q \in \mathbb{C}$ be an arbitrary non-zero complex number (but $q \neq \pm 1$). The statistical weights of the web models will be defined in terms of so-called q-numbers $[k]_q$, with $k \in \mathbb{N}$, defined by

$$[k]_q = \frac{q^k - q^{-k}}{q - q^{-1}}\,. \tag{116}$$

Note that the q-numbers reduce to the ordinary integers, $[k]_q \to k$, in the limit $q \to 1$. We shall also need the corresponding q-factorial and q-binomial coefficients:

$$[k]_q! = \prod_{1 \le i \le k} [i]_q\,, \qquad \begin{bmatrix} n \\ k \end{bmatrix}_q = \frac{[n]_q!}{[k]_q![n-k]_q!}\,,$$

with the convention $[0]_q! = 1$ and $\begin{bmatrix} n \\ 0 \end{bmatrix}_q = 1$.

We recall here a definition of the Hopf algebra $U_q(X)$ and its pivotal structure. Let d_i be the relatively prime positive integers such that $d_i A_{ij}$ is symmetric. Then, the $\mathbb{C}(q)$-algebra $U_q(X)$ is generated by E_i, F_i, q^{H_i} for $i \in [\![1,2]\!]$ satisfying the following relations:

$$q^{H_i} q^{H_j} = q^{H_j} q^{H_i}\,, \tag{117a}$$

$$q^{H_i} E_j q^{-H_i} = q^{A_{ij}} E_j\,, \qquad q^{H_i} F_j q^{-H_i} = q^{-A_{ij}} F_j\,, \tag{117b}$$

$$[E_i, F_j] = \delta_{ij} \frac{q^{d_i H_i} - q^{-d_i H_i}}{q^{d_i} - q^{-d_i}}\,, \tag{117c}$$

$$\sum_{m=0}^{1-A_{ij}} (-1)^m \begin{bmatrix} 1 - A_{ij} \\ m \end{bmatrix}_{q^{d_i}} E_i^{1-A_{ij}-m} E_j E_i^m = 0\,, \quad \text{if } i \neq j\,, \tag{117d}$$

$$\sum_{m=0}^{1-A_{ij}} (-1)^m \begin{bmatrix} 1-A_{ij} \\ m \end{bmatrix}_{q^{d_i}} F_i^{1-A_{ij}-m} F_j F_i^m = 0\,, \quad \text{if } i \neq j\,. \tag{117e}$$

It is a Hopf algebra with the coproduct

$$\Delta(E_i) = E_i \otimes q^{d_i H_i} + 1 \otimes E_i\,, \qquad \Delta(F_i) = F_i \otimes 1 + q^{-d_i H_i} \otimes F_i\,, \qquad \Delta(q^{H_i}) = q^{H_i} \otimes q^{H_i}\,, \tag{118}$$

the antipode

$$S(E_i) = -E_i q^{-d_i H_i}\,, \qquad S(F_i) = -q^{d_i H_i} F_i\,, \qquad S(q^{H_i}) = q^{-H_i}\,, \tag{119}$$

and the counit

$$\epsilon(E_i) = 0\,, \qquad \epsilon(F_i) = 0\,, \qquad \epsilon(q^{H_i}) = 1\,. \tag{120}$$

We use the notation $H_{\sum_i c_i \alpha_i} := \sum_i c_i d_i H_i$.

Appendix D. Explicit matrix elements of representations

We give in this section the matrices of our representations of interest of the generators of quantum groups in our chosen bases.

D.1. The A_2 web models

D.1.1. $U_{-q}(A_2)$ representations

In the basis $\{u_i, i \in [\![1,3]\!]\}$ of V_1 introduced in Section 6.2, we have the following representation of generators of $U_{-q}(A_2)$:

$$E_1 = \begin{bmatrix} 0 & 1 & 0 \\ 0 & 0 & 0 \\ 0 & 0 & 0 \end{bmatrix} \qquad E_2 = \begin{bmatrix} 0 & 0 & 0 \\ 0 & 0 & 1 \\ 0 & 0 & 0 \end{bmatrix}$$

$$F_1 = \begin{bmatrix} 0 & 0 & 0 \\ 1 & 0 & 0 \\ 0 & 0 & 0 \end{bmatrix} \qquad F_2 = \begin{bmatrix} 0 & 0 & 0 \\ 0 & 0 & 0 \\ 0 & 1 & 0 \end{bmatrix}$$

$$H_1 = \begin{bmatrix} 1 & 0 & 0 \\ 0 & -1 & 0 \\ 0 & 0 & 0 \end{bmatrix} \qquad H_2 = \begin{bmatrix} 0 & 0 & 0 \\ 0 & 1 & 0 \\ 0 & 0 & -1 \end{bmatrix}$$

In the basis $\{v_i, i \in [\![1,3]\!]\}$ of V_2 introduced in Section 6.2, we have the following representation of generators of $U_{-q}(A_2)$:

$$E_1 = \begin{bmatrix} 0 & 0 & 0 \\ 0 & 0 & 1 \\ 0 & 0 & 0 \end{bmatrix} \qquad E_2 = \begin{bmatrix} 0 & 1 & 0 \\ 0 & 0 & 0 \\ 0 & 0 & 0 \end{bmatrix}$$

$$F_1 = \begin{bmatrix} 0 & 0 & 0 \\ 0 & 0 & 0 \\ 0 & 1 & 0 \end{bmatrix} \qquad F_2 = \begin{bmatrix} 0 & 0 & 0 \\ 1 & 0 & 0 \\ 0 & 0 & 0 \end{bmatrix}$$

$$H_1 = \begin{bmatrix} 0 & 0 & 0 \\ 0 & 1 & 0 \\ 0 & 0 & -1 \end{bmatrix} \qquad H_2 = \begin{bmatrix} 1 & 0 & 0 \\ 0 & -1 & 0 \\ 0 & 0 & 0 \end{bmatrix}$$

D.1.2. $U_t(G_2^{(1)})$ evaluation representation

Let $u \in \mathbb{C}^*$. Consider the following representation V_u of $U_t(G_2^{(1)})$ given in the basis $\{u_1, u_2, u_3, v_1, v_2, v_3, 1\}$ where 1 denotes the basis vector of the trivial representation of $U_{-q}(A_2)$,

$$E_0 = \begin{bmatrix} 0 & 1 & 0 & 0 & 0 & 0 & 0 \\ 0 & 0 & 0 & 0 & 0 & 0 & 0 \\ 0 & 0 & 0 & 0 & 0 & 0 & 0 \\ 0 & 0 & 0 & 0 & 0 & 0 & 0 \\ 0 & 0 & 0 & 0 & 0 & 1 & 0 \\ 0 & 0 & 0 & 0 & 0 & 0 & 0 \\ 0 & 0 & 0 & 0 & 0 & 0 & 0 \end{bmatrix} \qquad F_0 = \begin{bmatrix} 0 & 0 & 0 & 0 & 0 & 0 & 0 \\ 1 & 0 & 0 & 0 & 0 & 0 & 0 \\ 0 & 0 & 0 & 0 & 0 & 0 & 0 \\ 0 & 0 & 0 & 0 & 0 & 0 & 0 \\ 0 & 0 & 0 & 0 & 0 & 0 & 0 \\ 0 & 0 & 0 & 0 & 1 & 0 & 0 \\ 0 & 0 & 0 & 0 & 0 & 0 & 0 \end{bmatrix}$$

$$E_1 = \begin{bmatrix} 0&0&0&0&0&0&0\\ 0&0&1&0&0&0&0\\ 0&0&0&0&0&0&0\\ 0&0&0&0&1&0&0\\ 0&0&0&0&0&0&0\\ 0&0&0&0&0&0&0\\ 0&0&0&0&0&0&0 \end{bmatrix} \qquad F_1 = \begin{bmatrix} 0&0&0&0&0&0&0\\ 0&0&0&0&0&0&0\\ 0&1&0&0&0&0&0\\ 0&0&0&0&0&0&0\\ 0&0&0&1&0&0&0\\ 0&0&0&0&0&0&0\\ 0&0&0&0&0&0&0 \end{bmatrix}$$

$$E_2 = u\begin{bmatrix} 0&0&0&0&0&0&0\\ 0&0&0&0&0&0&0\\ 0&0&0&0&0&0&\sqrt{[2]_t}\\ 0&0&0&0&0&0&0\\ 1&0&0&0&0&0&0\\ 0&1&0&0&0&0&0\\ 0&0&0&\sqrt{[2]_t}&0&0&0 \end{bmatrix} \qquad F_2 = \frac{1}{u}\begin{bmatrix} 0&0&0&0&1&0&0\\ 0&0&0&0&0&1&0\\ 0&0&0&0&0&0&0\\ 0&0&0&0&0&0&\sqrt{[2]_t}\\ 0&0&0&0&0&0&0\\ 0&0&0&0&0&0&0\\ 0&0&\sqrt{[2]_t}&0&0&0&0 \end{bmatrix}$$

$$H_0 = \begin{bmatrix} 1&0&0&0&0&0&0\\ 0&-1&0&0&0&0&0\\ 0&0&0&0&0&0&0\\ 0&0&0&0&0&0&0\\ 0&0&0&0&1&0&0\\ 0&0&0&0&0&-1&0\\ 0&0&0&0&0&0&0 \end{bmatrix} \qquad H_1 = \begin{bmatrix} 0&0&0&0&0&0&0\\ 0&1&0&0&0&0&0\\ 0&0&-1&0&0&0&0\\ 0&0&0&1&0&0&0\\ 0&0&0&0&-1&0&0\\ 0&0&0&0&0&0&0\\ 0&0&0&0&0&0&0 \end{bmatrix}$$

$$H_2 = \begin{bmatrix} -1&0&0&0&0&0&0\\ 0&-1&0&0&0&0&0\\ 0&0&2&0&0&0&0\\ 0&0&0&-2&0&0&0\\ 0&0&0&0&1&0&0\\ 0&0&0&0&0&1&0\\ 0&0&0&0&0&0&0 \end{bmatrix}$$

D.2. The G_2 web models

D.2.1. $U_q(G_2)$ representations

In the basis $\{e_i, i \in [\![1,7]\!]\}$ of V introduced in Section 6.3, we have the following representation of generators of $U_q(G_2)$:

$$E_1 = \begin{bmatrix} 0&1&0&0&0&0&0\\ 0&0&0&0&0&0&0\\ 0&0&0&[2]_q&0&0&0\\ 0&0&0&0&[2]_q&0&0\\ 0&0&0&0&0&0&0\\ 0&0&0&0&0&0&1\\ 0&0&0&0&0&0&0 \end{bmatrix} \qquad E_2 = \begin{bmatrix} 0&0&0&0&0&0&0\\ 0&0&1&0&0&0&0\\ 0&0&0&0&0&0&0\\ 0&0&0&0&0&0&0\\ 0&0&0&0&0&1&0\\ 0&0&0&0&0&0&0\\ 0&0&0&0&0&0&0 \end{bmatrix}$$

$$F_1 = \begin{bmatrix} 0&0&0&0&0&0&0\\ 1&0&0&0&0&0&0\\ 0&0&0&0&0&0&0\\ 0&0&1&0&0&0&0\\ 0&0&0&1&0&0&0\\ 0&0&0&0&0&0&0\\ 0&0&0&0&0&1&0 \end{bmatrix} \qquad F_2 = \begin{bmatrix} 0&0&0&0&0&0&0\\ 0&0&0&0&0&0&0\\ 0&1&0&0&0&0&0\\ 0&0&0&0&0&0&0\\ 0&0&0&0&0&0&0\\ 0&0&0&0&1&0&0\\ 0&0&0&0&0&0&0 \end{bmatrix}$$

$$H_1 = \begin{bmatrix} 1&0&0&0&0&0&0\\ 0&-1&0&0&0&0&0\\ 0&0&2&0&0&0&0\\ 0&0&0&0&0&0&0\\ 0&0&0&0&-2&0&0\\ 0&0&0&0&0&1&0\\ 0&0&0&0&0&0&-1 \end{bmatrix} \qquad H_2 = \begin{bmatrix} 0&0&0&0&0&0&0\\ 0&1&0&0&0&0&0\\ 0&0&-1&0&0&0&0\\ 0&0&0&0&0&0&0\\ 0&0&0&0&1&0&0\\ 0&0&0&0&0&-1&0\\ 0&0&0&0&0&0&0 \end{bmatrix}$$

D.2.2. $U_q(D_4^{(3)})$ evaluation representation

Let $u \in \mathbb{C}^*$. Consider the following representation V_u of $U_q(D_4^{(3)})$ given in the basis $\{1, e_1, e_2, e_3, e_4, e_5, e_6, e_7\}$ where 1 denotes the basis vector of the trivial representation of $U_q(G_2)$,

$$E_0 = \begin{bmatrix} 0&0&0&0&0&0&0&0\\ 0&0&0&0&0&0&0&0\\ 0&0&0&1&0&0&0&0\\ 0&0&0&0&0&0&0&0\\ 0&0&0&0&0&0&0&0\\ 0&0&0&0&0&0&1&0\\ 0&0&0&0&0&0&0&0\\ 0&0&0&0&0&0&0&0 \end{bmatrix} \qquad F_0 = \begin{bmatrix} 0&0&0&0&0&0&0&0\\ 0&0&0&0&0&0&0&0\\ 0&0&0&0&0&0&0&0\\ 0&0&1&0&0&0&0&0\\ 0&0&0&0&0&0&0&0\\ 0&0&0&0&0&0&0&0\\ 0&0&0&0&0&1&0&0\\ 0&0&0&0&0&0&0&0 \end{bmatrix}$$

$$E_1 = \begin{bmatrix} 0&0&0&0&0&0&0&0\\ 0&0&1&0&0&0&0&0\\ 0&0&0&0&0&0&0&0\\ 0&0&0&0&[2]_q&0&0&0\\ 0&0&0&0&0&[2]_q&0&0\\ 0&0&0&0&0&0&0&0\\ 0&0&0&0&0&0&0&1\\ 0&0&0&0&0&0&0&0 \end{bmatrix} \qquad F_1 = \begin{bmatrix} 0&0&0&0&0&0&0&0\\ 0&0&0&0&0&0&0&0\\ 0&1&0&0&0&0&0&0\\ 0&0&0&0&0&0&0&0\\ 0&0&0&1&0&0&0&0\\ 0&0&0&0&1&0&0&0\\ 0&0&0&0&0&0&0&0\\ 0&0&0&0&0&0&1&0 \end{bmatrix}$$

$$E_2 = u\begin{bmatrix} 0&-\frac{\sqrt{[3]_q}}{[2]_q}&0&0&0&0&0&0\\ 0&0&0&0&0&0&0&0\\ 0&0&0&0&0&0&0&0\\ 0&0&0&0&0&0&0&0\\ 0&\frac{1}{[2]_q}&0&0&0&0&0&0\\ 0&0&\frac{1}{[2]_q}&0&0&0&0&0\\ 0&0&0&\frac{1}{[2]_q}&0&0&0&0\\ -\frac{\sqrt{[3]_q}}{[2]_q}&0&0&0&\frac{1}{[2]_q}&0&0&0 \end{bmatrix} \qquad F_2 = \frac{1}{u}\begin{bmatrix} 0&0&0&0&0&0&0&-\sqrt{[3]_q}\\ -\sqrt{[3]_q}&0&0&0&1&0&0&0\\ 0&0&0&0&0&[2]_q&0&0\\ 0&0&0&0&0&0&[2]_q&0\\ 0&0&0&0&0&0&0&1\\ 0&0&0&0&0&0&0&0\\ 0&0&0&0&0&0&0&0\\ 0&0&0&0&0&0&0&0 \end{bmatrix}$$

$$H_0 = \begin{bmatrix} 0&0&0&0&0&0&0&0\\ 0&0&0&0&0&0&0&0\\ 0&0&1&0&0&0&0&0\\ 0&0&0&-1&0&0&0&0\\ 0&0&0&0&0&0&0&0\\ 0&0&0&0&0&1&0&0\\ 0&0&0&0&0&0&-1&0\\ 0&0&0&0&0&0&0&0 \end{bmatrix} \qquad H_1 = \begin{bmatrix} 0&0&0&0&0&0&0&0\\ 0&1&0&0&0&0&0&0\\ 0&0&-1&0&0&0&0&0\\ 0&0&0&2&0&0&0&0\\ 0&0&0&0&0&0&0&0\\ 0&0&0&0&0&-2&0&0\\ 0&0&0&0&0&0&1&0\\ 0&0&0&0&0&0&0&-1 \end{bmatrix}$$

$$H_2 = \begin{bmatrix} 0&0&0&0&0&0&0&0\\ 0&-2&0&0&0&0&0&0\\ 0&0&-1&0&0&0&0&0\\ 0&0&0&-1&0&0&0&0\\ 0&0&0&0&0&0&0&0\\ 0&0&0&0&0&1&0&0\\ 0&0&0&0&0&0&1&0\\ 0&0&0&0&0&0&0&2 \end{bmatrix}$$

D.3. The B_2 web models

D.3.1. $U_q(B_2)$ representations

In the basis $\{e_i, i \in [\![1,4]\!]\}$ of V_1 introduced in Section 6.4, we have the following representation of generators of $U_q(B_2)$:

$$E_1 = \begin{bmatrix} 0&1&0&0\\ 0&0&0&0\\ 0&0&0&1\\ 0&0&0&0 \end{bmatrix} \qquad E_2 = \begin{bmatrix} 0&0&0&0\\ 0&0&1&0\\ 0&0&0&0\\ 0&0&0&0 \end{bmatrix}$$

$$F_1 = \begin{bmatrix} 0 & 0 & 0 & 0 \\ 1 & 0 & 0 & 0 \\ 0 & 0 & 0 & 0 \\ 0 & 0 & 1 & 0 \end{bmatrix} \qquad F_2 = \begin{bmatrix} 0 & 0 & 0 & 0 \\ 0 & 0 & 0 & 0 \\ 0 & 1 & 0 & 0 \\ 0 & 0 & 0 & 0 \end{bmatrix}$$

$$H_1 = \begin{bmatrix} 1 & 0 & 0 & 0 \\ 0 & -1 & 0 & 0 \\ 0 & 0 & 1 & 0 \\ 0 & 0 & 0 & -1 \end{bmatrix} \qquad H_2 = \begin{bmatrix} 0 & 0 & 0 & 0 \\ 0 & 1 & 0 & 0 \\ 0 & 0 & -1 & 0 \\ 0 & 0 & 0 & 0 \end{bmatrix}$$

In the basis $\{v_i, i \in [\![1,5]\!]\}$ of V_2 introduced in Section 6.4, we have the following representation of generators of $U_q(B_2)$:

$$E_1 = \begin{bmatrix} 0 & 0 & 0 & 0 & 0 \\ 0 & 0 & [2]_q & 0 & 0 \\ 0 & 0 & 0 & [2]_q & 0 \\ 0 & 0 & 0 & 0 & 0 \\ 0 & 0 & 0 & 0 & 0 \end{bmatrix} \qquad E_2 = \begin{bmatrix} 0 & 1 & 0 & 0 & 0 \\ 0 & 0 & 0 & 0 & 0 \\ 0 & 0 & 0 & 0 & 0 \\ 0 & 0 & 0 & 0 & 1 \\ 0 & 0 & 0 & 0 & 0 \end{bmatrix}$$

$$F_1 = \begin{bmatrix} 0 & 0 & 0 & 0 & 0 \\ 0 & 0 & 0 & 0 & 0 \\ 0 & 1 & 0 & 0 & 0 \\ 0 & 0 & 1 & 0 & 0 \\ 0 & 0 & 0 & 0 & 0 \end{bmatrix} \qquad F_2 = \begin{bmatrix} 0 & 0 & 0 & 0 & 0 \\ 1 & 0 & 0 & 0 & 0 \\ 0 & 0 & 0 & 0 & 0 \\ 0 & 0 & 0 & 0 & 0 \\ 0 & 0 & 0 & 1 & 0 \end{bmatrix}$$

$$H_1 = \begin{bmatrix} 0 & 0 & 0 & 0 & 0 \\ 0 & 2 & 0 & 0 & 0 \\ 0 & 0 & 0 & 0 & 0 \\ 0 & 0 & 0 & -2 & 0 \\ 0 & 0 & 0 & 0 & 0 \end{bmatrix} \qquad H_2 = \begin{bmatrix} 1 & 0 & 0 & 0 & 0 \\ 0 & -1 & 0 & 0 & 0 \\ 0 & 0 & 0 & 0 & 0 \\ 0 & 0 & 0 & 1 & 0 \\ 0 & 0 & 0 & 0 & -1 \end{bmatrix}$$

D.3.2. First $U_t(A_4^{(2)})$ evaluation representation

Let $u \in \mathbb{C}^*$. Consider the following representation V_u of $U_t(A_4^{(2)})$ given in the basis $\{1, e_1, e_2, e_3, e_4, v_1, v_2, v_3, v_4, v_5\}$ where 1 denotes the basis vector of the trivial representation of $U_q(B_2)$,

$$E_0 = u \begin{bmatrix} 0 & \frac{\sqrt{[2]_t}(-t^2+1-t^{-2})}{t^2+t^{-2}} & 0 & 0 & 0 & 0 & 0 & 0 & 0 & 0 \\ 0 & 0 & 0 & 0 & 0 & 0 & 0 & 0 & 0 & 0 \\ 0 & 0 & 0 & 0 & 0 & \sqrt{[2]_t} & 0 & 0 & 0 & 0 \\ 0 & 0 & 0 & 0 & 0 & 0 & \sqrt{[2]_t} & 0 & 0 & 0 \\ -\sqrt{[2]_t} & 0 & 0 & 0 & 0 & 0 & 0 & \sqrt{[2]_t} & 0 & 0 \\ 0 & 0 & 0 & 0 & 0 & 0 & 0 & 0 & 0 & 0 \\ 0 & 0 & 0 & 0 & 0 & 0 & 0 & 0 & 0 & 0 \\ 0 & \frac{\sqrt{[2]_t}}{t^2+t^{-2}} & 0 & 0 & 0 & 0 & 0 & 0 & 0 & 0 \\ 0 & 0 & \frac{\sqrt{[2]_t}}{t^2+t^{-2}} & 0 & 0 & 0 & 0 & 0 & 0 & 0 \\ 0 & 0 & 0 & \frac{\sqrt{[2]_t}}{t^2+t^{-2}} & 0 & 0 & 0 & 0 & 0 & 0 \end{bmatrix}$$

$$F_0 = \frac{1}{u} \begin{bmatrix} 0 & 0 & 0 & 0 & \frac{\sqrt{[2]_t}(-t^2+1-t^{-2})}{t^2+t^{-2}} & 0 & 0 & 0 & 0 & 0 \\ -\sqrt{[2]_t} & 0 & 0 & 0 & 0 & 0 & 0 & \sqrt{[2]_t} & 0 & 0 \\ 0 & 0 & 0 & 0 & 0 & 0 & 0 & 0 & \sqrt{[2]_t}(t^2+t^{-2}) & 0 \\ 0 & 0 & 0 & 0 & 0 & 0 & 0 & 0 & 0 & \sqrt{[2]_t}(t^2+t^{-2}) \\ 0 & 0 & 0 & 0 & 0 & 0 & 0 & 0 & 0 & 0 \\ 0 & 0 & \sqrt{[2]_t} & 0 & 0 & 0 & 0 & 0 & 0 & 0 \\ 0 & 0 & 0 & \sqrt{[2]_t} & 0 & 0 & 0 & 0 & 0 & 0 \\ 0 & 0 & 0 & 0 & \frac{\sqrt{[2]_t}}{t^2+t^{-2}} & 0 & 0 & 0 & 0 & 0 \\ 0 & 0 & 0 & 0 & 0 & 0 & 0 & 0 & 0 & 0 \\ 0 & 0 & 0 & 0 & 0 & 0 & 0 & 0 & 0 & 0 \end{bmatrix}$$

$$H_0 = \begin{bmatrix} 0 & 0 & 0 & 0 & 0 & 0 & 0 & 0 & 0 & 0 \\ 0 & -2 & 0 & 0 & 0 & 0 & 0 & 0 & 0 & 0 \\ 0 & 0 & 0 & 0 & 0 & 0 & 0 & 0 & 0 & 0 \\ 0 & 0 & 0 & 0 & 0 & 0 & 0 & 0 & 0 & 0 \\ 0 & 0 & 0 & 0 & 2 & 0 & 0 & 0 & 0 & 0 \\ 0 & 0 & 0 & 0 & 0 & -2 & 0 & 0 & 0 & 0 \\ 0 & 0 & 0 & 0 & 0 & 0 & -2 & 0 & 0 & 0 \\ 0 & 0 & 0 & 0 & 0 & 0 & 0 & 0 & 0 & 0 \\ 0 & 0 & 0 & 0 & 0 & 0 & 0 & 0 & 2 & 0 \\ 0 & 0 & 0 & 0 & 0 & 0 & 0 & 0 & 0 & 2 \end{bmatrix}$$

$$E_1 = \begin{bmatrix} 0 & 0 & 0 & 0 & 0 & 0 & 0 & 0 & 0 & 0 \\ 0 & 0 & 1 & 0 & 0 & 0 & 0 & 0 & 0 & 0 \\ 0 & 0 & 0 & 0 & 0 & 0 & 0 & 0 & 0 & 0 \\ 0 & 0 & 0 & 0 & 1 & 0 & 0 & 0 & 0 & 0 \\ 0 & 0 & 0 & 0 & 0 & 0 & 0 & 0 & 0 & 0 \\ 0 & 0 & 0 & 0 & 0 & 0 & 0 & 0 & 0 & 0 \\ 0 & 0 & 0 & 0 & 0 & 0 & 0 & t^2 + t^{-2} & 0 & 0 \\ 0 & 0 & 0 & 0 & 0 & 0 & 0 & 0 & t^2 + t^{-2} & 0 \\ 0 & 0 & 0 & 0 & 0 & 0 & 0 & 0 & 0 & 0 \\ 0 & 0 & 0 & 0 & 0 & 0 & 0 & 0 & 0 & 0 \end{bmatrix}$$

$$F_1 = \begin{bmatrix} 0 & 0 & 0 & 0 & 0 & 0 & 0 & 0 & 0 & 0 \\ 0 & 0 & 0 & 0 & 0 & 0 & 0 & 0 & 0 & 0 \\ 0 & 1 & 0 & 0 & 0 & 0 & 0 & 0 & 0 & 0 \\ 0 & 0 & 0 & 0 & 0 & 0 & 0 & 0 & 0 & 0 \\ 0 & 0 & 0 & 1 & 0 & 0 & 0 & 0 & 0 & 0 \\ 0 & 0 & 0 & 0 & 0 & 0 & 0 & 0 & 0 & 0 \\ 0 & 0 & 0 & 0 & 0 & 0 & 0 & 0 & 0 & 0 \\ 0 & 0 & 0 & 0 & 0 & 0 & 1 & 0 & 0 & 0 \\ 0 & 0 & 0 & 0 & 0 & 0 & 0 & 1 & 0 & 0 \\ 0 & 0 & 0 & 0 & 0 & 0 & 0 & 0 & 0 & 0 \end{bmatrix}$$

$$H_1 = \begin{bmatrix} 0 & 0 & 0 & 0 & 0 & 0 & 0 & 0 & 0 & 0 \\ 0 & 1 & 0 & 0 & 0 & 0 & 0 & 0 & 0 & 0 \\ 0 & 0 & -1 & 0 & 0 & 0 & 0 & 0 & 0 & 0 \\ 0 & 0 & 0 & 1 & 0 & 0 & 0 & 0 & 0 & 0 \\ 0 & 0 & 0 & 0 & -1 & 0 & 0 & 0 & 0 & 0 \\ 0 & 0 & 0 & 0 & 0 & 0 & 0 & 0 & 0 & 0 \\ 0 & 0 & 0 & 0 & 0 & 0 & 2 & 0 & 0 & 0 \\ 0 & 0 & 0 & 0 & 0 & 0 & 0 & 0 & 0 & 0 \\ 0 & 0 & 0 & 0 & 0 & 0 & 0 & 0 & -2 & 0 \\ 0 & 0 & 0 & 0 & 0 & 0 & 0 & 0 & 0 & 0 \end{bmatrix}$$

$$E_2 = \begin{bmatrix} 0 & 0 & 0 & 0 & 0 & 0 & 0 & 0 & 0 & 0 \\ 0 & 0 & 0 & 0 & 0 & 0 & 0 & 0 & 0 & 0 \\ 0 & 0 & 0 & 1 & 0 & 0 & 0 & 0 & 0 & 0 \\ 0 & 0 & 0 & 0 & 0 & 0 & 0 & 0 & 0 & 0 \\ 0 & 0 & 0 & 0 & 0 & 0 & 0 & 0 & 0 & 0 \\ 0 & 0 & 0 & 0 & 0 & 0 & 1 & 0 & 0 & 0 \\ 0 & 0 & 0 & 0 & 0 & 0 & 0 & 0 & 0 & 0 \\ 0 & 0 & 0 & 0 & 0 & 0 & 0 & 0 & 0 & 0 \\ 0 & 0 & 0 & 0 & 0 & 0 & 0 & 0 & 0 & 1 \\ 0 & 0 & 0 & 0 & 0 & 0 & 0 & 0 & 0 & 0 \end{bmatrix}$$

$$F_2 = \begin{bmatrix} 0&0&0&0&0&0&0&0&0&0\\ 0&0&0&0&0&0&0&0&0&0\\ 0&0&0&0&0&0&0&0&0&0\\ 0&0&1&0&0&0&0&0&0&0\\ 0&0&0&0&0&0&0&0&0&0\\ 0&0&0&0&0&0&0&0&0&0\\ 0&0&0&0&0&1&0&0&0&0\\ 0&0&0&0&0&0&0&0&0&0\\ 0&0&0&0&0&0&0&0&0&0\\ 0&0&0&0&0&0&0&0&1&0 \end{bmatrix}$$

$$H_2 = \begin{bmatrix} 0&0&0&0&0&0&0&0&0&0\\ 0&0&0&0&0&0&0&0&0&0\\ 0&0&1&0&0&0&0&0&0&0\\ 0&0&0&-1&0&0&0&0&0&0\\ 0&0&0&0&0&0&0&0&0&0\\ 0&0&0&0&0&1&0&0&0&0\\ 0&0&0&0&0&0&-1&0&0&0\\ 0&0&0&0&0&0&0&0&0&0\\ 0&0&0&0&0&0&0&0&1&0\\ 0&0&0&0&0&0&0&0&0&-1 \end{bmatrix}$$

D.3.3. Second $U_t(A_4^{(2)})$ evaluation representation

Let $u \in \mathbb{C}^*$. Consider the following representation V'_u of $U_t(A_4^{(2)})$ given in the basis $\{1, e_1, e_2, e_3, e_4\}$ where 1 denotes the basis vector of the trivial representation of $U_q(B_2)$,

$$E_0 = u\begin{bmatrix} 0&-\sqrt{[2]_t}&0&0&0\\ 0&0&0&0&0\\ 0&0&0&0&0\\ 0&0&0&0&0\\ \sqrt{[2]_t}&0&0&0&0 \end{bmatrix} \quad F_0 = \frac{1}{u}\begin{bmatrix} 0&0&0&0&\sqrt{[2]_t}\\ -\sqrt{[2]_t}&0&0&0&0\\ 0&0&0&0&0\\ 0&0&0&0&0\\ 0&0&0&0&0 \end{bmatrix} \quad H_0 = \begin{bmatrix} 0&0&0&0&0\\ 0&-2&0&0&0\\ 0&0&0&0&0\\ 0&0&0&0&0\\ 0&0&0&0&2 \end{bmatrix}$$

$$E_1 = \begin{bmatrix} 0&0&0&0&0\\ 0&0&1&0&0\\ 0&0&0&0&0\\ 0&0&0&0&1\\ 0&0&0&0&0 \end{bmatrix} \quad F_1 = \begin{bmatrix} 0&0&0&0&0\\ 0&0&0&0&0\\ 0&1&0&0&0\\ 0&0&0&0&0\\ 0&0&0&1&0 \end{bmatrix} \quad H_1 = \begin{bmatrix} 0&0&0&0&0\\ 0&1&0&0&0\\ 0&0&-1&0&0\\ 0&0&0&1&0\\ 0&0&0&0&-1 \end{bmatrix}$$

$$E_2 = \begin{bmatrix} 0&0&0&0&0\\ 0&0&0&0&0\\ 0&0&0&1&0\\ 0&0&0&0&0\\ 0&0&0&0&0 \end{bmatrix} \quad F_2 = \begin{bmatrix} 0&0&0&0&0\\ 0&0&0&0&0\\ 0&0&0&0&0\\ 0&0&1&0&0\\ 0&0&0&0&0 \end{bmatrix} \quad H_2 = \begin{bmatrix} 0&0&0&0&0\\ 0&0&0&0&0\\ 0&0&1&0&0\\ 0&0&0&-1&0\\ 0&0&0&0&0 \end{bmatrix}$$

References

[1] A. Lafay, A.M. Gainutdinov, J.L. Jacobsen, $U_q(\mathfrak{sl}_n)$ web models and $\mathbb{Z}_n$ spin interfaces, J. Stat. Mech. 2021 (2021) 053104, arXiv:2101.00282.
[2] A. Lafay, A.M. Gainutdinov, J.L. Jacobsen, $U_q(\mathfrak{sl}_3)$ web models: locality, phase diagram and geometrical defects, Nucl. Phys. B 979 (2022) 115789, arXiv:2107.10106.
[3] G. Kuperberg, Spiders for rank 2 Lie algebras, Commun. Math. Phys. 180 (1996) 109–151, arXiv:q-alg/9712003.
[4] B. Nienhuis, Critical behavior of two-dimensional spin models and charge asymmetry in the Coulomb gas, J. Stat. Phys. 34 (1984) 731–761.
[5] B. Nienhuis, Coulomb gas formulation of two-dimensional phase transitions, in: C. Domb, J. Lebowitz (Eds.), Phase Transitions and Critical Phenomena, vol. 11, Academic Press, London, 1987, pp. 1–53.
[6] J.L. Jacobsen, Conformal field theory applied to loop models, in: A.J. Guttmann (Ed.), Polygons, Polyominoes and Polycubes, vol. 775, Springer, Heidelberg, 2009, pp. 347–424.
[7] A.M. Gainutdinov, J.L. Jacobsen, N. Read, H. Saleur, R. Vasseur, Logarithmic conformal field theory: a lattice approach, J. Phys. A, Math. Theor. 46 (2013) 494012, arXiv:1303.2082.
[8] E. Vernier, J.L. Jacobsen, H. Saleur, Non compact conformal field theory and the $a_2^{(2)}$ (Izergin-Korepin) model in regime III, J. Phys. A, Math. Theor. 47 (2014) 285202, arXiv:1404.4497.
[9] E. Vernier, J.L. Jacobsen, H. Saleur, A new look at the collapse of two-dimensional polymers, J. Stat. Mech. Theory Exp. 2015 (2015) 09001, arXiv:1404.4497.
[10] G.F. Lawler, Schramm-Loewner evolution, arXiv:0712.3256.
[11] J. Cardy, SLE for theoretical physicists, Ann. Phys. 318 (2005) 81–118, arXiv:cond-mat/0503313.
[12] S. Sheffield, Exploration trees and conformal loop ensembles, Duke Math. J. 147 (2009) 79–129, arXiv:math/0609167.
[13] R. Rhodes, V. Vargas, Gaussian multiplicative chaos and applications: a review, Probab. Surv. 11 (2014) 315–392, arXiv:1305.6221.
[14] A. Kupiainen, R. Rhodes, V. Vargas, Integrability of Liouville theory: proof of the DOZZ formula, Ann. Math. 191 (2020) 81–166, arXiv:1707.08785.
[15] M. Ang, X. Sun, Integrability of the conformal loop ensemble, arXiv:2107.01788.

[16] G. Delfino, J. Viti, On three-point connectivity in two-dimensional percolation, J. Phys. A, Math. Theor. 44 (2010) 032001, arXiv:1009.1314.
[17] M. Picco, R. Santachiara, J. Viti, G. Delfino, Connectivities of Potts Fortuin–Kasteleyn clusters and time-like Liouville correlator, Nucl. Phys. B 875 (2013) 719–737, arXiv:1304.6511.
[18] J.L. Jacobsen, H. Saleur, Bootstrap approach to geometrical four-point functions in the two-dimensional critical Q-state Potts model: a study of the s-channel spectra, J. High Energy Phys. 2019 (2019) 84, arXiv:1809.02191.
[19] Y. He, J.L. Jacobsen, H. Saleur, Geometric four-point functions in the 2D critical Q-state Potts model: the interchiral conformal bootstrap, J. High Energy Phys. 2020 (2020) 019, arXiv:2005.07258.
[20] L. Grans-Samuelsson, R. Nivesvivat, J.L. Jacobsen, S. Ribault, H. Saleur, From combinatorial maps to correlation functions in loop models, SciPost Phys. 15 (2023) 147, arXiv:2302.08168.
[21] B. Nienhuis, Exact critical point and critical exponents of O(n) models in two dimensions, Phys. Rev. Lett. 49 (1982) 1062.
[22] R.J. Baxter, q colourings of the triangular lattice, J. Phys. A, Math. Gen. 19 (1986) 2821.
[23] B. Nienhuis, Critical spin-1 vertex models and $O(n)$ models, Int. J. Mod. Phys. B 04 (1990) 929–942.
[24] S.O. Warnaar, B. Nienhuis, Solvable lattice models labelled by Dynkin diagrams, J. Phys. A, Math. Gen. 26 (1993) 2301.
[25] G. Takács, Quantum affine symmetry and scattering amplitudes of the imaginary coupled $D_4^{(3)}$ affine Toda field theory, Nucl. Phys. B 502 (1997) 629–648, arXiv:hep-th/9701118.
[26] G. Takács, The R-matrix of the $U_q(D_4^{(3)})$ algebra and $G_2^{(1)}$ affine Toda field theory, Nucl. Phys. B 501 (1997) 711–727, arXiv:hep-th/9702196.
[27] H.W.J. Blöte, B. Nienhuis, Critical behaviour and conformal anomaly of the O(n) model on the square lattice, J. Phys. A, Math. Gen. 22 (1989) 1415.
[28] A. Lafay, A.M. Gainutdinov, J.L. Jacobsen, Coulomb Gas description of the A_2 web models, In preparation, 2024.
[29] U. Grimm, S.O. Warnaar, Yang-Baxter algebras based on the two-colour BWM algebra, J. Phys. A, Math. Gen. 28 (1995) 7197–7207, arXiv:hep-th/9506119.
[30] G. Kuperberg, The quantum G_2 link invariant, Int. J. Math. 05 (1994) 61–85, arXiv:math/9201302.
[31] P. Fendley, V. Krushkal, Link invariants, the chromatic polynomial and the Potts model, Adv. Theor. Math. Phys. 14 (2010) 507–540, arXiv:0806.3484.
[32] Rodney J. Baxter, H.N.V. Temperley, S.E. Ashley, Triangular Potts model at its transition temperature, and related models, Proc. R. Soc. Lond. A 358 (1978) 535–559.
[33] J.L. Jacobsen, J. Salas, A.D. Sokal, Spanning forests and the q-state Potts model in the limit $q \to 0$, J. Stat. Phys. 119 (2005) 1153–1281, arXiv:cond-mat/0401026.
[34] M. Jimbo, Quantum R matrix for the generalized Toda system, Commun. Math. Phys. 102 (1986) 537–547.
[35] V.N. Tolstoy, S.M. Khoroshkin, The universal R-matrix for quantum untwisted affine Lie algebras, Funct. Anal. Appl. 26 (1992) 69–71.
[36] I. Damiani, The R-matrix for (twisted) affine quantum algebras, arXiv:1111.4085.
[37] R.B. Zhang, M.D. Gould, A.J. Bracken, From representations of the braid group to solutions of the Yang-Baxter equation, Nucl. Phys. B 354 (1991) 625–652.
[38] G.W. Delius, M.D. Gould, Y.-Z. Zhang, On the construction of trigonometric solutions of the Yang-Baxter equation, Nucl. Phys. B 432 (1994) 377–403, arXiv:hep-th/9405030.
[39] G.W. Delius, M.D. Gould, Y.-Z. Zhang, Twisted quantum affine algebras and solutions to the Yang-Baxter equation, Int. J. Mod. Phys. A 11 (1996) 3415–3437, arXiv:q-alg/9508012.
[40] F.Y. Wu, K.Y. Lin, On the triangular Potts model with two- and three-site interactions, J. Phys. A, Math. Gen. 13 (1980) 629–636.
[41] J.L. Jacobsen, J. Salas, C.R. Scullard, Phase diagram of the triangular-lattice Potts antiferromagnet, J. Phys. A, Math. Theor. 50 (2017) 345002, arXiv:1702.02006.
[42] A. Lafay, Geometrical lattice models, algebraic spiders and applications to random geometry, Thesis, Sorbonne Université, 2022.
[43] Y. Ikhlef, J. Cardy, Discretely holomorphic parafermions and integrable loop models, J. Phys. A, Math. Theor. 42 (2009) 102001, arXiv:0810.5037.
[44] Y. Ikhlef, R. Weston, M. Wheeler, P. Zinn-Justin, Discrete holomorphicity and quantized affine algebras, J. Phys. A, Math. Theor. 46 (2013) 265205, arXiv:1302.4649.
[45] V. Riva, J. Cardy, Holomorphic parafermions in the Potts model and stochastic Loewner evolution, J. Stat. Mech. Theory Exp. 2006 (2006) 12001, arXiv:cond-mat/0608496.
[46] S. Smirnov, Conformal invariance in random cluster models. I. holomorphic fermions in the Ising model, Ann. Math. 172 (2010) 1435–1467.
[47] D. Chelkak, S. Smirnov, Universality in the 2D Ising model and conformal invariance of fermionic observables, Invent. Math. 189 (2012) 515–580, arXiv:0910.2045.
[48] S. Smirnov, Critical percolation in the plane: conformal invariance, Cardy's formula, scaling limits, C. R. Acad. Sci., Ser. 1 Math. 333 (2001) 239–244.
[49] M. Khristoforov, S. Smirnov, Percolation and $O(1)$ loop model, arXiv:2111.15612.